Fuel Particle Heat Exchange during Wildland Fire Spread

A Dissertation

Presented in Partial Fulfillment of the Requirements for the

Degree of Doctorate of Philosophy

with a

Major in Natural Resources

in the College of Graduate Studies

University of Idaho

by

Jack D. Cohen

Major Professor: Penelope Morgan, Ph.D.

Committee Members: Donald Elger, Ph.D.; Alistair Smith, Ph.D.; Mark Finney, Ph.D.

Department Administrator: Anthony Davis, Ph.D.

May 2015

Authorization to Submit Dissertation

This dissertation of Jack D. Cohen, submitted for the degree of Doctor of Philosophy with a major in Natural Resources and titled "Fuel Particle Heat Exchange during Wildland Fire Spread," has been reviewed in final form. Permission, as indicated by the signatures and dates below, is now granted to submit final copies to the College of Graduate Studies for approval.

Major Professor: _____ Date: _____
Penelope Morgan, Ph.D.

Committee Members: _____ Date: _____
Donald Elger, Ph.D.

_____ Date: _____
Alistair Smith, Ph.D.

_____ Date: _____
Mark Finney, Ph.D.

Department Administrator: _____ Date: _____
Anthony Davis, Ph.D.

Abstract

A wildland fire spreads when thermal energy heats up nearby fuel particles leading to their ignition. This heat transfer can only involve convection and radiation heat transfer. It is commonly assumed that radiation heat transfer is the dominant mechanism; that is, fire spread is primarily governed by radiation heat transfer. The purpose of this study was to quantity the contributions of convection and radiation prior to ignition and to test the assumption that radiation heat transfer is the dominant mechanism. The study used (a) mathematical modeling and (b) experimental methods. The mathematical model involved a two-dimensional, transient, finite-difference solution to the conduction heat equation using standard heat transfer equations. The mathematical model was not tuned to match the experimental data because the purpose of the model was to represent the physical processes. One set of experiments controlled fuel particle exposures to a radiant panel and another set of experiments had particles exposed to flame fronts during spreading fire. During the controlled experiments, irradiances were between 29.8 kW/m^2 and 36.4 kW/m^2. Fuel particles were cooled by free convection in some experiments and forced convection in others. All experimental fuel particles were fabricated from yellow poplar (*Liriodendron tulipifera*) and square in cross section. Particle sizes were 1, 3, 6, 9 and 12 mm for the controlled experiments and 1 and 12 mm for the fire spread experiments. The temperatures versus time plots predicted by the numerical model closely matched the shapes of the measured temperature profiles. Thus the mathematical model accurately captured the physics. Both experimental and numerical results from the controlled experiments showed that radiation heat transfer was not sufficient to ignite the 1 mm particle due to convective cooling. Experimental and numerical results from the fire spread experiments showed that convection (not radiation) was the dominant mechanism responsible for heating 1 mm particles to ignition for conditions relevant to wildland fires. These results indicate the need to consider both convective and radiative heat transfer at fuel particle scales in physical wildland fire spread models.

Keywords: wildland fire spread, fuel particle heat exchange, wildland fire modeling

Acknowledgements

This project was made possible by the funding and support of the U.S. Forest Service, Rocky Mountain Research Station and Fire and Aviation Management. I wish to express many thanks to my advisor, Penny Morgan and committee members Don Elger, Karl Rink, Alistair Smith and Mark Finney. Thank you to Randy Pryhorocki, the machinist, welder and mirror polisher who made my designs into experimental equipment. And I am especially indebted to Mark Finney for being a daring, skeptical research colleague, a continual source of discussion, ideas and inspiration, and the person who convinced Fire and Aviation Management to fund our research.

Table of Contents

List of Figures

List of Tables

Chapter One

Dissertation Overview

Physical processes of fuel particle ignition are fundamental to flame spread in wildland fires (Fons 1946) but have received surprisingly little research attention. In this dissertation, I address the mechanisms of dead woody fuel particle heating prior to ignition during wildland fire spread. Wildland fire spread is distinct from industrial or urban contexts because the particles comprising wildland fuel beds widely range in size, have non-uniform, heterogeneous arrangements and consequently respond differently to radiation and convection heat transfer (Williams 1982). Here, I specifically examine the effects of particle surface length (frequently its size) on particle surface heating by radiation and convection and distinguish the difference between particle geometry and surface area-to-volume ratio related to heat exchange. Using experiments coupled with physical modeling I describe how particle boundary conditions and thus particle heat exchange are influenced by a particle's surface length. From this research I provide an experimentally supported theoretical basis for fuel particle heating leading to ignition and fire spread in wildland fuels.

I have written this dissertation as a single document. The format is compatible with the *International Journal of Wildland Fire* so I can easily revise chapters to meet their publication requirements. I do not intend to submit Chapter 2 for publication in a peer reviewed journal, and the principal parts of Chapter 3 have already been published by my coauthors and I, Finney et al. (2013). I intend to publish the research found in Chapters 4 and 5. However, to maintain information continuity and coherence for the dissertation, these chapters are too long for a peer reviewed journal and thus I will later modify them to submit for publication.

Six chapters comprise my dissertation including this overview. In four chapters, Chapters 2 through 5, I present technical information. In the last one, Chapter 6, I summarize the research approach, describe the findings, and put the research findings in context by discussing its limitations and the need for further research.

1.1 Chapter 2 – Fuel Particle Heat Exchange and Wildland Fire Spread

In this chapter I establish the background and rationale for research on particle ignition. I specifically address fuel particle heat exchange leading to ignition during flame zone propagation through wildland vegetation fuel beds. I review fire spread models currently used for fire management and research and find that the assumptions of radiant heating for ignition are physically inconsistent with measured particle heating response.

1.2 Chapter 3 – A Physical Basis for Size Affecting Fuel Particle Heat Exchange

In this chapter I examine physical mechanisms for fuel particle heating that are addressed through experiments and modeling in later chapters. I demonstrate ignition behavior of fine and coarse particles to thermal radiation that qualitatively suggests the organization of physical processes involved in ignition. Based on these exploratory experiments I present the physical justification for investigating specific research questions in Chapters 4 and 5.

1.3 Chapter 4 – Convective Cooling of Irradiated Fuel Particles

Here I present the design and results of experiments that determine fuel particle temperature changes during exposure to thermal radiation. I develop a model of fuel particle heat exchange and compare it to experimental measurements. Through experiments and modeling I addressed research questions (1, 2 and 3) developed in Chapter 3 and found that 1) radiation heating was insufficient to significantly pyrolyze the finest fuel particles, 2) convective heat exchange increased for decreased particle size, and 3) surface area-to-volume ratio does not determine heat exchange at the fuel particle surface. Thus, I show that convective cooling can keep fine fuel temperatures below what is necessary for ignition while coarser fuels under similar radiant heating conditions can ignite and this is not determined by fuel particle surface area-to-volume ratio.

1.4 Chapter 5 – Fuel Particle Heating Leading to Ignition in Spreading Laboratory Fires

In this chapter I describe experiments and modeling of fuel particle response to the changing thermal environment experienced during the approach of a spreading fire in a wind tunnel. These experiments subject fuel particles to radiation from the flame front as well as convective cooling and heating from the ambient air flow and the flame zone. Irradiances and air temperatures are measured as well as fuel particle surface temperatures. I exercise the numerical model from Chapter 4 to understand how fine fuel particles exchange heat leading to ignition during fire spread. Using experiments and modeling I addressed research questions (4, 5 and 6) developed in Chapter 3 and found that 4) none of experimental fires had measured radiation sufficient to heat fuel particles to ignition, 5) convection was the dominant heat transfer mechanism responsible for fine fuel particle heat exchange just before ignition, and 6) convective heating was the principal mechanism for fine particle ignition. Thus, I reveal that radiation was not the primary mechanism for any of the fire spread experiments and fine fuel particles convectively heated to ignition primarily from the intermittent pulses of hot gases generated by the spreading fire.

1.5 Chapter 6 – The Research: Significance, Limitations and Further Considerations

In this chapter I summarize my research approach and describe my findings. I put the research findings in context by discussing its limitations and the need for further research to provide a more comprehensive description of fuel particle heating during wildland fire spread. From my research findings I discuss the significance to and implications for physically modeling flame zone spread in porous fuel beds.

1.6 References

Fons WL (1946) Analysis of fire spread in forest fuels. *Journal of Agricultural Research* **72**: 93-121.

Finney MA, Cohen JD, McAllister SS, Jolly WM (2013) On the need for a theory of wildland fire spread. *International Journal of Wildland Fire* **22**(1): 25-36.

Williams FA (1982) Urban and wildland fire phenomenology. *Progress Energy Combustion Science* **8**: 317-354.

Chapter Two

Fuel Particle Heat Exchange and Wildland Fire Spread

2.1 Introduction

Wildland fire spread is known to be the result of continued ignition of fuels adjacent to the flame front (Fons 1946). Yet, the physical processes of fuel particle heat exchange leading to ignition are poorly understood (Finney et al. 2013), and this means that current wildland fire spread models either do not explicitly represent physical processes or instead rely on assumptions of heat transfer and ignition mechanisms. After reviewing 19 physical or quasi-physical fire spread models, Sullivan (2009a) found that the models were predicated on differing assumptions of physical processes responsible for wildland fire spread. Many of these assumptions are not consistent with experimental evidence, particularly pertaining to ignition which is not explicitly known at fuel particle scales. For example, the common assumption that thermal radiation is the primary mechanism governing fire spread (Finney et al. 2013) is inconsistent with previous experimental results (Fang and Steward 1969; Anderson 1969; Baines 1990).

Attempts to produce physical fire spread models have not been founded on a basic physical understanding of ignition processes because fundamental experimentation has been insufficient to understand how wildland fires spread (Baines 1990; Sullivan 2009a; Finney et al. 2013). Grishin (1997, p. 81) identifies five phases of developing a physical fire spread model: 1) analyze the phenomenon and identify the physical processes, 2) represent the physical processes in a mathematical model, 3) determine a solution method for the equation set, 4) verify the solution of the equation set, and 5) validate that the solution satisfies the application for real conditions. Both Phase 1 and Phase 2 involve experimentation to explicitly identify and represent fire spread processes.

It is from the first two phases that a phenomenological theory can be established (Finney et al. 2013). Prior investigations by Baines (1990), Weber (1991), and Sullivan

(2009a), however, reveal that Phase 1 has not adequately occurred. Phase 2 has therefore, been based on assumptions rather than experimentally confirmed descriptions of physical processes. Nevertheless, considerable effort has been put into Phase 3 and Phase 4 (Sullivan 2009a) because of the complexity of numerical methods required for solving the governing equations of the numerical models. Phase 5 requires experiments similar to Phases 1 and 2 and has occurred only sporadically for the physical models (Sullivan 2009a). Validation attempts (for example, by Linn et al. 2005; Mell et al. 2007) based on *a posteriori* observational data establish the degree of agreement for models but not model accuracy (Oreskes et al. 1997; Sullivan 2009a; Finney et al. 2013). Based on Sullivan (2009a) and Finney et al. (2013), it appears that current physical fire spread models primarily result from modeling efforts (Phases 3 and 4) without the prerequisite experimental research of Phases 1 and 2.

The long-term value of research into the physics of fire spread is the potential for improving the reliability of modeling for fire management. Operational predictions by models are of use on active fires and for pro-active fuel reduction activities. In the western U.S. fuel treatment has been demonstrated to be effective at mitigating undesirable wildfire behavior (Graham et al. 2004; Noss et al. 2006; Joint Fire Sciences Program 2007; Reinhardt et al. 2008; Keeley et al. 2009). The need to evaluate fuel treatment efficacy has been recognized and post-fire studies indicate treatments can offer sufficient reductions in fire behavior under wildfire conditions; however, the ability to *a priori* design effective fuel treatments is highly uncertain (Graham et al. 2004; Joint Fire Sciences Program 2007; Stephens et al. 2009; Cochrane et al. 2012). In the U.S., the Rothermel (1972) fire spread model is the method for evaluating potential fire behavior changes due to fuel treatment (Graham et al. 2004; Stephens et al. 2009; Cochrane et al. 2012), but its reliability is restricted to the conditions used for development (Graham et al. 2004; Stephens et al. 2009; Sullivan 2009b) and its empirical formulation offers no physical rationale for connecting fuel structure to fire behavior. This is problematic because the fuel treatment conditions needing evaluation (for example, horizontally and vertically discontinuous fuels, live tree foliage fuels and extreme weather conditions, Graham et al. 2004) are significantly outside the range of experimental conditions used to develop the Rothermel (1972) fire spread rate model. Thus, increasing the reliability and range of conditions beyond current empirical and physically-

based wildland fire spread models cannot occur without a fundamental understanding based on experimental evidence.

Since ignition is the foundation of wildfire spread (Fons 1946), then understanding fuel particle heat exchange, ignition processes, and the conditions for sustained ignition is the required basis for predicting fire spread and spread rate. In this chapter I provide background on the spread of flaming combustion in wildland fuel beds, review how current models address fuel particle heating during wildland fire spread, and report experimental observations of fuel particle heating that are inconsistent with physical processes currently assumed for modeling. From this exposition, I outline critical experimental research that is needed to provide a physical basis for fuel particle heat exchange and thereby identify the research addressed in Chapters 4 and 5.

2.2 Wildland Flame Spread

Dead and live vegetation comprise the fuel for wildland fires burning in ground, surface and canopy strata. Fires burning in these fuel strata have been correspondingly described as ground fires, surface fires and crown (canopy) fires (Graham et al. 2004; NWCG 2014). Depending on the fuel, weather and topographic conditions, wildland fires can spread through these strata independently or in association. Ground fires burn and spread through compact dead vegetation in various stages of decay just above and within the soil such as duff, roots and organic soils. Ground fires primarily burn with smoldering combustion (surface oxidation of carbonaceous char with associated pyrolysis [Drysdale 1998]). Because smoldering combustion is not significant for flame front propagation, these fires are not considered in this discussion. Surface and crown fires spread with flaming combustion (oxidation of pyrolysates – the vaporous thermal decomposition products of dead and live vegetation [Drysdale 1998]). Surface fires typically spread through dead and live vegetation at and just above ground level and crown fires primarily spread through the foliage and twigs of shrub and tree canopies (Graham et al. 2004; NWCG 2014). Although some shrub types can have significant persistent dead fine fuels, canopy fuels are typically living vegetation (Montygierd-Loyba and Keeley 1987; Riggan et al. 1988; Paysen and Cohen 1990). Surface

and crown fire propagation occurs by the flaming front directly heating adjacent fuels to ignition (although firebrand/ember spot ignitions can be significant in overall fire growth).

Van Wagner (1977) described crown fires as passively and actively spreading. By his definitions, passive crown fires burn in a series of canopy ignitions initiated by sufficiently intense surface fire spreading beneath a shrub or tree canopy. Commonly, ignitions start on the main stem and foliage at the crown base and spread upward (torching) after the surface fire has spread under the canopy fuels. Horizontal fire spread with the occurrence of passive crown fire is primarily determined by the surface fire (NWCG 2014). Van Wagner (1977) defined active crown fires as spreading by horizontal propagation through shrub and tree canopies. Although the flame fronts of active crown fires typically include fuels from the canopy to the surface (NWCG 2014), the horizontal fire spread is primarily determined by the canopy propagation.

2.2.1 Structure of Wildland Fuel Beds

Surface and canopy fuels are heterogeneous at all spatial scales. They include a range of sizes of both fuel particles and spaces between fuel particles. Surface and canopy fuels commonly include a mixture of dead and live fuels ranging in fuel particle cross-section of less than one millimeter for conifer needles, some shrub foliage and grasses (Rothermel and Anderson 1966; Rothermel and Philpot 1973) to hundreds of millimeters (e.g. dead branches and tree stems). The size distribution by mass of dead and live fuels depends on the vegetation type (e.g. grass, shrub, and tree). Based on current fuel models used for fire spread modeling (Anderson 1982; Scott and Burgan 2005), surface fuels are largely composed of deposited dead shrub and tree debris (e.g. needles, leaves, twigs and branches) and cured herbaceous vegetation (e.g. dead grasses and forbs). Shrub and tree canopy fuels are primarily foliage and typically living (Montygierd-Loyba and Keeley 1987; Riggan et al. 1988; Paysen and Cohen 1990; Scott and Reinhardt 2005). Although I did not find published space distances between fuel particles, observations of various fuel types readily reveal that fuel gaps can range in scale over three orders of magnitude from millimeters between fuel particles in surface litter to meters within and between forest tree canopies.

2.2.2 Fuel Particle Sizes and Flame Spread

Understanding how fires spread in heterogeneous fuels requires an understanding of how size influences fuel particle ignition and fuel burning rates. Rothermel (1972) found larger fuels (greater than 12 mm in diameter) made negligible contributions to fire spread in the presence of finer fuels. Rothermel (1972) stated that:

> "*The fuels having the highest surface-area-to-volume ratio (fine fuels) will respond the fastest; therefore, these will be involved in the leading portions of a fire.*"

Consequently, the maximum sized particle Rothermel (1972) used for laboratory experiments that generated his fire spread model was 12.7 mm (0.5 inch). This is important because Rothermel's (1972) fire spread model has become the basis for the primary operational fire behavior models used by U.S. fire managers (for example, the National Fire Danger Rating System, Deeming et al. 1978; BEHAVE, Andrews et al. 2005; FARSITE, Finney 1998).

The dominant influence of fine fuels on fire spread appears to be consistently observed in fires spreading through fuel beds of multiple particle sizes and is the consensus assumption of wildland fire scientists. The Rothermel (1972) fire spread model, originally developed using fuel beds of single-sized particles, has been applied to actual fuel beds of multiple fuel sizes by using surface area-weighted-mass averaging to emphasize the fine fuel influence (Rothermel 1972; Albini 1976). For management applications, fire model fuel inputs have been organized into sets of fuel bed characteristics called 'fuel models' (Rothermel 1972; Albini 1976; Cohen and Deeming 1985; Scott and Burgan 2005). Scott and Burgan (2005) provide a brief description of expected surface fire behavior at the propagating flame front primarily related to the fine fuel surface area-to-volume ratio and mass load for each of their fuel models. Scott and Reinhardt (2005) describe available conifer canopy fuel as live and dead foliage, 0 to 3 mm living branch wood, and 0 to 6 mm dead branch wood because larger sized dead and live canopy fuels "do not burn in the short period of time of flaming during a crown fire (less than one minute)." In several decades of observations and experiments (e.g. Fons 1946; Rothermel 1972; Pagni and Peterson 1973; Call and Albini 1997; Morvan and

Dupuy 2004; Stocks et al. 2004b) fine live and dead vegetation have been identified as the primary fuels involved in flame front propagation. To help understand these findings and observations I use physical logic to examine how fine fuels primarily govern the propagating flame front.

The fine fuels primarily involved in fire spread typically have higher surface area per unit volume (SA/V) than less involved fuels. For constant fuel material and conditions, the unit volume can be considered the unit mass. Heating the fuel mass occurs through the surface according to the temperature difference between the fuel particle surface (hotter) and its interior mass (cooler). For a given fuel surface temperature, the greater the SA/V, the greater the fuel heating per unit mass.

The following example illustrates how this occurs by comparing the potential heating of coarse and fine particles. The coarse particle is a wood stick with a 12 mm square cross-section and 120 mm long (this is sufficiently long to neglect the end area). The coarse particle will heat through a surface area of 5760 mm^2. If the coarse particle is separated into identical pieces 1 mm square (at the upper size of fine fuels) and these particles all have the same surface temperature as before, the same mass is heated through 12 times the surface area or 69,120 mm^2. The higher SA/V of the 1-mm sticks results in greater per unit mass heating for the same heat exposure. In general, any energy and mass exchange of a fuel particle occurs through its surface. So for given surface conditions, increasing surface area per unit mass will increase the energy and mass exchange rates per unit mass. Thus for given surface conditions, higher SA/V fuels have higher thermal response rates, reduced times to ignition, and thereby higher rates of spread.

The fuel burning rate per unit mass also increases with increased SA/V. Assume the fuel particle spacing in the fuel bed allows sufficient air flow for combustion and all fuel particle surface temperatures are the same and sufficient for combustion. These conditions produce the same initial lineal burning rates for the 12 mm and 1 mm fuel particles (Drysdale 1998) but result in different mass consumption rates and thus heat release rates. For example, a 12-mm fuel particle that burns 0.5 mm of the wood on all sides consumes about 16 percent of its mass. If the 12-mm particle is divided into 144 1-mm particles burning at the same lineal rate on all sides, the entire fuel mass equivalent to the 12-mm particle consumes

within the same time period. Given the same heat release per unit mass burned, the 1-mm heat release rate is more than 6 times greater. In general, the smaller the fuel particle size the shorter the burning consumption time and the larger the per unit mass energy release rate. Thus, the fine fuels govern both the heat release rate and the burning duration of the propagating flame front. Importantly, the flame front is the heat source for igniting adjacent fuels to sustain fire spread.

Sustained fire spread depends on the rate of fuel mass ignited to equal or exceed the rate of fuel mass consumed. The spread threshold occurs at the minimum fuel mass ignition rate capable of maintaining the flame front as a sufficient heat source for sustained fire spread (Finney et al. 2013). For example, on a per unit mass basis, if the time to ignition exceeds the fuel consumption time then the flame zone depth decreases resulting in reduced heat transfer from the flame front. Reduced fuel heating results in longer times to ignition until ignition does not occur and fire spread ceases (Finney et al. 2013). The relation between the flame front and fire spread is dynamically non-linear and particularly important near spread-no-spread threshold conditions (Finney et al. 2013).

In the previous example, the fuel particles are assumed to burn without significantly reduced air flow within the fuel bed; however, densely arranged fuel beds can influence fuel particle burning characteristics. Thus, the effect of fuel bed packing density on particle burning must be determined.

2.2.3 Fuel Bed Density and Fine Fuel Burning

The concept that fuel bed density influences fuel particle heat transfer and burning rates is clearly demonstrated by packing 144 1-mm particles into the size of a 12-mm particle, which would heat and burn like a 12-mm particle. Closer packing of fine fuels reduces radiation and convection heat exchange to inner particles and pyrolysate-air mixing is restricted during burning. Rothermel (1972) experimentally determined influences of fuel bed density (packing ratio) on heat release rates for given sized fuel particles. Block (1971) found that fuel particle burning times in experimental wood crib fires depended on fuel crib density (porosity). For a given fuel particle size, fuel bed geometry influenced particle burning times for densely

packed fuels; whereas, for loosely packed fuels, particle thickness primarily influenced burning time. Block's (1971) results qualitatively agree with Rothermel's (1972) findings but are not reliable for quantitatively determining fuel bed arrangement influences on burning wildland fuel beds (McAllister, personal communication).

Laboratory and field burning experiments along with fuel bed data indicate shrub and tree canopy fuel beds are loosely packed and thus, fuel particle burning rates are primarily determined by SA/V. Anderson (1969) examined fuel burning residence times of laboratory test fires in loosely packed (low bulk density), shallow depth fuel beds. He qualitatively described these fuel beds as having particle spacing distant enough such that burning was primarily controlled by fuel particle thermal properties but close enough to remain in the flame convection of surrounding particles. His highest fuel bed porosity was 1.84×10^{-2} m^3/m^2 (Anderson 1969, p.16). Using laboratory test fires, Anderson (1969) and Burrows (2001) found that fuel particle burning residence times in fuel beds with this porosity were largely a function of particle thickness. Using Anderson's (1969) definition of porosity (the same as Fons 1946) and canopy fuel data, I calculated the canopy fuel porosity for conifers in eastern Canada and the western United States (Van Wagner 1977; Scott and Reinhardt 2005; Brown 1970). From these sample data I specifically chose canopy fuels that produced the lowest canopy porosity (highest packing density) and found the porosity to be 2.96×10^{-1} m^3/m^2, more than an order of magnitude greater than Anderson's (1969) most porous experimental fuel beds. Because the canopy fuels have higher porosities than surface fuel beds with burning rates primarily determined by fuel particle SA/V (Anderson 1969), I assume canopy fuel particle burning rates are not influenced by fuel bed packing density at the propagating flame front. To confirm this assumption I further examine the propagating flame zone canopy fuel consumption and burning residence time data from experimental crown fires.

The propagating crown fire flame front primarily burns the fine fuels that include foliage and fine stems. During the International Crown Fire Modeling Experiment (ICFME, Stocks et al. 2004a), all needle foliage and 86 percent of 0–5 mm size class fuels (cylindrical shape assumed) were consumed during crowning (Stocks et al. 2004b), consistent with the findings of Morvan and Dupuy (2004). Canopy fuels >30 mm in diameter had negligible

consumption and of the total canopy fuel mass consumed (<30 mm in diameter), 43 percent was needle foliage and 79 percent was canopy fuel that included needles and stems <5 mm in diameter (Stocks et al. 2004b). The ICFME results were also consistent with a prior analysis of crown fire fuel consumption done by Call and Albini (1997). Fine fuel consumption primarily occurred during the burning residence time of the crown fire's propagating flame front. Given that crown fire flame fronts primarily burn fine fuels, observed flame front burning residence times can be compared to calculated canopy fine fuel particle burning residence times to evaluate whether or not canopy fine fuels burn without significant influences of fuel bed packing arrangement.

Propagating crown fire flame front residence times determined by Taylor et al. (2004) and Cohen (2004) are close but over-estimate calculated burning residence times not influenced by fuel bed arrangement (Anderson 1969). Using canopy level temperature measurements (durations > 300 C) and video, Taylor et al. (2004) measured an average crown fire residence time to be 31 seconds with a range from 19 – 45 seconds for all experimental crown fires in jack pine (*Pinus banksiana*). Cohen (2004) analyzed different video records for the same fires and found an average crown fire residence time of 34 seconds with a range of 26 – 41 seconds. During the 1988 Yellowstone Fires, Despain et al. (1996) used video to estimate burning durations of lodgepole pine (*Pinus contorta*) canopies averaging 15 – 20 seconds. Based on Anderson's (1969, p. 15) burning particle residence time and an estimated jack pine needle SA/V equal to 5250 m^{-1} (Harlow and Harrar 1969, description p. 76), an individual needle consumes in 14 seconds and a lodgepole pine needle consumes in 12 seconds (estimated SA/V = 6470 m^{-1}; Brown, 1970). For the 5 mm diameter size limit of fine fuels, a fuel particle (SA/V = 800 m^{-1}) consumes in 94 seconds.

Measured crown fire residence times longer than that of individual needles, should be expected. The measurement resolution of crown fire residence times using temperature measurements and video observation (Taylor et al. 2004; Cohen 2004) incorporates a volume of flame front orders of magnitude greater than that of a conifer needle. From video records (Cohen 2004), I observed that all the fine fuels of an entire tree canopy did not ignite and burn simultaneously; ignition progressed through canopies commonly in a non-steady, multi-directional manner. This would contribute uncertainty and lengthen measured residence times

due to flames passing through locations already burned. Nevertheless, the fuel consumption data and canopy flame front residence time analysis are consistent with crown fires primarily burning as a loosely packed canopy fine fuel bed.

In conclusion, flame fronts spread through wildland fuel beds composed of different sized fuel particles separated by air spaces. The heat source for spread is the propagating flame front and the fine fuel component of wildland fuel beds primarily governs propagating flame front spread and heat release rates. The finer the fuels, the greater are the flame front heat release rates. However, the finer the fuels, the shorter are the durations of burning and thus the shorter are the durations of the heat source for heating fuels to ignition. Anderson (1969) found burning residence time independent of fuel bed influences for his most porous surface fuel beds. Because conifer canopy fuels are significantly more porous than Anderson's fuel beds and measured flaming durations are close to expected fuel particle residence times, I conclude that fine fuel particles in porous surface fuel beds and conifer canopies have burning durations independent of fuel bed influences. I further assume that fine fuel heat exchange is primarily determined by fuel particle characteristics for porous fuel beds. Given the principal importance of fine fuels for propagating flame zone heat release rates and spread, understanding fuel particle heat exchange and particularly heat exchange of fine fuels is critical for understanding flame zone spread.

2.3 Current Fire Spread Modeling

In this section I examine the basis of current fire spread modeling with a focus on fuel particle heating leading to ignition. Although there are many aspects of wildland fire that need attention (for example, soil heating, smoldering combustion, tree canopy scorch, large scale fire growth and fire-atmosphere interactions), flame spread conditions are sufficiently different from these other wildland fire aspects to warrant specific attention.

Sullivan (2009a, b) has categorized fire spread models into two general types: "empirical and quasi-empirical" models and "physical and quasi-physical" models. Empirical and quasi-empirical fire spread models associate measured explanatory variables with measured response variables. The typical response variable is fire spread rate measured over

some time period. Physical and quasi-physical models calculate fire spread rate by using in varying degrees physical descriptions of fire spread processes.

Empirical and quasi-empirical fire spread models have been developed from measured data associations and are not intended to describe specific physical mechanisms of fuel particle heat exchange and ignition. Using laboratory and field experiments and wildfires, researchers have associated measured fire behavior (principally spread rate and flame length) and post-fire measured fuel consumption with measured characteristics of the fuel, weather and topography. The researchers derive mathematical models associating the characteristics of spreading fires to the initial conditions using curve fitting techniques without describing fundamental physical processes that can be generalized beyond the data conditions (Weber 1991; Sullivan 2009a, b). Current operational fire models used for fire management purposes in the U.S., Canada, Australia and elsewhere are empirical and quasi-empirical.

Empirical models are not developed from physical principles. For example, wildfire characteristics are predicted using the Canadian Fire Behavior Prediction Model based on associations of field measurements of environmental conditions and fuel types specific to measured fire behavior characteristics of selected wildfires and experimental burns (Hirsch 1996). Similarly, Australia and others use the empirically based McArthur grassland and forest fire meters (Noble et al. 1980). More recently the existing empirical associations of the Australian wildland fire meters have been refined using measurements of experimental field burns (Gould et al. 2007; Project Vesta, http://www.csiro.au/Outcomes/Safeguarding-Australia/VestaTechReport.aspx).

Quasi-empirical models are developed using general theoretical principles (for example, conservation of energy) to determine and mathematically connect the experimentally determined empirical associations (Sullivan 2009b). The Rothermel fire spread model is quasi-empirical and uses conservation of energy as the governing principle for the rate of spread equation (Rothermel 1972). The terms of Rothermel's spread rate equation (for example, optimum reaction velocity, moisture damping coefficient, propagating flux ratio and wind and slope factors) were determined using curve fitting of experimental data. These empirical associations implicitly account for the physical mechanisms specific to the experimental conditions but do not describe the physical processes in generalized

theoretical terms. Although the Rothermel (1972) fire spread model has been the basis for established, widely used fire management decision models such as the U.S. National Fire Danger Rating System (Deeming et al. 1977; Cohen and Deeming 1985), FIRECAST (Cohen 1986), BehavePlus (Andrews et al. 2005), FARSITE (Finney 1998) and FlamMap (Finney et al. 2006), the Rothermel (1972) model is not based on a fundamental understanding of fire spread processes.

The reliability of empirical and quasi-empirical fire spread models is limited to the range of conditions used in generating the model associations. Sullivan (2009b) notes the difficulty of developing scaling rules for variable associations from experimental burns to fire spread conditions outside the range of experimental conditions. The empirical and quasi-empirical model associations do not necessarily remain constant and thus, cannot be generalized. Reliability problems can arise when the empirical and quasi-empirical models are applied to conditions outside their experimental range. The model error cannot be quantified and corrected without doing experiments at the expanded range of conditions. Additionally, empirical and quasi-empirical fire spread models have reliability problems near behavior thresholds because wildland fire spread is a dynamically non-linear process (Finney et al. 2013). Fuel ignition adjacent to the flaming front resulting in fire spread depends on the flaming front conditions, and those conditions depend on how the previous fuel ignited and burns. At fire spread thresholds, non-linear behaviors alter response characteristics to explanatory variables. The fire spread response becomes highly sensitive to conditions making the required measurement resolutions and reproducibility of experiments unworkable and thus unattainable (Finney et al. 2013; Schneider and Griffies 1999). For example, crown fire spread is outside the range of conditions that generated the Rothermel spread model and using a similar approach for modeling crown fire spread thresholds is impractical. Alternatively, fire spread conditions outside a range of experimental capability might be predicted to some known degree using a theoretical approach that describes fire spread in terms of the governing physical processes – a physical model (Finney et al. 2013).

Physically-based models of fire spread currently exist that use representations of physical processes such as radiation and convection heat transfer and chemical kinetics (Weber 1991; Sullivan 2009a; Sullivan 2009b). These models are largely experimental and

not used for management applications due to the required computation time limiting the spatial extent addressed. However, they are being used by researchers for management-related issues. As with any computational model, assumptions are paramount. Finney et al. (2013) examined physically-based fire spread models (for example, those described by Porterie et al. 2000; Porterie et al. 2003; Morandini et. al. 2002; Morvan and Dupuy 2004; Morandini et al. 2005; Zhou et. al. 2005; Mell et. al. 2006, 2007a, b; and Simeoni et al. 2011) and concluded that the fundamental processes of fuel particle ignition and thus fire spread were largely assumed without an experimental basis. The governing equations for heat and mass transfer and chemical kinetics are well established, but they represent different physical processes which do not have equal influence on outcomes. Typically, the importance of a process depends on the phenomenon and its context, but without an experimental basis it cannot be explicitly known what processes occur and how they occur at fuel particle scales (Finney et al. 2013). Numerical methods compound the challenge of making appropriate assumptions. Physically-based fire spread model grid lengths (e.g. Morvan and Dupuy 2004; Mell et al. 2007a, b) are influenced by numerical methods and computational demands resulting in modeled scales greater than fuel particle scales. Baines (1990) observed that modelers "have (for the most part) used their own judgment as to what is important" when numerically describing fire spread. Baines (1990) stated:

> "*Models for fire propagation have then been constructed based on heuristic arguments with little reference to experimental data. Where some experiments have been described, the measurements are only partially complete, and the data has* (sic) *been employed to estimate parameter values rather than to test the model or the mechanisms involved.*"

In particular, radiation has been assumed to be the principal heating mechanism responsible for wildland fire spread by many modelers (Sacadura 2005). Sen and Puri (2008) in their survey of radiation in wildland fire modeling state that:

> "*Radiation has been unsurprisingly identified as the controlling heat transfer mechanism that fixes the rate of spread of wildland fires.*"

Although radiation is the most commonly invoked mechanism for heating during fire spread, analysis of other factors such as convection have been lacking (Baines 1990). I know of no research literature that provides definitive experimental evidence of heat transfer processes in general and none to support radiation as the primary heat transfer mechanism governing fire spread in wildland surface and canopy fuel beds.

Modeling by Frank Albini played an important role in establishing radiation as the governing mechanism of wildland fire spread. But he (Albini 1980, 1985, 1986, 1996) assumed radiation heating governed fire spread without an experimental basis. Albini's contributions have been considered central (Sacadura 2005) and his assumption of radiation as the dominant heat transfer mechanism in fires has been a standard premise for others (Morvan and Dupuy 2004; Mell et al. 2006, 2007a , b). Albini (1985) reasoned that under most cases, a developed flame zone blocks the ambient wind and therefore flame does not extend into adjacent fuel. Without supporting experiments, he then assumed the flame front to be a steady radiating planar surface with radiation heat transfer the mechanism governing fire spread. Albini also assumed radiation was the principal mechanism for fire spread in his crown fire spread model (Butler et al. 2004). Although Albini (1986) recognized convective cooling of preheated fuels from fire-induced inflow, he never questioned the sufficiency of radiation for ignition and thus fire spread. Model parameters were adjusted to calibrate model spread rates to actual spread rates (Butler et al. 2004) without examining and understanding fuel particle heat exchange processes.

The radiation assumption has not been accepted without scrutiny. Baines (1990) and Weber (1991) questioned radiation as the dominant mechanism responsible for fire spread and both examined the surface fire data from the laboratory experiments of de Mestre et al. (1989). Baines (1990) and Weber (1991) found that radiation models could not account for how fuel particles preheated ahead of a flame zone. They both determined that radiation calculations could be adjusted to meet fuel temperature ignition criteria and thus make spread rates match actual fires; however, the increased magnitude of radiation heating necessary for the actual spread rate resulted in modeled fuel temperatures significantly greater than observed temperatures (Fig. 2.1). The measured fuel temperatures during preheating (de Mestre et al. 1989) had a significantly different profile than those predicted by the radiation-

based models (Figure 1). Thus, calibrating the model to the spread rate misrepresented the heat transfer processes. Baines (1990) hypothesized that convective cooling might influence fuel temperatures and added a simple Newtonian convection cooling term with a constant convection coefficient to the radiation model of de Mestre et al. (1989; model 2 in Fig. 2.1). The addition of convective cooling resulted in modeled fuel temperatures closely approximating the experimental measurements (thin solid line in Fig. 2.1; Baines 1990) until flame front-fuel distances were within a few centimeters. I suggest this indicates that: 1) convective cooling from ambient air significantly cools irradiated fuel particles, and 2) the increase in fuel particle irradiance in the last few centimeters cannot account for the rapid fuel particle heating to significant pyrolysis temperatures.

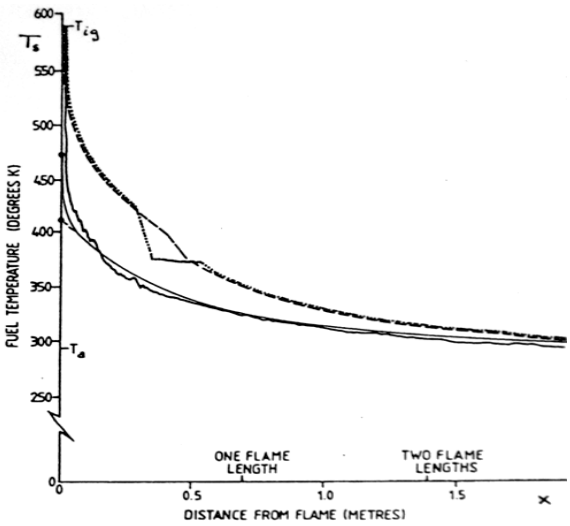

Fig. 2.1 Fuel particle temperature: actual and modeled. The fine dashed line (model 1) has moisture evaporated at 373 K and the coarse dashed line (model 2) has continuously evaporated moisture complete at 373 K. but both represent radiation only models. The solid wavy line is the measured fuel temperature and the steady solid line is modeled fuel temperature with radiation and convection. (Graph from Baines 1990)

It is not explicitly known how fuel particles exchange heat to produce the rapid temperature rise leading to ignition. Fuel particle temperatures at which pyrolysis rates are capable of sustaining ignition do not occur at temperatures below 550 K (Fairbridge et al. 1978; Tillman et al. 1981; Simmons 1995; Drysdale 1998). Thus, the uncertainty in flame front position corresponding to measured fuel temperatures in Fig. 2.1 (de Mestre et al. 1989) means that the possibility of convective fuel particle heating from flame contact cannot be discounted. Similarly, Fang and Steward (1969) found that 60 percent of heating to ignition occurred in the last 2.5 cm of fire spread but their experiments could not resolve the mechanisms of heat transfer in this short distance and time. Anderson (1969) found that radiation was insufficient and stated: “Experimental testing of a mathematical model show that radiation heat transfer accounted for no more than 40% of total heat flux required to maintain rate of spread.” How a fuel particle heats to ignition remains unresolved.

Fire spread is the result of ignitions from particle to particle in discontinuous, non-steady advances (Fons 1946); however, fire researchers have largely focused on predicting fire spread rate rather than explicitly determining heat exchange and ignition processes. Although experimental fire spread measurements have been made, explicit fuel particle heating and ignition processes have not been resolved (for example, Silvani et al. 2009, 2012; Liu et al. 2014). As a result, explicit fuel particle heat exchange is largely unknown. In the absence of a fundamental understanding, fire spread modelers, including Linn (1997), Morandini et al. (2002), Morvan and Dupuy (2004), Zhou et al. (2005), Mell et al. (2006, 2007b) have assumed that heat exchange and ignition mechanisms are the same for average fuel bed properties at computational grid scales as they are at fuel particle scales. However, if the heat exchange of individual fuel particles depends on size and is not accounted for in the model bulk fuel averages, then ignition and combustion modeling will be unreliable.

The arguments of Baines (1990) and Weber (1991) suggest that radiation may not alone explain the ignition behavior of fuel particles in spreading fires. If convective heat transfer is critical, then a series of investigations must be undertaken to reveal how convective heating and cooling influence ignition. First, the axiomatic non-steadiness of flames means that temporal and spatial details of flame motion must be understood. Flame or fluid motions carry hot and cold gasses (including air) to contact fuel particles across voids in wildland fuel beds. Heating by flame contact means that the flame front must laterally extend across voids to contact fuels and the frequency and duration of flame contact must heat fuel particles sufficiently for sustained ignition and fire spread. Conversely, fuel particle convective heating exchange thermal response to intermittent flame contact must produce ignition.

In summary, current fire spread models, whether based on empirical associations or attempted physical descriptions of fire spread processes, have not been developed from an explicit understanding of wildland fire spread (Finney et al. 2013). Current operational wildland fire models are based on empirical associations generated from fire experiments. The reliability of the empirical associations is limited to the experimental range of conditions. In the U.S. most operational fire models are based on Rothermel's (1972) empirically-derived fire spread model and thus, model reliability is largely limited to laboratory experiments of

surface fire spread in relatively compact dead fuel beds (Anderson 1969). The fuels burning in crown fires are not compact and shallow. Physically-based fire spread models attempt to describe in varying degrees fundamental fire spread processes. However, current physical models are based on fuel particle heat exchange and ignition assumptions unsupported by experiments. Model developers have largely assumed radiation to be the primary heat transfer mechanism for fuel particle heating leading to ignition despite experimental evidence suggesting an insufficiency of radiation for fire spread. Experiments are needed to resolve the mechanisms of fuel particle heat exchange leading to ignition and fire spread. Fire spread model reliability over a wide range of conditions depends on understanding the fundamental processes and fuel particle heat exchange is a critical component.

2.4 How Do Fuels Heat To Ignition?

During fire spread, only two heat transfer mechanisms exist for heating adjacent fuels to ignition from a flame front: radiation from emitting solids within flames (soot and especially burning fuel particles) and contact from hot flame gases. Rothermel (1972) and Porterie et al. (2000) describe the ignition and fire spread sequence as follows:

1. The flame front heats fine fuels resulting in increased fuel temperature;
2. Temperatures increase sufficiently to produce pyrolysates;
3. Pyrolysate production rates are sufficient to produce a combustible pyrolysate-air mixture; and
4. The combustible mixture is ignited by flames and the flame zone advances to the ignited fuel.

However, this does not tell us whether fuels are heated due to radiation, convection, or a combination of both. Anderson (1969) found from experiments that radiation was not sufficient for fire spread. McCarter and Broido (1965) conducted laboratory burning experiments with small fuel cribs in still air that compared surface fire spread rates with fuels adjacent to the flame front being screened and unscreened from flame radiation above the fuel bed. The resulting fire spread rates were indistinguishable and indicated flame radiation (from above the fuel bed) had negligible effects on particle ignition and spread. de Mestre et al.

(1985) conducted similar experiments with the same results. During deep-fuel laboratory experiments (Finney et al. 2010) significant "smoky" pyrolysate emissions were not observed within the fuel bed. Gaps between fuels appeared clear prior to flame contact and ignition indicating radiation was not sufficient for ignition (Fig. 2.2). Lastly, I observed from video recordings taken inside forest stands during the International Crown Fire Modeling Experiment multiple cases of understory black spruce (*Picea mariana*) canopy foliage neither igniting nor significantly pyrolyzing as the flame front approached even after surrounding densely packed surface litter and large stem fuels pyrolyzed and ignited. Only after flames contacted the black spruce did I observe the canopies ignite and burn.

The apparent lack of significant pyrolysis from fuels adjacent to the flaming region indicates insufficient heating by radiation and thus fuel temperatures too low for significant thermal decomposition. These observations are consistent with Baines' (1990) analysis (Fig. 2.1) of the de Mestre et al. (1989) experiments. Rothermel and Anderson (1966) show experimental results of an instrumented fuel particle having a temperature of about 177 C at flame arrival. This fuel surface temperature is 100 C too low (275 C) to produce flammable pyrolysates and 150 C below typical minimum fuel surface temperatures (325 C) that produce pyrolysis rates sufficient for piloted ignition (Fairbridge et al. 1978; Tillman et al. 1981; Simmons 1995; Drysdale 1998). Similarly, Rothermel (1972) presents three fuel temperature graphs with flame-particle distances corresponding to fire spread with the wind ("heading"), without wind, and into the wind ("backing") (Fig. 2.3). As with the results of Rothermel and Anderson (1966), Fang and Steward (1969) and de Mestre et al. (1989), fuel surface temperatures are significantly below a minimum 325 C required to produce flammable pyrolyzates at rates

Fig. 2.2 This experimental fire is spreading from right to left through a 1.2 m deep (vertical length) fine excelsior fuel bed (shredded *Populus spp*.). Observations revealed the ignition of adjoining fuels without significant pre-ignition pyrolysate emissions (clear gaps) and only after flame contact. (photograph by Jack Cohen, US Forest Service)

capable of sustaining ignition. Fuel particles do not achieve the typical ignition temperature until flame-fuel distances are within 2.5 cm. Within the last 2.5 cm, air temperatures and fuel temperatures increase rapidly and are indistinguishable (Fig. 2.3), suggesting flames are then in contact with fuel particles.

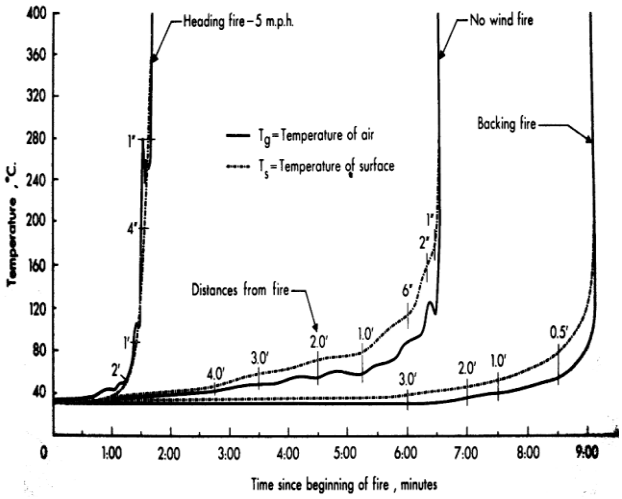

Fig. 2.3 Graph from Rothermel (1972) showing the temperatures of fuel particle surfaces and adjacent air for heading, no wind and backing fire spread. No fuel surface temperature greater than 325 C occurs until fire-fuel distances are less than 2.5 cm (indicated in inches; 2.54 cm/1.0 inch) with air and fuel temperatures indistinguishable.

By reviewing the state of knowledge of wildland fuel composition, particle heating and ignition, fuel bed burning characteristics, and fire modeling assumptions, it is clear that there is no evidence for an explicit physical understanding of the heat exchange processes leading to fuel particle ignition during wildland fire spread. Research required to develop this understanding must begin by addressing the following questions:

- *What heat transfer mechanisms are responsible for the fuel particle temperature profiles provided by Rothermel and Anderson (1966), Rothermel (1972), and de Mestre et al. (1989)?*
- *To what extent is radiation heat transfer responsible for heating fuel particles to ignition during fire spread?*
- *To what extent is convection heat transfer responsible for heating fuel particles in the unresolved heating-to-ignition portion of the fuel particle temperature profiles?*

However, to address these questions I need better physical insight to define specific research questions that effectively examine the knowledge gaps. In Chapter 3 I present exploratory experiments that form the physical basis for defining my research questions addressed in Chapters 4 and 5.

2.5 Conclusion

Wildland fire spread results from the sustained ignition of fuel particles through a fuel bed. For loosely packed surface and canopy fuel beds, burning fine fuels primarily determine fire spread and the propagating flame front intensity. The ignition of fine fuels is principal to how most wildland fires spread and thus, reliably determining how wildland fire spread occurs depends on explicitly understanding fuel particle ignition processes for fine fuels. Although ignition is the basis for fire spread, researchers have largely pursued *rate of spread* questions and not fuel *ignition* questions. As a result, the processes of heat exchange leading to fuel particle ignition remain unresolved and assumed by model developers. Modelers have commonly assumed radiation as the primary heating mechanism governing wildland fire spread and discounted convection heating and cooling as major factors. However, the experimental evidence does not support this assumption. Radiation may not be sufficient for heating fine fuels to ignition and thus for fire spread. Importantly, no experiments have resolved fuel particle heat exchange leading to ignition. Without sufficient understanding of fire spread processes in general and fuel particle heat exchange specifically, we cannot expect to achieve reliable modeling of wildland fire spread.

2.6 References

Albini FA (1976) Estimating wildfire behavior and effects. USDA Forest Service, Intermountain Forest and Range Experiment Station, General Technical Report INT-GTR-30. (Ogden, UT)

Albini FA (1980) Thermochemical properties of flame gases from fine wildland fuels. USDA Forest Service, Intermountain Forest and Range Experiment Station, Research Paper INT-RP-243. (Ogden, UT)

Albini FA (1985) A model for fire spread in wildland fuels by radiation. *Combustion Science and Technology* **42**(5-6), 229-258.

Albini FA (1986) Wildland fire spread by radiation – a model including fuel cooling by natural convection. *Combustion Science and Technology* **45**(1-2), 101-113.

Albini FA (1996) Iterative solution of the radiation transport equations governing spread of fire in wildland fuel. *Combustion, Explosion, and Shock Waves* **32**(5), 534-543.

Anderson HE (1969) Heat transfer and fire spread. USDA Forest Service, Intermountain Forest and Range Experiment Station, Research Paper INT-RP-69. (Ogden, UT)

Anderson HE (1982) Aids to determining fuel models for estimating fire behavior. USDA Forest Service, Intermountain Forest and Range Experiment Station, General Technical Report INT-GTR-122. (Ogden, UT)

Andrews PL, Bevins CD, Seli RC (2005) BehavePlus fire modeling system, version 3: Users guide. USDA Forest Service, Rocky Mountain Research Station, General Technical Report RMRS-GTR-106WWW Revised. (Ft. Collins, CO)

Baines PG (1990) Physical mechanisms for the propagation of surface fires. *Mathematical Computer Modeling* **13**(12), 83-94.

Block JA (1971) A theoretical and experimental study of nonpropagating free-burning fires. In 'Thirteenth Symposium (International) on Combustion' **13**(1), 971-978. (The Combustion Institute: Pittsburgh, PA)

Brown JK (1970) Ratios of surface area to volume for common fine fuels. *Forest Science* **16**, 101-105.

Burrows ND (2001) Flame residence times and rates of weight loss of eucalypt forest fuel particles. *International Journal of Wildland Fire* **10**, 137-143.

Butler BW, Finney MA, Andrews PL, Albini FA (2004) A radiation-driven model for crown fire spread. *Canadian Journal of Forest Research* **34**(8), 1588-1599.

Byram GM (1959) Combustion of forest fuels, Ch.3 'Forest Fire: Control and Use.' (McGraw-Hill: New York)

Calkin DE, Cohen JD, Finney MA, Thompson MP (2014) How risk management can prevent future wildfire disasters in the wildland-urban interface. *Proceedings of the National Academy of Sciences* **111**(2), 746-751.

Call PT, Albini FA (1997) Aerial and surface fuel consumption in crown fires. *International Journal of Wildland Fire* **7**(3), 259-264.

Cochrane MA, Moran CJ, Wimberly MC, Baer AD, Finney MA, Beckendorf KL, Eidenshink J, Zhu Z (2012) Estimation of wildfire size and risk changes due to fuel treatments. *International Journal of Wildland Fire* **21**, 357-367.

Cohen JD (1986) FIRECAST: user's manual. USDA Forest Service, Pacific Southwest Forest and Range Experiment Station, General Technical Report PSW-GTR-90. (Berkeley, CA)

Cohen JD (2004) Relating flame radiation to home ignition using modeling and experimental crown fires. *Canadian Journal of Forest Research* **34**(8), 1616-1626.

Cohen JD, Deeming JE (1985) The national fire danger rating system: basic equations. USDA Forest Service, Pacific Southwest Forest and Range Experiment Station, General Technical Report PSW-GTR-82. (Berkeley, CA)

Countryman CM, Philpot CW (1970) Physical characteristics of chamise as a fuel. USDA Forest Service, Pacific Southwest Forest and Range Experiment Station, Research Paper PSW-GTR-66. (Berkeley, CA)

de Mestre N, Rothermel RC, Wilson R, Albini F (1985) Radiation screened fire propagation. University of New South Wales, Faculty of Military Studies, Department of Mathematics Report. Unpublished Report on file at the USDA Forest Service Fire Sciences Laboratory, Missoula, Montana.

de Mestre NJ, Catchpole EA, Anderson DH, Rothermel RC (1989) Uniform propagation of a planar fire front without wind. *Combustion Science and Technology* **65**, 231-244.

Deeming JE, Burgan RE, Cohen JD (1977) The national fire danger rating system—1978. USDA Forest Service, Intermountain Forest and Range Experiment Station, General Technical Report INT-GTR-39. (Ogden, UT)

Despain DG, Clark DL, Reardon JJ (1996) Simulation of crown fire effects on canopy seed bank in lodgepole pine. *International Journal of Wildland Fire* **6**, 45-49.

Drysdale D (1998) ‘An Introduction to Fire Dynamics.’ (Wiley: New York)

Fang JB, Steward FR (1969) Flame spread through randomly packed fuel particles. *Combustion and Flame* **13**, 392-398.

Fairbridge C, Ross RA, Sood SP (1978) A kinetic and surface study of the thermal decomposition of cellulose powder in inert and oxidizing atmospheres. *Journal of Applied Polymer Science* **22**, 497-510.

Finney MA (1998) FARSITE: Fire Area Simulator—model development and evaluation. USDA Forest Service, Rocky Mountain Forest and Range Experiment Station, Research Paper RMRS-RP-4. (Ft. Collins, CO)

Finney MA, Britain S, Seli RC (2006) FlamMap ver. 3.0 (beta). Online at ***www.firelab.org***

Finney MA, Cohen JD, Yedinak KM, Grenfell IC (2010) An examination of fire spread thresholds in discontinuous fuelbeds. *International Journal of Wildland Fire* **19**, 163-170.

Finney MA, Cohen JD, McAllister SS, Jolly WM (2013) On the need for a theory of wildland fire spread. *International Journal of Wildland Fire* **22**(1), 25-36.

Fons WL (1946) Analysis of fire spread in forest fuels. *Journal of Agricultural Research* **72**, 93-121.

Gould JS, McCaw WL, Cheney NP, Ellis PF, Knight IK, Sullivan AL (2007) Project Vesta – Fire in dry eucalypt forest: fuel structure, fuel dynamics and fire behavior. Ensis-CSIRO. Canberra, AU.

Graham RT, McCaffrey S, Jain TB (2004) Science basis for changing forest structure to modify wildfire behavior and severity. USDA Forest Service, Rocky Mountain Research Station, General Technical Report RMRS-GTR-120. (Ft. Collins, CO)

Grishin AM (1997) ‘Mathematical Modeling of Forest Fires and New Methods of Fighting Them. English Translation Edition. (Ed. F Albini) (Publishing House of Tomsk State

University: Tomsk, Russia) [Translated from Russian by M Czuma, L Chikina, L Smokotina]

Harlow WM, Harrar ES (1969) 'Textbook of Dendrology.' (McGraw-Hill: New York)

Hirsch KG (1996) Canadian forest fire behavior prediction (FBP) system: user's guide. Canadian Forest Service, Northern Forestry Centre. Special Report 7. (Edmonton, AB)

Joint Fire Sciences Program (2007) Tested by fire: what happens when wildfires meet fuel treatments? Fire Science Brief (1). www.firescience.gov

Keeley JE, Aplet GH, Christensen NL, Conard SG, Johnson EA, Omi PN, Peterson DL, Swetnam TW (2009) Ecological foundations for fire management in north American forest and shrubland ecosystems. USDA Forest Service, Pacific Northwest Experiment Station , General Technical Report PNW-GTR-779. (Portland, OR)

Linn RR (1997) A transport model for prediction of wildfire behavior. Los Alamos National Laboratory, Technical Report LA-13334-T. (Los Alamos, NM)

Linn R, Winterkamp J, Colman J, Edminster C, Bailey JD (2005) Modeling interactions between fire and atmosphere in discrete element fuel beds. *International Journal of Wildland Fire* **14**(1), 37–48. doi:10.1071/WF04043

Lui N, Wu J, Chen H, Zhang L, Deng Z, Satoh K, Viegas DX, Raposos JR (2014) Upslope spread of a linear flame front over a pine needle fuel bed: the role of convection cooling. In press. 'Proceedings of the Combustion Institute.' http://dx.doi.org/10.1016/j.proci.2014.05.100.

McCarter RJ, Broido A (1965) Radiative and convective energy from wood crib fires. *Pyrodynamics* **2**, 65-68.

Mell WE, Manzello SL, Maranghides A (2006) Numerical modeling of fire spread through trees and shrubs. 'Proc. of the 5th International Conference on Forest Fire Research.' November, 2006, Coimbra, Portugal.

Mell, W.E.; Jenkins, M.A.; Gould, J.; Cheney, P. (2007a) A physics-based approach to modeling grassland fires. *International Journal of Wildland Fire* **16**(1), 1-22.

Mell WE, Jenkins MA, Gould J, Cheney P (2007b) A physics-based approach to modeling grassland fires, accessory publication. *International Journal of Wildland Fire* **16**(1), 1-22.

Montygierd-Loyba TM, Keeley JE (1987) Demographic structure of *Ceanothus megacarpus* chaparral in the long absence of fire. *Ecology* **68**, 211-213.

Morandini F, Santoni PA, Balbi JH, Ventura JM, Mendes-Lopes JM (2002) A two-dimensional model of fire spread across a fuel bed including wind combined with slope conditions. *International Journal of Wildland Fire* **11**, 53-64.

Morandini F, Simeoni A, Santoni PA, Balbi JH (2005) A model for the spread of fire across a fuel bed incorporating the effects of wind and slope. *Combustion Science and Technology* **177**, 1381-1418.

Morvan D, Dupuy JL (2004) Modeling the propagation of a wildfire through a Mediterranean shrub using a multiphase formulation. *Combustion and Flame* **138**, 199-210.

National Wildfire Coordinating Group (NWCG) (2014) Glossary of wildland fire terminology. PMS 205, October 2014 update. Online at *www.nwcg.gov/pms/pubs/glossary/PMS205.pdf*

Noss RF, Franklin JF, Baker WL, Schoennagel T, Moyle PB (2006) Managing fire-prone forests in the western United States. *Frontiers in Ecology and the Environment* **4**(9), 481-487.

Pagni PJ, Peterson TG (1973) Fire spread through porous fuels. 'Fourteenth Symposium (International) on Combustion' **14**(1), 1099-1107. (Pittsburgh, PA)

Paysen TE, Cohen JD (1990) Chamise chaparral dead fuel fraction is not reliably predicted by age. *Western Journal of Applied Forestry* **5**(4):127-131.

Porterie B, Morvan D, Loraud JC, Larini M (2000) Firespread through fuel beds: modeling of wind aided fires and induced hydrodynamics. *Physics of Fluids* **12**(7), 1762-1782.

Porterie B, Loraud JC, Bellemare LO, Consalvi JL (2003) A physically based model of the onset of crowning. *Combustion Science and Technology* **175**, 1109-1141.

Reinhardt, E.D.; Keane, R.E.; Calkin, D.E.; Cohen, J.D. (2008) Objectives and considerations for wildland fuel treatment in forested ecosystems of the interior western United States. *Forest Ecology and Management* **256**, 1997-2006.

Riggan PJ, Goode S, Jacks PM, Lockwood RN (1988) Interaction of fire and community development in chaparral of southern California. *Ecological Monographs* **58**, 155-176.

Rothermel RC (1972) A mathematical model for predicting fire spread in wildland fuels. USDA Forest Service, Intermountain Forest and Range Experiment Station, Research Paper INT-RP-115. (Ogden, UT)

Rothermel RC, Philpot CW (1973) Predicting changes in chaparral flammability. *Journal of Forestry* **71**, 164-169.

Rothermel RC, Anderson HE (1966) Fire spread characteristics determined in the laboratory. USDA Forest Service, Intermountain Forest and Range Experiment Station, Research Paper INT-RP-30. (Ogden, UT)

Sacadura JF (2005) Radiative heat transfer in fire safety science. *Journal of Quantitative Spectroscopy and Radiative Transfer* **93**, 5-24.

Sen S, Puri IK (2008) Thermal radiation modeling in flames and fires. Ch. 8 'Transport Phenomena in Fires.' (WIT Press-Cambridge Printing: Southampton, UK)

Scott JH, Burgan RE (2005) Standard fire behavior fuel models: a comprehensive set for use with Rothermel's surface fire spread model. USDA Forest Service, Rocky Mountain Forest and Range Experiment Station, General Technical Report RMRS-GTR-153. (Ft. Collins, CO)

Schneider T, Griffies SM (1999) A conceptual framework for predictability studies. *Journal of Climate* **12**, 3133-3155.

Silvani X, Morandini F, MuzyJ-F (2009) Wildfire spread experiments: fluctuations in thermal measurements. *International Communication in Heat and Mass Transfer* **36**(9), 887-892.

Silvani X, Morandini F, Dupuy JL (2012) Effects of slope on fire spread observed through video images and multi-point thermal measurements. *Experimental Thermal and Fluid Science* **41**, 99-111.

Scott, J.H.; Reinhardt, E.D. (2005) Stereo photo guide for estimating canopy fuel characteristics in conifer stands. USDA Forest Service, Rocky Mountain Forest and Range Experiment Station, General Technical Report RMRS-145.

Simeoni A, Salinesi P, Morandini F (2011) Physical modeling of forest fire spreading through heterogeneous fuel beds. *International Journal of Wildland Fire* **20**(5), 625-632.

Stephens SL, Moghaddas JJ, Edminster C, Fiedler CE, Haase S, Harrington M, Keeley JE, Knapp EE, McIver JD, Metlen K, Skinner CN, Youngblood A (2009) Fire treatment effects on vegetation structure , fuels, and potential fire severity in western U.S. forests. *Ecological Applications* **19**(2), 305-320.

Simmons RF (1995) Fire chemistry, Ch. 7 'Combustion Fundamentals of Fire.' (Academic Press: New York)

Stocks BJ, Alexander ME, Lanoville RA (2004a) Overview of the International Crown Fire Modelling Experiment (ICFME). *Canadian Journal of Forest Research* **34**, 1543-1547.

Stocks BJ, Alexander ME, Wotton BM, Stefner CN, Flannigan MD, Taylor SW, Lavoie N, Mason JA, Hartley GR, Maffey ME, Dalrymple GN, Blake TW, Cruz MG, Lanoville RA (2004b) Crown fire behavior in a northern jack pine-black spruce forest. *Canadian Journal of Forest Research* **34**: 1548-1560.

Sullivan AL (2009a) Wildland surface fire spread modeling, 1990-2007. 1: Physical and quasi-physical models. *International Journal of Wildland Fire* **18**(4), 349-368.

Sullivan AL (2009b) Wildland surface fire spread modeling, 1990-2007. 2: Empirical and quasi-empirical models. *International Journal of Wildland Fire* **18**(4), 369-386.

Taylor SW, Wotton BM, Alexander ME, Dalrymple GN (2004) Variation in wind and crown fire behaviour in a northern jack pine – black spruce forest. *Canadian Journal of Forest Research* **34**, 1561-1576.

Tillman DA, Amadeo JR, Kitto WD (1981) 'Wood Combustion.' (Academic Press: New York)

Van Wagner CE (1977) Conditions for the start and spread of crown fire. *Canadian Journal of Forest Research* **7**, 23-34.

Weber RO (1991) Modelling fire spread through fuel beds. *Progress in Energy Combustion Science* **17**: 67-82.

Zhou X, Mahalingam S, Weise D (2005) Modeling of marginal burning state of fire spread in live chaparral shrub fuel bed. *Combustion and Flame* **143**, 183-198.

Chapter Three

A Physical Basis for Size Affecting Fuel Particle Heat Exchange

3.1 Introduction

The contributions of radiation and convection to wildland fire spread have not been resolved (for example, Rothermel and Anderson 1966; Fang and Steward 1969; Rothermel 1972; de Mestre et al. 1989; Silvani et al. 2009; Silvani et al 2012; Liu et al. 2014). However, these heat transfer mechanisms govern fuel particle heating leading to ignition and fire spread. Thus, understanding the mechanisms of fuel particle heat exchange is required for understanding how fires spread. Understanding how fires spread is the foundation for developing physical fire models. From experiments to better describe radiant heating of fuel particles, Latham (personal communication) found he could not heat fine fuel particles to ignition from radiation. With a simple demonstration experiment I confirmed his results. These findings are inconsistent with the assumption that radiation is the governing mechanism of wildland fire spread but in agreement with Anderson (1969), Baines (1990) and Weber (1991). I conducted an exploratory experiment and physical reasoning to examine the heat transfer mechanisms of fuel particles leading to ignition during wildland fire spread. In this chapter I discuss my experiment and theoretical analysis that lead to specific research questions of fuel particle heat exchange that are addressed in Chapters 4 and 5.

3.1.1 Unexpected Experimental Results of Irradiated Particles

In an experiment to predict the thermal irradiance of fine fuel particles during wildland fire spread, Don Latham a scientist at the Fire Sciences Laboratory could not heat fine fuels to ignition. He used a small gas-fired radiant panel as the thermal radiation source and irradiated fine fuel particles in still air. Much to his surprise he found that the particle temperatures ceased to increase well below the ignition threshold. After learning of his experimental

results, I examined his work (unpublished) and used his measured irradiances to calculate the potential for piloted ignition (Tran et al. 1992; Cohen 2004). My piloted ignition calculation was based on a thermal irradiance-ignition time correlation for thermally thick wood slabs that had been successfully applied to wood walls (Tran et al. 1992; Cohen 2004). According to this calculation Latham's fine fuel particles, irradiated at 30 kW/m^2, should have heated to piloted ignition in 65 seconds. To further pursue this discrepancy, I conducted qualitative exploratory experiments that repeated Latham's experimental findings.

3.1.2 Qualitative Exploratory Experiments

I experimentally repeated Latham's fine fuel results and demonstrated significant heating differences between fine woody fuels and coarse wood blocks. For expediency I used readily available wood materials. I chose aspen excelsior (*Populus tremuloides*) to be the fine fuel and small blocks of Douglas-fir (*Pseudotsuga menziesii*) as the coarse fuel (Fig. 3.1a). At irradiances greater than 20 kW/m^2, these different wood species have a negligible effect on piloted ignition time (Spearpoint and Quintiere 2001). The fuels were not dried and the moisture contents unknown but the wood materials had been in the same indoor environment for weeks before testing, so I assumed each had the same moisture content. The fine and coarse fuel particles were separately positioned at the same location in front of a gas fired radiant panel. The fine and coarse fuels were exposed to measured irradiances of 37 kW/m^2 (± 0.5 kW/m^2), greater than the 30 kW/m^2 of Latham's experiments. Every one of five repetitions resulted in the irradiated wood block pilot-igniting in 35 seconds (± 1 second) (Figs. 1b and 1c), and this time-to-ignition was predicted by a piloted ignition time correlation (Tran et al. 1992; Cohen 2004). However, the same number of repetitions for the fine excelsior fuels resulted in neither ignition nor significant observable pyrolysis after several minutes (Figs. 1d and 1e). These experiments confirmed Latham's observations for fine fuels as did more than a dozen other demonstrations. The fine excelsior fuels did not appear to heat sufficiently for piloted ignition but the wood blocks did.

a) Exposed fuels **b) 20 seconds** **c) 35 seconds**

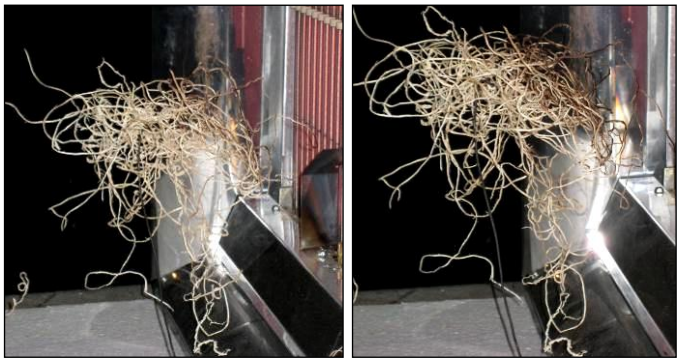

d) 40 seconds **e) 5 minutes**

Fig. 3.1 a) The excelsior (*Populus spp*.) on the left with less than a 1 mm cross-section and the Douglas-fir (*Pseudotsuga menziesii*) wood block with dimensions 25 mm x 38 mm x 13 mm (height, width, depth) were equally irradiated; b) The wood block pyrolyzing after 20 seconds of irradiation; c) Piloted ignition at 35 seconds of irradiation (pilot not shown); d and e) The excelsior neither ignited nor significantly pyrolyzed despite the same irradiance - shown after 40 seconds and 5 minutes of irradiance. (photographs from Jack Cohen, US Forest Service)

These demonstrations raise major questions concerning how fuel particles heat leading to ignition during wildand fire spread. How does size affect fuel particle heat exchange? Given the importance of fine fuels to wildland fire spread, what heat exchange processes account for the different ignition responses of small and large particles? And if, as it appears, radiation is not sufficient for fine fuel ignition how do fine fuel particles ignite during fire spread.

I confirmed that fuel particle size differences resulted in different radiative heating and posited a theoretical basis to physically explain this difference in heat exchange. Based on this exploratory experiment and conceptual model of particle heat exchange I developed detailed questions (end of this chapter) that I addressed with further experimentation (discussed in Chapters 4 and 5).

3.2 Exploratory Fuel Particle Heating Experiment

I conducted an exploratory experiment to confirm heating differences of irradiated fuel particles and then developed a theoretical basis to physically explain the results. The experiments discussed above demonstrated different piloted ignition results but without particle temperature measurements I could not confirm heating differences. I measured temperatures of two different sized irradiated fuel particles to determine whether or not there was a significant heating difference. This exploratory experiment was not sufficient for conclusively describing fuel particle heat exchange; rather, I used this experiment to test my perceptions of fuel particle heat exchange, guide my development of a physical explanation, and provide a basis for defining specific research questions for further experimentation.

3.2.1 Methods

I thermally irradiated two different sized fuel particles. To reduce potential variations in thermal response, the two different sized fuel particles were made from a single piece of yellow poplar (*Liriodendron tulipifera*). The particles were precisely machined to square cross-sections of 1 mm (± 10%) and 12 mm (± 5%) with a 120 mm length (Figure 2a). A 1-mm particle size was chosen to be within the range of fine dead fuels and foliage consumed in the propagating flame fronts of typical surface and canopy fuels (0 – 5 mm, Morvan and Dupuy 2004; Stocks et al. 2004). Similarly, a 12-mm particle was selected to be outside this range but often present in wildland fuel beds (Anderson 1982; Scott and Burgan 2005; Scott and Reinhardt 2005). Both fuel particle sizes were dried to less than one-percent moisture content (dry mass basis), sealed in an air tight bag and allowed to attain ambient temperature.

A gas fired, ceramic element radiant heating panel (0.486 m wide x 0.375 m high) was used as the radiant source (Fig. 3.2b). To check the radiant panel's emissive spectral range, I measured the panel's ceramic surface temperature at the center of each of the 12 rectangular sections (Fig. 3.2b) with a 0.076 mm K-type bare thermocouple. The temperatures ranged from 1230 K to 1260 K and were within the range of wildland flame temperatures at the spreading flame front as measured by Butler et al. (2004) and Taylor et al. (2004). Assuming burning vegetation and the panel thermally radiate as gray bodies, the panel temperatures and

thus its spectral characteristics are similar to actual flames with a peak power wavelength of about 2.3 microns (Incopera and DeWitt 2002). Thus the radiant panel can serve as a reasonable facsimile for vegetation fires regarding wood spectral reflection and absorption (Janssens 1991).

I exposed the coarse particle and fine fuel particle separately (Fig. 3.2a) in quiescent air (no wind) to an irradiance of 41 (±0.2) kW/m^2. To receive this exposure, fuel particles were centered on and 0.10 m from the radiant panel surface. The particle irradiance was measured at the fuel particle position prior to particle exposures using a Medtherm® Schmidt-Boelter, water-cooled total heat flux sensor (Medtherm 1997). The particle position was inspected to assure it was not within the panel's flame convection. An aluminum radiation shield prevented heating during fuel particle placement and precisely controlled the particle exposure. A full particle radiation exposure occurred in less than 0.2 seconds when the shield was removed.

a)

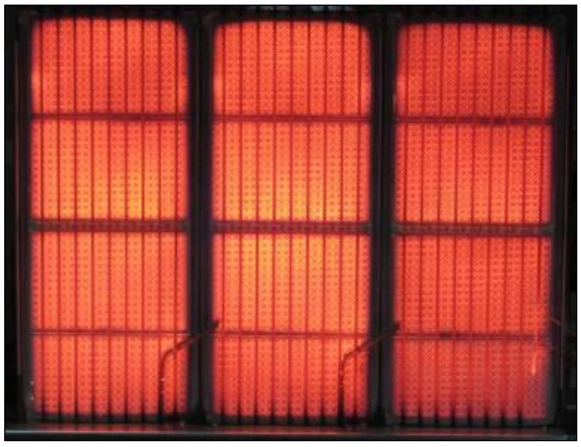

b)

Fig. 3.2 a) Experimental fuel particles have 1 mm (left) and 12 mm (right) square cross-sections and are 120 mm in length; b) Ceramic element, gas-fired radiant panel 0.486 m wide and 0.375 m high with surface temperatures between 1230 K and 1260 K. (photographs from Jack Cohen, US Forest Service)

One experimental test had fuel particles with temperature measurements; however, fine and coarse fuel particles were exposed without temperature measurements to practice the experimental procedure. After establishing the procedure, I did five experimental tests that measured the irradiance but did not measure temperatures of the exposed 1-mm and 12-mm particles. After these five practice tests I instrumented the fuel particles for measuring temperature.

Fuel particle temperatures were measured on the particle surface facing the radiant panel. A 1-mm and 12-mm fuel particle was instrumented with a thermocouple (Type K,

0.076 mm diameter wire) imbedded on the particle's surface at the center of the irradiated side. Because wood conductivity is lower in the cross-grain direction, the particle was oriented such that the side facing the radiant panel was as close to parallel as possible with the wood grain. When heating produced significant, observable pyrolysates, a small gas pilot flame was introduced immediately above the top surface of the fuel particle and forward of the front surface (not shown).

3.2.2 Results

Consistent with the prior demonstration experiments, the 1-mm particle did not pilot-ignite during the radiation exposure that resulted in the 12-mm particle igniting. For all six sets of fuel particles the 12-mm fuel particle significantly emitted pyrolysates shortly after the initial exposure (Fig. 3.3a) followed by piloted ignition (Fig. 3.3b, pilot not shown). By comparison, none of the 1-mm particles either produced observable pyrolysates or significant particle charring during the 2 minute exposure duration (Fig. 3.3c). Importantly, the 2-minute exposure was several times longer than the measured average burning residence times of active crown fires discussed in Chapter 2 (Cohen 2004; Despain et al. 1996; Taylor et al. 2004).

a) 15 seconds **b) 26 seconds**

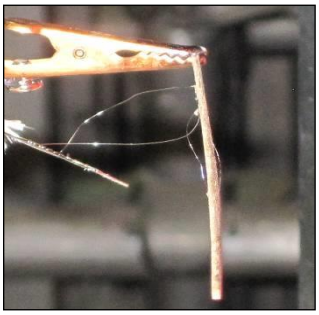

c) 2 minutes

Fig. 3.3 a) The 12 mm fuel particle pyrolyzing after 15 seconds of exposure to an irradiance of 41 (±0.2) kW/m^2. b) The same 12 mm fuel particle pilot ignited after 26 seconds (pilot flame not shown). c) For the same irradiance, the 1 mm fuel particle neither ignited nor significantly pyrolyzed after 2 minutes of exposure. (photographs from Jack Cohen, US Forest Service)

For the instrumented 1-mm and 12-mm particles the surface temperatures initially increased at similar rates indicating similar net heating. After less than 2 seconds of exposure and a surface temperature of about 130 C, the 1-mm rate of temperature increase significantly

reduced indicating reduced net particle heating compared to the 12-mm particle (Fig. 3.4). The surface temperature of the 12-mm particle continued to monotonically increase to piloted ignition (Fig. 3.4). By comparison, the 1-mm particle ceased its significant temperature increase and varied between 160 C and 200 C until the exposure ceased (Fig. 3.4). The lack of significant charring for the six 1-mm (instrumented and non-instrumented) tests is consistent with the maximum 160 C to 200 C temperature range of the measured 1-mm particle (Fairbridge et al. 1978; Tillman et al. 1981; Simmons 1995).

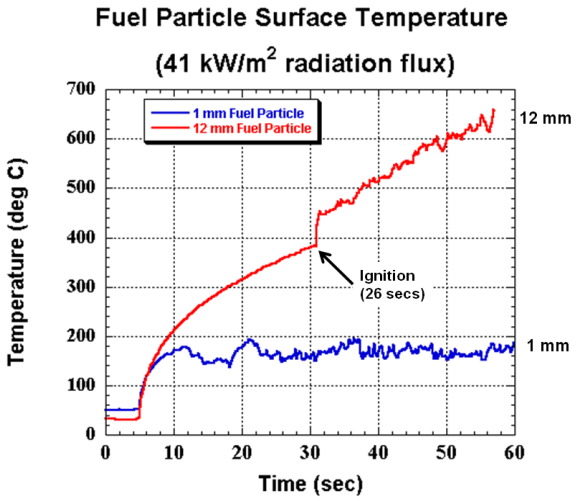

Fig. 3.4 The 1 mm and 12 mm particles were separately exposed to an irradiance of 41 (±0.2) kW/m^2. The fuel particle surface temperatures were measured with an imbedded thermocouple in the irradiated surface. The 12 mm particle pilot ignited after 26 seconds of exposure as indicated by the sudden temperature increase. Note that the particle irradiance starts at 5 seconds. An exposure of 26 seconds is at 31 seconds on the graph.

The measured particle temperatures (Fig. 3.4) can be compared to the photo times in Fig. 3.3. The observable pyrolysates shown after 15 seconds of exposure in Fig. 3.3a correspond to a temperature of 314 C in Fig. 3.4 (20 seconds on the time axis). Piloted ignition (Fig. 3.3b) occurred at about 380 C in Fig. 3.4 and corresponds to the abrupt temperature jump 26 seconds after the initial exposure.

3.2.3 Discussion

3.2.3.1 Different fuel particle size results in different heat exchange

The fine fuels neither ignited nor significantly charred in Latham's fine fuel experiments, my demonstration experiments and my exploratory fuel particle experiment. Importantly, the fine fuels of all my experiments did not ignite with higher irradiances than for Latham's experiments. All of the coarse fuels of my experiments heated to piloted ignition. The validated piloted ignition calculation of Tran et al. (1992) and Cohen (2004) predicted to the nearest second the coarse particle ignition times of 35 seconds for an irradiance of 37 kW/m^2

(qualitative experiments) and 26 seconds for an irradiance of 41 kW/m^2 (1-mm and 12-mm experiment). The correspondence between the calculated piloted ignition time and the actual coarse particle ignition time indicates the heat exchange processes for the coarse particles and the piloted ignition correlation are equivalent. However, the consistent failure to predict the fine particle results indicates significant heat exchange differences due to particle sizes smaller than the 12-mm particle.

The diverging 1-mm and 12-mm particle temperature profiles (Fig. 3.4) and corresponding differences in observable pyrolysis (Fig. 3.3) also indicate significant heat exchange differences between the two equally irradiated fuel particles. Significant pyrolysis rates and flammable products occur above 275 C (Fairbridge et al. 1978; Tillman et al. 1981; Simmons 1995; Drysdale 1998), so the lack of observable pyrolysates from the 1-mm fuel particle (Fig. 3.3c) was consistent with the surface temperatures remaining below 200 C. By comparison, the readily observable pyrolysates (Fig. 3.3a) and piloted ignition (Fig. 3.3b) of the 12-mm fuel particle were consistent with the surface temperatures exceeding 300 C leading to piloted-ignition at 380 C (Fairbridge et al. 1978; Tillman et al. 1981; Simmons 1995; Drysdale 1998). Recall from Chapter 2 (Fig. 3.2) that during deep-fuel bed fire experiments significant pyrolysis of the fine fuels was not observed as the flame front spread to adjacent fuels. Based on the consistent results of the exploratory experiments, it appears the flame zone radiation and fine fuel heat exchange during the deep-fuel fire spread could not heat the fuels to significant pyrolysis temperatures before flame contact. Given the same wood material, moisture content and irradiances, the different results of the 1-mm and 12-mm particle temperatures and corresponding pyrolysis appear to be from differences in the heat exchange due to particle size.

Based on the exploratory experiments, I suggest fuel particle thermal boundary conditions are a principal factor determining fuel heating and thus fire spread. In the following section I use established heat transfer theory (e.g. Incropera and DeWitt 2002; Kays et al. 2005) and physical reasoning to explain how thermal boundary conditions might govern fuel particle heating and how that can vary for different sized particles.

3.2.3.2 A physical explanation of fuel particle heat exchange

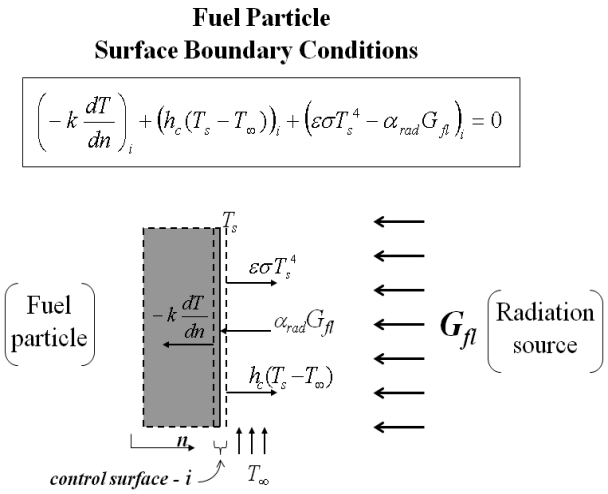

Fig. 3.5 The conditions at the particle (control) surface determine fuel particle heating and cooling. The left-hand-side terms of the conservation of energy equation at the control surface represent (left to right) conduction at the fuel particle surface, convection and net radiation.

Masses exchange heat through their surfaces, so heat exchange of an opaque fuel particle is determined by the particle surface temperature. In turn, the particle surface temperature is a function of the following boundary conditions (Fig. 3.5):

- Absorbed irradiance at the (control) surface ($\alpha_{rad}G_{fl}$) from the flame zone source (G_{fl}),
- Emitted radiation from the particle (control) surface ($\varepsilon\sigma T_s^4$),
- Convection heat exchange at the particle (control) surface ($h_c(T_s - T_\infty)$), and
- Energy conduction at the fuel particle (control) surface ($-k(dT/dn)$).

where:

α_{rad} = absorptivity, ε = gray body emissivity, σ = Stefan-Boltzmann constant, G_{fl} = irradiance; h_c = convection heat transfer coefficient, k = particle conductivity, T_s = particle surface temperature, T_∞ = ambient air temperature, dT/dn = temperature gradient normal to control surface, *control surface – i* = particle surface boundary through which energy passes.

For this analysis I assume the control surface corresponds exactly to the fuel particle surface. Thus, each boundary condition is represented by a term in the conservation of energy equation (Fig. 3.5) at the fuel particle surface. The particle surface temperature results from the interaction of the net radiation ($\varepsilon\sigma T_s^4 - \alpha_{rad}G_{fl}$)[1], natural and forced convection ($h_c(T_s$ -

[1] The flame irradiance, $G_{fl} = F_{fl,s}(\varepsilon\sigma T_{fl}^4)$, where $F_{fl,s}$ = the flame-particle view factor, T_{fl} = radiative flame temperature, and ε, σ are as defined above. The view factor, $F_{fl,s}$ is geometrically complicated to calculate and highly variable in time for flame fronts and thus measured for my experiments.

T_∞)), and conduction into the particle (heating, $(dT/dn) < 0$) or out of the particle (cooling, $(dT/dn) > 0$) at the surface ($-k(dT/dn)$) (Incopera and DeWitt 2002).

Fuel particle heat transfer is the result of temperature differences between the particle surface and its radiative and convective surroundings. If the particle surface temperature (T_s) is lower than its surroundings then convective and radiative particle heating occurs. Conversely, a higher particle surface temperature than its surroundings results in particle cooling. A particle can have a lower surface temperature than its radiative surroundings and heat to a surface temperature higher than the surrounding air. This results in convective cooling. In general, the greater the temperature difference, the higher the heat transfer rate. For given wildland fuels and flame front characteristics, the heat transfer rate due to radiation and conduction is largely influenced by temperature differences with the particle surface. From the conservation of energy equation (Fig. 3.5), the coefficients of the radiation and conduction terms are either material properties or a physical constant and they change little or not at all compared to temperature differences. However, convection heat transfer rates are not only determined by temperature differences but significantly by flow rate, gas temperature and density, and particle configuration and size (Incopera and DeWitt 2002; Kays et al. 2005). The importance of the convective conditions is demonstrated through the properties and conditions used for deriving the heat transfer coefficient (h_c) (Incopera and DeWitt 2002; for example, forced convection Table 7.9 and free convection Table 9.2).

As a flame front approaches fuel particles, the particles initially heat from absorbed radiation resulting in surface temperatures higher than ambient air temperatures. I conducted my exploratory experiments with quiescent air surroundings so the increased particle surface temperatures formed thermal boundary layers adjacent to the particle surfaces resulting in free convection (and negligible forced convection). When the surface temperature rises above the ambient air temperature, a fluid (air) thermal and buoyant flow boundary layer develops (Incropera and DeWitt 2002, Chapter 9) that displaces ambient air with heated air. As the thermal boundary layer next to the particle thickens with vertical flow length, less ambient cool air mixes into the surface boundary further reducing particle surface cooling. Thermal and flow boundary thickening similarly occurs during forced convection resulting in reduced convective cooling as well (Incopera and DeWitt 2002, Chapter 7). Researchers have found

for a wide range of conditions and contexts that the flow length (size) of a heated surface influences cooling by free and forced convection (Tibbals et al. 1964; Martin 1965; Alvares et al. 1970; Garg and Steward 1971).

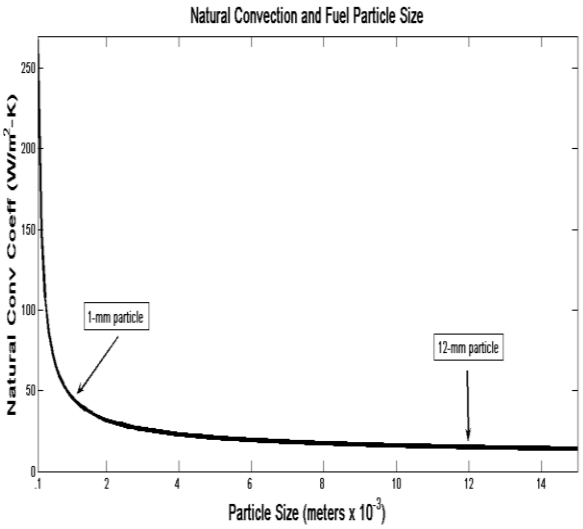

Fig. 3.6 The natural convection average heat transfer coefficient becomes highly sensitive to particle size at less than 1 mm and insensitive to size at 12 mm and larger. The convection coefficient calculations assume irradiance and environmental temperatures are constant with a fuel surface temperature of T_s = 197 C (470K).

3.2.3.3 The effect of size on convection heat exchange

Based on the exploratory experimental results, I suggest the two different-sized fuel particles heated differently because their surface lengths produced different boundary layers and thus different convective cooling. The 12-mm particle produced a thicker boundary layer across most of its heated surface than the 1-mm particle resulting in less convective cooling and thereby heating to ignition. A thinner thermal boundary layer with greater convective cooling can explain the non-ignition of the 1-mm particle during the same exposures that resulted in ignition of the 12-mm particle and even much larger wall sections (Tran et al. 1992; Cohen 2004).

The thermal boundary layer and thus the rate of convective heat exchange are not related to surface area-to-volume ratio (SA/V). As I discussed in Chapter 2, the SA/V influences the rate of heat exchange per unit fuel mass and thus the thermal response rate of a particle to a change in surface temperature. However, SA/V *per se* does not determine particle boundary conditions and thus the surface temperature. That means different fuel particle shapes and configurations (e.g. leaves and needles, orientation, and packing) having the same SA/V but different surface lengths have potentially different rates of free and forced convection heat exchange both cooling and heating.

To further explore this boundary condition argument, I used a common free convection heat transfer coefficient correlation (Incopera and DeWitt 2002, Eq. 9.27) to

examine the effect of heated vertical surface length on convection heat exchange as represented by the convection coefficient (Fig. 3.6). I calculated the average particle convection coefficient, h_c as a function of vertical surface length, L, to show the general influence of surface length (L) on the convection coefficient (h_c). My examination is a heuristic exercise; I am not suggesting this correlation as a specific application to fire spread modeling. I calculated a laminar, free convection average heat transfer coefficient based on the conditions of my particle heating experiment. The particle size, L is the vertical length of the side exposed to radiant heating. As the radiation is absorbed, the fuel particle surface temperature increases resulting in a buoyant, free convection surface boundary layer (Incropera and DeWitt 2002; Kays et al. 2005). To calculate the average free convection heat transfer coefficient I used the maximum 1-mm particle surface temperature of 470K (197 C), measured at mid-length ($L/2$). At this temperature the 1-mm particle heat transfer coefficient, and thus the assumed heat exchange rate was high enough to keep the particle from exceeding 470 K (Fig. 3.4). From Fig. 3.4, it is evident by the rate of temperature increase that the 12-mm particle convection heat transfer coefficient was not sufficient at 470 K or greater temperature to prevent the particle from heating to ignition.

As the vertical surface length decreases, the convection coefficient nonlinearly increases and thus increases the convective heat exchange rate (Fig. 3.6). I suggest this physically explains how the fine fuel (1-mm particle) did not ignite under the same conditions that resulted in coarse fuel (12-mm) ignition. This also explains how the ignition correlation (Tran et al. 1992; Cohen 2004) predicted the 12-mm particle ignition but not the 1-mm particle. The ignition correlation was developed using wood samples with vertical surface lengths of 50 mm to 100 mm and thicknesses greater than 19 mm (Janssens 1991). This is larger than the 12-mm particle and wood blocks of my exploratory experiments. Inspection of Fig. 3.6 indicates small convective heat exchange differences for vertical surface lengths greater than 12 mm and thus a negligible difference with the ignition correlation. Based on Fig. 3.6, the convection heat exchange rate of a12-mm particle and a wood wall both satisfy the convection conditions of the piloted ignition correlation. The ignition correlation fails for 1-mm particles and based on Fig. 3.6 the convection heat exchange rate is significantly greater for 1-mm particles and rapidly increases as particles get smaller. For perspective, the 1-mm particle is at the coarse limit of fine fuels (Scott and Burgan 2005) and larger than the

wood excelsior of the qualitative experiments. The 1-mm particle is also coarser than some western U.S. coniferous and shrub foliage that commonly burns in active crown fires (Rothermel and Anderson 1966; Rothermel and Philpot 1973). Assuming the average convection coefficient represents a general relationship between surface length and the rate of convective heat exchange, fine fuel particles with surface lengths smaller than 1 mm will have non-linearly increasing rates of convective heat exchange resulting in significant cooling from ambient air and rapid heating from flame contact.

3.2.3.4 Questions for continued fuel particle heat exchange research

Based on the results of my experiments and the literature (Chapter 2), I have defined my fuel particle research through the following questions that will be addressed in Chapters 4 and 5:

1) Does fuel particle size influence net radiation heating for ignition?
2) Do all thermally irradiated fuel particles undergo the same convection heat exchange?
3) Does fuel particle surface area-to-volume ratio determine convective heat exchange?
4) Is radiation always sufficient to heat fine fuels to ignition during fire spread?
5) What heat transfer mechanisms account for fuel particle heating in the final unresolved time and distance between the flaming front and adjacent fuel particles?
6) Can convection be the primary mechanism heating fine fuel particles to ignition resulting in fire spread?

3.2.4 Conclusion

Exploratory experiments, physical analysis, and the literature indicate that for fine fuels radiation heating can be insufficient for ignition due to convective cooling. Exploratory experiments consistently resulted in fine fuel particles not heating to ignition for the same conditions that produced piloted ignitions of coarse particles. From my physical analysis I showed how convective heat exchange increases with decreasing particle size sufficiently to keep irradiated fine fuels from igniting. Anderson (1969) concluded that radiation heating provided 40 percent of the energy required for fire spread in fine fuels and thus insufficient

for fire spread. Baines (1990) showed that a radiation model without convective cooling could not reasonably replicate measured fine fuel particle temperatures during an approaching flame front. However, when measured fuel temperatures rapidly increased near the flame front, radiation was insufficient and without convective heating Baines' (1990) model could not account for the observed particle temperature increasing to ignition.

Convective heat exchange must govern fire spread in fine fuels if radiation is insufficient for ignition. I found from established convection heat transfer theory and convection coefficient correlations that surface flow length influences the thermal boundary conditions that largely govern surface temperatures. For given conditions, the convective heat exchange non-linearly increases with decreasing flow length. Thus, the fuel particle size (flow length) influences particle temperatures. For fine fuels convective cooling can reduce radiant heating to prevent ignition and convective heating of fine fuels from flame contact would be highly effective in producing ignitions resulting in fire spread. Based on this I posit that convective heat exchange is primarily governs fuel particle temperatures leading to ignition in porous fine fuel dominated wildland surface and canopy fuel beds. I articulated questions for my further research (addressed in Chapters 4 and 5) to evaluate the degree to which convection is the principal heat transfer mechanism (cooling and heating) for fine fuels (1 mm and less).

3.3 References

Alvares NJ, Blackshear PL Jr, Kanury AM (1970) The influence of free convection on the ignition of vertical cellulosic panels by thermal radiation. *Combustion Science and Technology* **1**, 407-413.

Anderson HE (1969) Heat transfer and fire spread. USDA Forest Service, Intermountain Forest and Range Experiment Station, Research Paper INT-RP-69. (Ogden, UT)

Anderson HE (1982) Aids to determining fuel models for estimating fire behavior. USDA Forest Service, Intermountain Forest and Range Experiment Station, General Technical Report INT-GTR-122. (Ogden, UT)

Baines PG (1990) Physical mechanisms for the propagation of surface fires. *Mathematical Computer Modeling* **13**(12), 83-94.

Butler BW, Cohen J, Latham DJ, Schuette RD, Sopko P, Shannon KS, Jimenez D, Bradshaw LS (2004) Measurements of radiant emissive power and temperatures in crown fires. *Canadian Journal of Forest Research* **34**(8), 1577-1587.

Cohen JD (2004) Relating flame radiation to home ignition using modeling and experimental crown fires. *Canadian Journal of Forest Research* **34**(8), 1616-1626.

de Mestre NJ, Catchpole EA, Anderson DH, Rothermel RC (1989) Uniform propagation of a planar fire front without wind. *Combustion Science and Technology* **65**, 231-244.

Despain DG, Clark DL, Reardon JJ (1996) Simulation of crown fire effects on canopy seed bank in lodgepole pine. *International Journal of Wildland* Fire **6**, 45-49.

Drysdale D (1998) 'An Introduction to Fire Dynamics.' (John Wiley: New York)

Fairbridge C, Ross RA, Sood SP (1978) A kinetic and surface study of the thermal decomposition of cellulose powder in inert and oxidizing atmospheres. *Journal of Applied Polymer Science* **22**, 497-510.

Fang JB, Steward FR (1969) Flame spread through randomly packed fuel particles. *Combustion and Flame* **13**, 392-398.

Garg DR, Steward FR (1971) Piloted ignition of cellulosic materials containing high void spaces. *Combustion and Flame* **17**, 287-294.

Incopera FP, DeWitt DP (2002) 'Fundamentals of Heat and Mass Transfer.' 5th edn. (John Wiley: New York)

Janssens M (1991) Piloted ignition of wood: a review. *Journal of Fire and Materials* **15**, 151-167.

Kays WM, Crawford ME, Weigand B (2005) 'Convective Heat and Mass Transfer.' 4th edition. (McGraw-Hill: New York)

Lui N, Wu J, Chen H, Zhang L, Deng Z, Satoh K, Viegas DX, Raposos JR (2014) Upslope spread of a linear flame front over a pine needle fuel bed: the role of convection cooling. 'Proceedings of the Combustion Institute.' (The Combustion Institute: Pittsburgh, PA) http://dx.doi.org/10.1016/j.proci.2014.05.100.

Martin S (1965) Diffusion-controlled ignition of cellulosic materials by intense radiant energy. In 'Tenth Symposium (International) on Combustion.' 17-20 August 1964, Cambridge, England. pp. 877-896. (The Combustion Institute: Pittsburgh, PA)

Medtherm Corporation. (1997) 'Heat Flux Transducers'. Bulletin 118. Huntsville, Alabama.

Morvan D, Dupuy JL (2004) Modeling the propagation of a wildfire through a Mediterranean shrub using a multiphase formulation. *Combustion and Flame* **138**, 199-210.

Rothermel RC (1972) A mathematical model for predicting fire spread in wildland fuels. USDA Forest Service, Intermountain Forest and Range Experiment Station, Research Paper INT-RP-115. (Ogden, UT)

Rothermel RC, Philpot CW (1973) Predicting changes in chaparral flammability. *Journal of Forestry* **71**, 164-169.

Rothermel RC, Anderson HE (1966) Fire spread characteristics determined in the laboratory. USDA Forest Service, Intermountain Forest and Range Experiment Station, Research Paper INT-RP-30. (Ogden, UT)

Scott JH, Burgan RE (2005) Standard fire behavior fuel models: a comprehensive set for use with Rothermel's surface fire spread model. USDA Forest Service, Rocky Mountain Forest and Range Experiment Station, General Technical Report RMRS-GTR-153. (Ft. Collins, CO)

Scott JH, Reinhardt ED (2005) Stereo photo guide for estimating canopy fuel characteristics in conifer stands. USDA Forest Service, Rocky Mountain Forest and Range Experiment Station, General Technical Report RMRS-GTR-145. (Ft. Collins, CO)

Silvani X, Morandini F, MuzyJ-F (2009) Wildfire spread experiments: fluctuations in thermal measurements. *International Communication in Heat and Mass Transfer* **36**(9), 887-892.

Silvani X, Morandini F, Dupuy JL (2012) Effects of slope on fire spread observed through video images and multi-point thermal measurements. *Experimental Thermal and Fluid Science* **41**, 99-111.

Simmons RF (1995) Fire Chemistry, Ch. 7 'Combustion Fundamentals of Fire.' (Academic Press: New York)

Spearpoint MJ, Quintiere JG (2001) Predicting the piloted ignition of wood in the cone calorimeter using an integral model – effect of species, grain orientation and heat flux. *Fire Safety Journal* **36**, 391-415.

Stocks BJ, Alexander ME, Wotton BM, Stefner CN, Flannigan MD, Taylor SW, Lavoie N, Mason JA, Hartley GR, Maffey ME, Dalrymple GN, Blake TW, Cruz MG, Lanoville RA (2004) Crown fire behavior in a northern jack pine-black spruce forest. *Canadian Journal of Forest Research* **34**, 1548-1560.

Taylor SW, Wotton BM, Alexander ME, Dalrymple GN (2004) Variation in wind and crown fire behaviour in a northern jack pine – black spruce forest. *Canadian Journal of Forest Research* **34**, 1561-1576.

Tibbals EC, Carr EK, Gates DM, Kreith F (1964) Radiation and convection in conifers. *American Journal of Botany* **51**(5), 529-538.

Tillman DA, Amadeo JR, Kitto WD (1981) 'Wood Combustion.' (Academic Press: New York)

Tran HC, Cohen JD, Chase RA (1992) Modeling ignition of structures in wildland/urban interface fires. In 'Proceedings of the 1st International Fire and Materials Conference; 24-25 September 1992, Arlington, VA. pp. 253-262. (Interscience Communications Limited: Hamshire, UK)

Weber RO (1991) Modelling fire spread through fuel beds. *Progress in Energy Combustion Science* **17**: 67-82.

Chapter Four

Convective Cooling of Irradiated Fuel Particles

4.1 Introduction

Fuel particle ignition is the basis for wildland fire spread, yet the literature offers few experiments where heated fuel particle boundary conditions and particle temperatures have been measured and I found none that resolved the fuel heating mechanisms as particles were heating to ignition (from Chapter 2). In this chapter I continue from the exploratory research discussed in Chapter 3. From the exploratory experiment I found significant surface temperature differences between the 12 mm particle and the 1 mm particle. These measured particle temperatures were consistent with the observed pyrolysis and piloted ignition of the 12 mm particle as well as the lack thereof for the 1 mm particle (Fairbridge et al. 1978; Tillman et al. 1981; Simmons 1995; Drysdale 1998). This led me to develop a theoretical explanation that identified the higher convective heat exchange of the 1 mm as the reason for the lower temperatures. Based on the findings in Chapter 3 I designed controlled laboratory experiments and developed a theoretically based numerical model to examine the mechanisms of fuel particle heat exchange.

I used controlled laboratory experiments with a theoretically based numerical model to describe how particle geometry influenced convective cooling. With specially designed experimental equipment I exposed a range of fuel particle sizes from 1 mm to 12 mm to radiant heating and free and forced convective cooling. I controlled the magnitude and duration of the particle irradiance as well as the air flow during forced convection tests. To examine fuel particle heat exchange I measured irradiances and air speeds and temperatures along with fuel particle surface temperatures. However, these measurements without theoretical computations do not explain how fuel particles exchange heat. To computationally determine the heat exchange, I designed and developed a 2-dimensional, transient heat transfer model that included radiation and convection boundary conditions. Using this experiment-modeling combination I examined convective cooling differences due to particle

size, demonstrated how convective heat transfer is related to particle boundary development, and described how boundary conditions largely determine particle heat exchange at the surface and particle surface area-to-volume ratio determines a particle's heat exchange response rate.

4.2 Methods

The research methods involved the design and development of special laboratory equipment, the development of a numerical model to compute fuel particle heat exchange, and the experimental procedures for examining fuel particle heat exchange. I designed the equipment, model and procedures to address fuel particle heat exchange related to particle size, convective cooling and surface area-to-volume ratio.

4.2.1 Experimental Equipment

I designed and developed equipment to use for experiments to examine radiative fuel particle heating with free and forced convection. The equipment was composed of several components: the radiant panel and mirrors, the shutter door, the low speed wind tunnel and

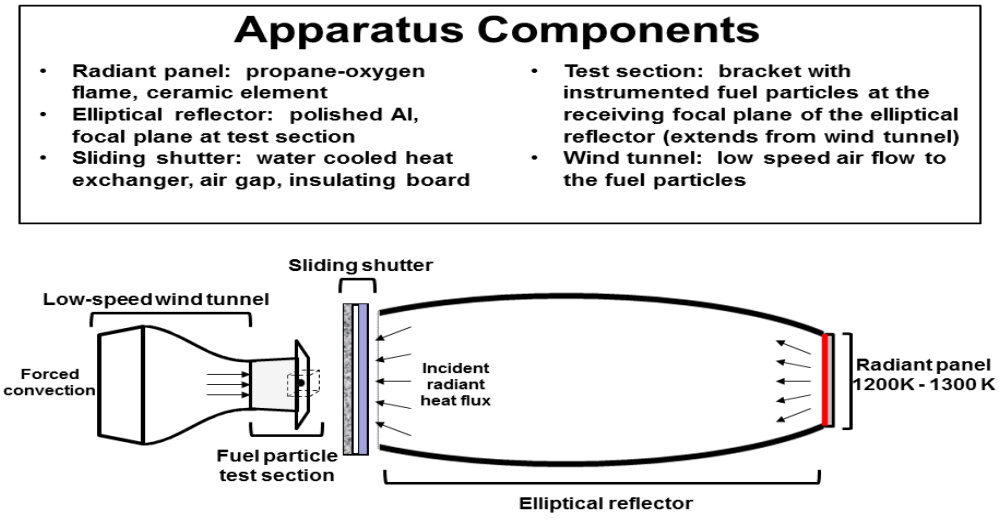

Fig. 4.1 I designed this radiant panel-elliptical mirror and low speed wind tunnel apparatus to investigate the heat exchange of various sized fuel particles during radiant heating and convective cooling.

the test section with instrumented fuel particles (Fig. 4.1). In addition, I created the means to capture images of the density gradient and related air flow adjacent to the heated particle surface using schlieren optics (Settles 2001, Ch. 2). Below I describe each experimental component as well as sensor calibration and exposure characterization of the equipment.

4.2.1.1 Radiant Panel and Mirrors

I developed a radiant panel for irradiating fuel particles. The gas fired, ceramic element panel was the same one described in Chapter 3 (Methods). However, for this apparatus oxygen was injected into the propane and air mixture to increase the panel's emissive power. The propane and oxygen flow rates were adjusted to select a desired irradiance of 29 kW/m^2 to 36 kW/m^2 at the opposite mirror focal plane (irradiance measurements taken the same as described in Chapter 3, Methods). The average measured panel surface temperatures (measurements described in Chapter 3, Methods) ranged from 1222K to 1290K and remained within the range of expected wildland fire flame front temperatures (Butler et al. 2004; Taylor et al. 2004).

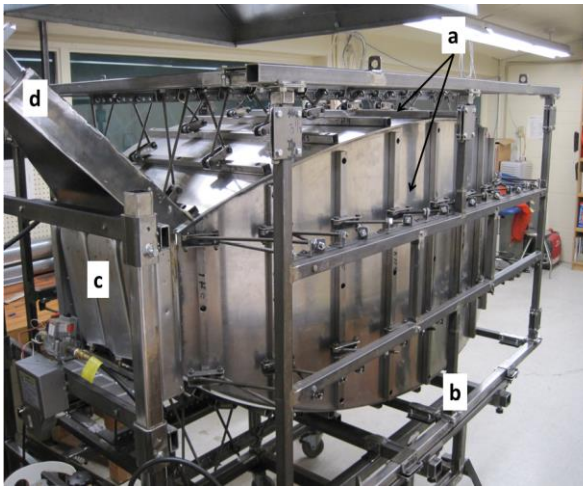

Fig. 4.2 This is the radiant panel (c) and the mirror assembly (a). The mirror assembly is supported by the shaping frame and support carriage (b). The gas fired radiant is panel (c) is vented through the exhaust duct (d).

I added mirrors so that air could be blown across the exposed fuel particle to produce forced convective cooling without disturbing the radiant panel. This allowed fuel particles to be placed 2.0 m from the radiant panel and have sufficient irradiance for the experiments. The mirrors were cut from sheet aluminum (5000 series), polished to a mirror finish, and joined to form orthogonal ellipses. The exterior mirror frame not only held the mirrors in place but served to bend and adjust the mirror elements into the elliptical shape (Fig. 4.2). The widths of the vertical and horizontal mirror elements matched the dimensions of the radiant panel

face (Fig. 4.3). Ellipses have two focal points so the elliptical mirror system had two focal planes. The radiant panel face was at one focal plane and 2.0 m away, fuel particles were placed at the opposite focal plane. The mirrors were cut 0.15 m short of the receiving focal plane to allow space for the shutter door (Figs. 4.1 and 4.4).

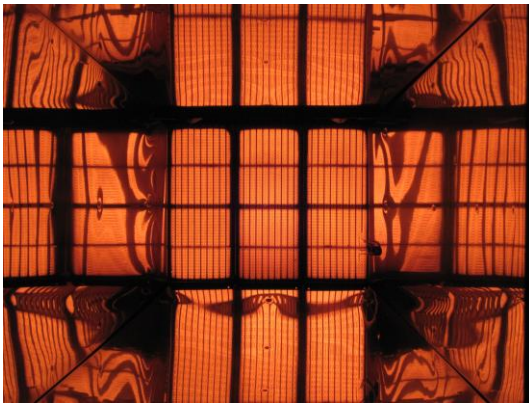

Fig. 4.3 Looking into the mirror cavity at the hot radiant panel. The panel is at the photo center surrounded by the mirror reflections that increase the irradiance at the exposed fuel particle.

4.2.1.2 Shutter Door

I designed the shutter for precise control of fuel particle radiant exposures and to provide a heat shield from the radiant panel while preparing for a test. The center opening, double traverse doors were composed of three layers: the heat exchanger, air gap and insulting panel (Figs. 4.1 and 4.4). The heat exchanger doors were machined from 0.18 meter, 6000 Series aluminum plate to be water cooled (18 liters/min at 10 – 20 C) through a multi-channeled, single pass configuration. The side facing the radiant panel had a thin black radiation absorbing coating. When the shutter was closed during operation, the heat exchanger absorbed nearly all radiation emitted by the panel. The insulating panel (0.12 m thick Micore® 300) on the test section side of the heat exchanger (Fig. 4.1) served to isolate the heat exchanger and radiant panel-mirror system from the fuel particle and be thermally the same as the room surroundings prior to exposure. The 0.12 m air gap aided in reducing heat transfer between the insulting panel and the heat exchanger.

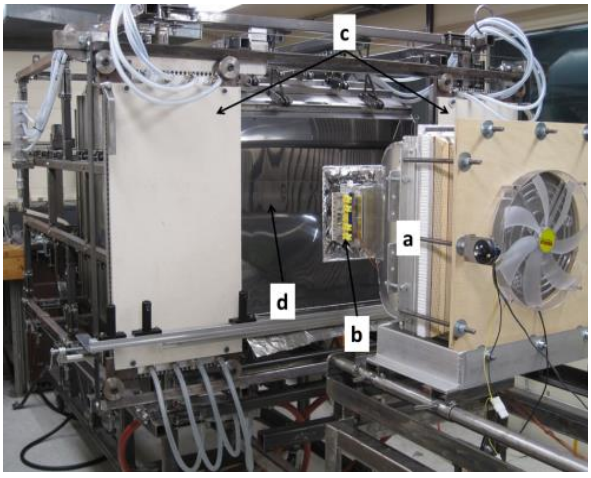

Fig. 4.4 The low speed wind tunnel (a), the fuel particle test section (b), the shutter door/heat exchanger (c) and the mirrors (d). The positions of the wind tunnel-test section assembly (a and b) and shutter door are as they would be for an experimental test.

4.2.1.3 Low Speed Wind Tunnel

The low speed wind tunnel produced air flow across the fuel particle mounted on the test section and also served as the mounting bracket for the test section (Fig. 4.4). I designed the low speed wind tunnel to provide steady, uniform air flow (Mehta and Bradshaw 1979; Bell and Mehta 1988) for the radiant panel experiments. The axial fan forced air into the diffuser section with its increasing square cross-sectional area containing a set of three screens to produce uniform flow over the tunnel cross-section. Immediately down-flow of the diffuser section was a honey-comb flow straightener that largely eliminated cross flows. After the honey-comb, air flowed through a set of screens to further equalize the cross-sectional flow velocity before entering the contraction section. The wind tunnel cross-section was reduced in the contraction section that is specifically designed (Bell and Mehta 1988) to increase air velocity while maintaining a uniform, steady flow. A test section bracket with heat flux sensors (Fig. 4.5) or fuel particles (Fig. 4.6) was attached to the end of the contraction section.

I designed the wind tunnel (with the test section) to move on a stationary carriage that was rigidly fixed to the exterior frame supporting the radiant panel and mirror assembly (Fig. 4.4). To provide working room when attaching or removing test section brackets, the wind tunnel was moved back, away from the shutter doors. After completing preparations, the wind tunnel-test section assembly was moved forward into its radiant exposure position.

4.2.1.4 Test Sections

The test section was where heat flux sensors or fuel particles were mounted for radiant panel experiments. The test section bracket was attached to the end of the wind tunnel contraction section and flush with the inside tunnel surfaces. The test section bracket added 0.10 m to the wind tunnel length (Fig. 4.5 and 4.6). The bracket cross-section was 0.16 m square so that fuel particle mid-sections experienced uniform, steady air flow during forced convection experiments. Because irradiances could not be measured during fuel particle exposures, a separate test section was equipped with heat flux sensors.

Heat flux test section: Fuel particle irradiance was measured using two Medtherm® Schmidt-Boelter, water-cooled total heat flux sensors (Fig. 4.5). The heat flux sensors have a hemispherical view, reliable to a 150 degree solid angle and a response time constant of 0.25 sec (Medtherm 1997). The sensors are horizontally mounted 0.025 m apart at their centers to a bracket designed to horizontally adjust the position of the sensor pair. The heat flux test section was designed to center the pair of heat flux sensors at the same position as the front face, mid-section any fuel particle regardless of particle size.

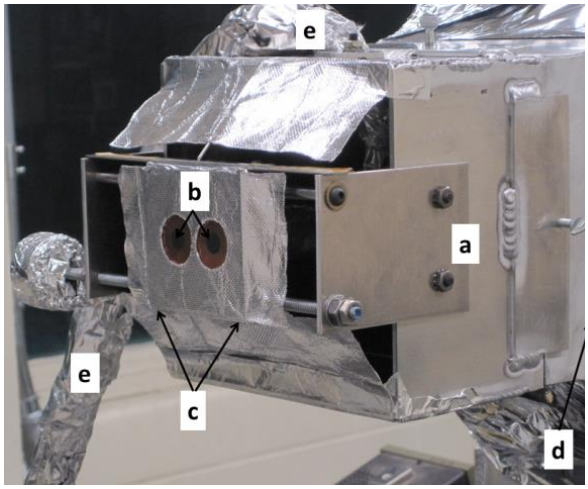

Fig. 4.5 The heat flux sensor test section (a) is attached to the wind tunnel (d). The two heat flux sensors (b) are mounted into the adjustable bracket (c) with the wire connectors and cooling tubes inside a reflective sheath (e).

Fuel particle test section: I measured fuel particle surface temperature and the surrounding air temperature with thermocouples. For all temperature measurements I used bare-wire K-type thermocouples that were 50.0 x 10^{-6} m (50 µm) in size. I computed the minimum thermocouple time constant for the maximum experimental air speed of 1.0 m/s at 0.07 sec (Incopera and DeWitt 2002; Sasaki et al. 1994). Thermocouple time constants increase for slower air speeds. For measuring fuel particle surface temperatures I embedded the 50 µm thermocouples in the fuel particle surface (Figs. 4.6 and 4.7). Fine, shallow grooves were scored into the particle surface for the thermocouple wire. The thermocouple leads were secured several cm on either side of the junction with cyanoacrylate glue and the thermocouple junction was bedded in a minute amount of heat flux compound to enhance thermal conductivity between the thermocouple and the particle surface. To measure ambient air temperatures at the fuel particle, I suspended a 50 µm bare thermocouple from stiff wire leads within 0.01 m of the fuel particle (Figs. 4.6 and 4.7).

Fuel particles with thermocouples were mounted on the test section bracket to minimize influences from the apparatus and facilitate temperature measurements during the experiments. Fuel particles were attached to the test section bracket with wire struts and the bare wire thermocouple leads were guided to connectors on thermocouple plug receptors (Fig. 4.6). Before an experimental run, an aluminum radiation reflector was mounted on the test section bracket to shield the thermally sensitive thermocouple wire guides and plug connectors (Fig. 4.6). The fragile fuel particle-thermocouple assembly became part of the test section bracket that could be quickly mounted to the wind tunnel, connected to plug-in leads from the data logger and moved to the radiant exposure position ready for data collection.

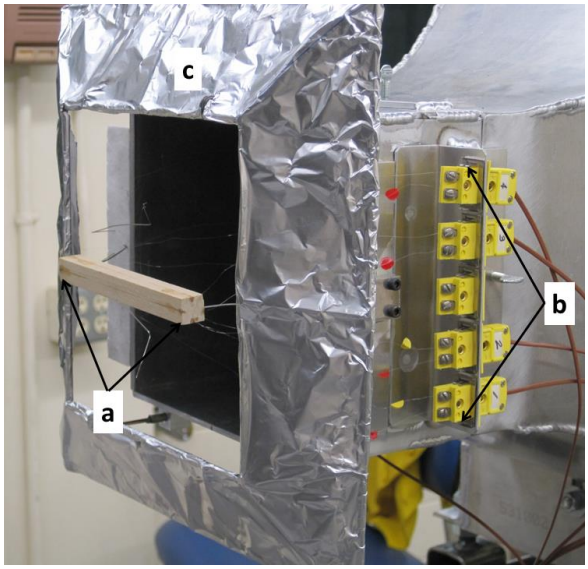

Fig. 4.6 The fuel particle (a) is attached to the test section bracket with stiff wire struts. The bare thermocouple wires are guided through separators and then attached to the plug connectors (b). The yellow and red tabs identify the thermocouple polarity. A reflecting shroud (c) shields the temperature-sensitive wire guides and connectors and prevents the heating of the fuel particle surroundings.

4.2.1.5 Schlieren Optical Imaging

I used a basic schlieren optical lens system to image air density gradients produced by fuel particle heating and disturbed air flow (Settles 2001, Ch. 2). The schlieren system used a high intensity light source, optical pin-hole, collimating and focusing lenses, and a knife edge (a razor blade) that produced flow images captured with video during free and forced convective conditions. Because heated particles produced hot air, air densities were reduced from ambient and thus, density gradients were negative. This resulted in dark patterns at flow boundaries corresponding to the air density rate of change.

4.2.1.6 Calibrating the Sensors and Characterizing the Apparatus

Preceding the fuel particle experiments I calibrated the heat flux sensors, analyzed for thermocouple irradiance error, determined the irradiances to the top, bottom and front (panel facing) sides of a fuel particle at the testing position and determined air flow uniformity. The following describes my procedures:

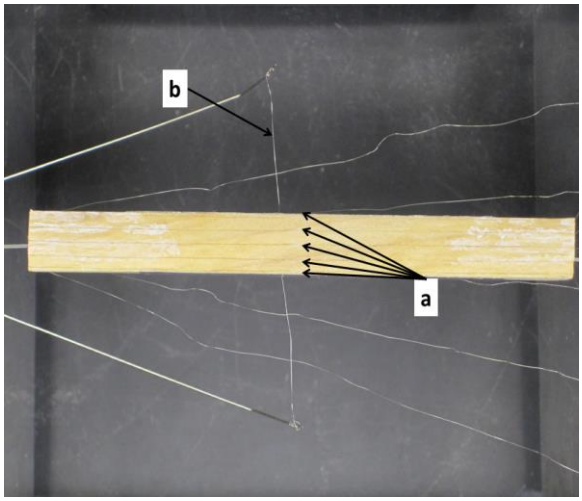

Fig. 4.7 This 12 mm x 12 mm fuel particle has five 50 µm thermocouples (a) imbedded in its front surface. The fine lines running the length of the fuel particle are the bare thermocouple wires with the thermocouple junctions (point of temperature measurement) just to the left of the arrow heads. A 50 µm air thermocouple (b) is suspended at the back of the particle. The fuel particle has been radiantly heated during a test and the white chalky color at the particle ends is from thermally decomposed cyanoacrylate glue.

- Both Medtherm® total heat flux sensors were calibrated using a Mikron® 300 black body cavity calibrator. I chose six cavity temperatures corresponding to irradiances of 30, 40, 50, 60, 70 and 100 kW/m^2. From the calibration data I produced linear regression equations of the sensors' voltage output corresponding to the black body cavity calibrator's temperature and thus the sensor irradiance. Both sensors were highly linear with correlation coefficients greater than 0.9999. I included the regression equations in my data logger program to produce direct measured irradiance during a test and later processing.
- My computational analysis of 50 µm K-type thermocouples exposed to an irradiance of 36 kW/m2 indicated a negligible radiation temperature error of less than one percent.
- Using the sensor positioning adjustment of the sensor mount, I determined the average irradiance to be horizontally uniform across the fuel particle span (0.12 m) within ±0.1 kW/m^2.
- From radiometer measurements at the focal plane, I found significant irradiances that would occur to the top and bottom of exposed fuel particles and not just the front face. For an average front facing irradiance (G_f) ranging from 30 kW/m^2 to 36 kW/m^2 I found an average irradiance of (0.327 G_f) kW/m^2 for the particle top and an average bottom irradiance of (0.254G_f) kW/m^2.

- Using a hot-wire anemometer to determine air speed for a range of 0.24 m/s to 1.2 m/s, I measured uniform flow speeds (±0.02 m/s) across the inside of the test section at distances greater than 0.02 m from the walls. The maximum air speed was 1.5 m/s without disturbing the radiant panel.

4.2.2 Experimental Procedures

4.2.2.1 Fuel Particle Testing

I designed a test procedure that I used for all the experiments that addressed fuel particle heat exchange related to particle size, convective cooling and surface area-to-volume ratio. Because heat flux sensors and fuel particles could not be mounted simultaneously, I measured average irradiances immediately before and after the fuel particle test run and produced an assumed constant average irradiance corresponding to the measured fuel particle temperatures. I describe the experimental procedure as follows:

- The instrumented fuel particle mounted on the test section was placed in a drying oven at a temperature of 60 C for 24 hours. Subsequently, the particle and test section were placed in a dry-cabinet at room temperature where fuel particles equilibrated for 24 hours or more to room temperature and moisture contents less than 3 percent (dry weight basis). Fuel particles remained in the dry-cabinet until just prior to a test run.
- The radiant panel experiments began with me starting exhaust fans, water flow through the heat exchanger-shutter door and igniting the gas-fired radiant panel. After running for 5 minutes or more the panel reached operating temperature and was ready for final propane and oxygen flow adjustments to come close to target irradiances. I made panel output adjustments by monitoring measured irradiances.
- The heat flux sensors and the thermocouples were connected to a data logger connected to a lap top computer. Heat flux measurements were made at 10 per second and thermocouple temperature measurements were made at 50 per second. In each case, the measurement rate was more than twice the Nyquist frequency (two times the sensor time constant) to prevent data aliasing (Fritschen and Gay 1979, p. 201).

- An experimental run started with pre-test heat flux sensor measurements to produce a 10-second average irradiance as close to 35.0 kW/m^2 as attainable. Then the shutter door was closed and the heat flux sensor test section was disconnected from the data logger and removed. The fuel particle test section was then attached and connected to the data logger. For the forced convection tests I measured average (n=10) air flow speed about 0.02 m upwind of the fuel particle with a hot-wire anemometer and adjusted the fan to meet a 1.0 m/s flow speed. The shutter door was opened to start the test run. The test was completed when either the fuel particle front face temperature increased to 300 C or when varying temperatures continued at less than 300 C for one minute. Then the shutter door was closed, the particle test section was removed and the heat flux test section was re-installed. A post-test 10-second average irradiance was measured to complete the experimental test.

4.2.2.2 Fuel Particle Size and Convective Heat Exchange

I subjected individual fuel particle of various sizes to approximately the same radiative and convective exposure to identify differences in heat exchange. The fuel particles I used for all the heat exchange experiments were not natural vegetative fuels. Fuel particles were made of *Liriodendron tulipifera* wood machined to various sizes. Fuel particles were all 120 mm long and had 1, 3, 6, 9 and 12 mm square cross-sections. I conducted three replications of each fuel particle size at irradiances between 29.8 kW/m^2 and 36.4 kW/m^2 during both free and forced convective (1.00 ± 0.02 m/s) conditions to determine ignition potential based on particle size. I monitored particle temperatures during the experiment and ended the test when the front side temperature exceeded 300 C or after a one minute exposure, whichever came first. Each particle heating test had different irradiances within the above range. Because particle temperatures are not linearly determined by the irradiance, each modeled test used the test-specific irradiance to predict particle temperatures and thereby examine particle heat transfer mechanisms. I selected the last set of fuel particle tests that had an irradiance range between 34.9 kW/m^2 and 35.4 kW/m^{2}for the physical modeling analysis.

4.2.2.3 Convective Cooling and Boundary Conditions

With these demonstrations I described fuel particle thermal boundary conditions. I used schlieren imaging and vertically arranged thermocouples on the front face of a 12 mm fuel particle to describe convection as the mechanism for fuel particle cooling. The schlieren optical system was used to image the thermal boundary of an irradiated 12 x 12 x 120 mm (width, height and length) particle for quiescent air and flow speeds of about 0.5 m/s and 1.0 m/s. To determine the vertical temperature profile, I instrumented fuel particles of 12 x 12 x 120 mm and 12 x 1 x 120 mm with five 50 µm vertically arranged thermocouples at a spacing of 0.5 mm, 3 mm, 6 mm, 9 mm and 11.5 mm at the middle of the particle front face. The attempted particle irradiance was 30.0 kW/m^2 for both quiescent air and an attempted flow speed of 1.00 m/s to produce a surface temperature profile of the irradiated particle associated with the schlieren images.

4.2.2.4 Boundary Conditions and Surface Area-to-Volume Ratio (SAV)

Using different sizes and configurations of fuel particles I investigated surface area-to-volume ratio (SA/V) as an influence on heat exchange. Two fuel particles had square cross-sections of 1 mm x 1 mm and 12 mm x 12 mm with SA/Vs of 4000 m^{-1} and 333 m^{-1} respectively. Two other particles had rectangular cross-sections of 1mm x 12 mm (width and height) and 0.5 mm x 12 mm with SA/Vs of 2167 m^{-1} and 4167 m^{-1} respectively. As with the particle size tests above, each test had a different irradiance. For this set of experiments irradiances were between 34.9 kW/m^2 and 35.2 kW/m2 for quiescent air and a forced flow speed of 1.00 m/s. Using my physical model, I predicted front surface temperatures and displayed fuel particle temperatures for the particle cross-section.

4.2.3 Numerical Particle Heat Exchange Model

I developed a two-dimensional numerical model of transient fuel particle heat transfer to further examine particle heat exchange. I used the heat transfer model heuristically with the recognition that it serves as a complex hypothesis (Oreskes et al. 1994) for examining fuel

particle heat exchange compared to observed results. The numerical model was designed to calculate a two-dimensional profile of surface and interior temperatures at the mid-length of an experimental fuel particle given the measured initial particle temperatures, the measured irradiance at sides exposed to panel radiation and the measured ambient air temperature and flow velocity. The model was intended to be used heuristically for understanding heat transfer processes leading to particle ignition during fire spread and not as a predictive tool. Model parameters were based on the most appropriate simplifying assumptions related to experimental conditions and the model was not adjusted after experiments to match model results with measured particle temperatures. The following describes the assumptions based on the experimental conditions and the resulting governing equations that comprise the computational model.

4.2.3.1 Assumptions and Governing Equations

Interior particle temperatures:

1) Heat exchange was non-steady state (transient conditions).

($\frac{dT}{dt} \neq 0$);

where: T = temperature, t = time.

2) No internal heat was generated (positive or negative); pyrolysis and water evaporation were neglected but that restricted model reliability to temperatures to less than 275 C (Fairbridge et al. 1978; Tillman et al. 1981; Simmons 1995; Drysdale 1998).

($q'''_{gen} = 0$);

where: q'''_{gen} = rate of energy generation per unit volume.

3) The fuel particle was a solid with negligible mass advection;

$$\left[\frac{dT}{dt} = \frac{\partial T}{\partial x}\frac{\partial x}{\partial t} + \frac{\partial T}{\partial y}\frac{\partial y}{\partial t} + \frac{\partial T}{\partial z}\frac{\partial z}{\partial t} + \frac{\partial T}{\partial t} = \frac{\partial T}{\partial t}\right];$$

$$(\frac{\partial x}{\partial t}=\frac{\partial y}{\partial t}=\frac{\partial z}{\partial t}=0)$$

where: *x*, *y*, *z* are unit dimensions of width, height and length, respectively.

4) The lengthwise surface temperatures were uniform so the *z*-axis temperature gradient and the end effects were negligible and a mid-section, 2-dimensional temperature profile is descriptive of most of the particle.

$(\frac{\partial T}{\partial z}=0)$;

where: *z* is the long particle axis.

5) The fuel particle was materially uniform with the conductivity (*k*), heat capacity (C_p), and thermal diffusivity (α) determined at each computational node as a function of temperature. Density changes were negligible and pressure was constant.

6) The fuel particle was a rectangular solid having a square or rectangular cross-section. All exposed particles are oriented such that the longest cross-sectional side is vertical and faced the radiant panel (Fig. 4.8).

The Modeled Particle and Conditions

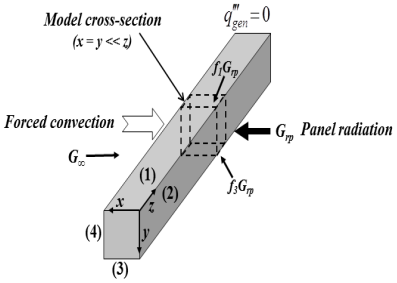

- *Initial uniform particle temperature in equilibrium with surroundings,*
- *Constant, uniform irradiance from radiant panel at face 2 (G_{rp}) and fractionally less irradiances at faces 1 and 3 (f_1G_{rp} and f_3G_{rp}),*
- *Constant, uniform irradiance from surroundings (G_∞) to face 4 and negligible compared to panel radiation on faces 1, 2, and 3,*
- *Constant forced air flow toward face 4 or quiescent,*
- *No internal energy generation,*
- *Temperature gradients negligible in the z direction, a 2-D model.*

Fig. 4.8 Model assumptions related to the particle and boundary conditions.

Based on assumptions (1), (5) and (6) the conduction heat diffusion equation in Cartesian coordinates was expressed as Equation 1:

$$\frac{\partial^2 T}{\partial x^2}+\frac{\partial^2 T}{\partial y^2}+\frac{\partial^2 T}{\partial z^2}+\frac{\dot{q}gen}{k}=\frac{1}{\alpha}\frac{dT}{dt} \qquad (1)$$

$$\frac{\partial^2 T}{\partial x^2}+\frac{\partial^2 T}{\partial y^2}=\frac{1}{\alpha}\frac{\partial T}{\partial t} \qquad (2)$$

Based on assumptions (2), (3) and (4) I reduced Equation 1 to become Equation 2, a 2-dimensional, solid particle, transient heat diffusion equation with no internal energy generation. Equation 2 was the governing equation for determining interior fuel particle

temperatures given the surface temperatures that were determined by the boundary conditions at the particle surface.

Boundary conditions:

The fuel particle boundary conditions were expressed as terms in a conservation of energy equation at the particle surface (Fig. 4.9). I expressed each boundary term of the equation in the numerical model based on the following assumptions:

7) The radiant panel, fuel particle and ambient surroundings were gray bodies (that is, each has a full thermal spectrum with an emissivity less than 1). The mirrors did not change the reflected spectra.

8) The radiosity of the radiant panel was independent of all other radiating surfaces.

9) The measured panel irradiance at the fuel particle (G_{rp}) was uniform and constant during particle exposure. For the focal plane position, panel irradiances to the particle's top ($f_1 G_{rp}$) and bottom ($f_3 G_{rp}$) sides were a constant fraction of the front side irradiance. Irradiance from the ambient surroundings was negligible compared to panel radiances to sides 1, 2 and 3.

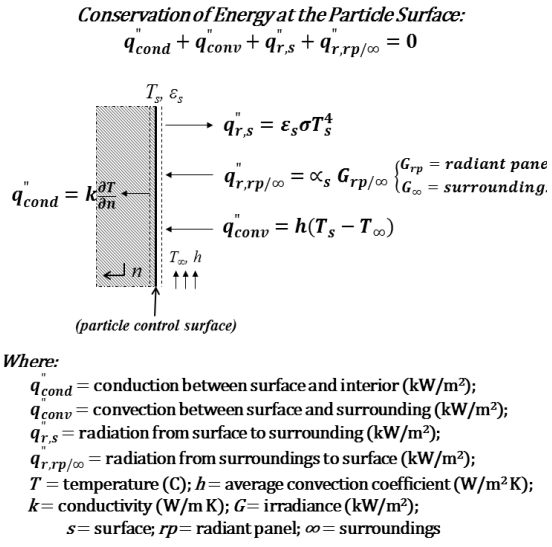

Fig. 4.9 Conservation of energy is the governing equation for the energy exchange at the fuel particle surface (the control surface of reference). The equation applies to all 4 surfaces of the particle cross-section; however, specific terms change due to differing boundary conditions.

10) The unmeasured irradiance to the particle's back side was from the surroundings (apparatus and room) having constant, uniform temperature T_∞ and emissivity ($\varepsilon_\infty = 0.9$). The irradiance to a small object in a large enclosure was expressed as

$$G_\infty = \varepsilon_\infty \sigma T_\infty^4 ,$$

where: σ = Stefan-Boltzman constant.

11) The fuel particle had constant emissivity ($\varepsilon_s = 0.9$) equal to its absorptivity (α_s), ($\varepsilon_s = \alpha_s$ is Kirchoff's Law; Incopera and DeWitt 2002, p. 739).

12) Air flow was either quiescent (free convection) or at a constant speed (forced convection); air temperatures were measured during particle heating.

13) Convection heat exchange was Newtonian (convective heat transfer term as represented in Fig. 4.9).

14) I applied Equation 9.27 to calculate the vertical surface average free-convection coefficient for quiescent air conditions and Equations 9.30 and 9.32 for heated upper and lower surfaces, respectively (all equations from Incopera and DeWitt 2002). The fuel particle was never colder than the surroundings; free convection always cooled the particle.

15) I used existing forced convection coefficient correlations for my fuel particle heat transfer model. Available convection correlations for noncircular cylinders were created for Reynolds numbers two or more orders of magnitude higher than my experimental flow conditions. Thus, I used correlations for circular cylinders at my experimental range of Reynolds numbers ($Re_L \approx 10^1$ to 10^2). I judged these to be a better approximation than using correlations for non-circular cylinders at significantly higher Reynolds number flows ($Re_L \approx 10^3$ to 10^5). I used the Hilpert correlations based on circular cylinders in cross flow (Incopera and DeWitt 2002, Equation 7.55b with Table 7.2). However, I could not use circular cylinder correlations for the thin rectangular particles (12 mm x 1 mm and 12 mm x 0.5 mm). Using the same Hilpert correlation equation (Incopera and DeWitt 2002, Equation 7.55b), I approximated correlation parameters for a vertical plate (Sparrow et al. 2004, Table 1) with guidance for low Reynolds numbers from circular cylinder correlation parameters (Incopera and DeWitt 2002, Table 7.2).

16) Experimental conditions were either free convection dominated or forced convection dominated for all particles tested using the Grashof (Gr_L) and Reynolds (Re_L) number ratio criteria: free convection neglected, $Gr_L/Re_L^2 << 1$; forced convection neglected, $Gr_L/Re_L^2 >> 1$ (Incopera and DeWitt 2002, p. 539).

17) The physical properties of air were determined by the particle-air film temperature in accordance with the convection coefficient correlations represented by Equations 9.27, 9.30, 9.32 and 7.55b from Incopera and DeWitt (2002).

18) Irradiance and air flow at the fuel particle were independent of one another.

19) The initial conditions were uniform fuel particle temperatures (surface and interior) in thermal equilibrium with the radiating surfaces of the surroundings with the temperature designated as that of the particle front side.

4.2.3.2 Numerical Methods

The governing equations that described the transient, nonlinear heat exchange of the fuel particle with radiative and convective boundary conditions are not analytically solvable. A numerical solution to the governing equations therefore involved converting the continuous equations to a set of linear finite difference equations that were iteratively computed for a small grid spacing and time step. Given initial and boundary conditions I numerically computed a mid-section, 2-dimensional grid of fuel particle temperatures at each time step.

The numerical model required that the grid size and time steps had to be small enough to approximate steady and uniform conditions for each nodal computation. With this requirement considered I used a finite difference, explicit numerical modeling method (Incopera and DeWitt 2002, Ch. 5; Patankar 1980, pp. 56-57). For the range of fuel particle sizes (1 mm to 12 mm), I used a range of grid lengths from 25 μm to 100 μm, and for all particles a time step of 5.0×10^{-4} seconds. For example, the 1-mm particle had a 41 x 41 grid of computational nodes at a spacing of 25 μm and the 12-mm particle had a 121 x 121 grid of computational nodes at a spacing of 100 μm. For the rectangular particles I used the 25 μm grid length. I verified that the explicit method computations were stable and the model results were independent of grid size and time step (Incopera and DeWitt 2002, Ch. 5).

To model fuel particle temperatures during the experiments, the model required input data that consisted of the initial and boundary conditions from the experimental test. The initial conditions specified a uniform particle and surface temperature. Prior to radiant

exposure the measured particle and air temperatures were all within plus or minus 1 degree Celsius of each other. Thus, the temperature of the surroundings was designated to be the fuel particle temperature. Radiation boundary conditions due to the radiant panel were constant and determined by the measured average irradiance for the front side and the fractional irradiances were calculated for the top and bottom sides. The radiation boundary conditions on the back side of the particle were from the large gray body surroundings (laboratory space and apparatus) at the constant initial particle temperature. The convection boundary conditions were the measured air temperatures during the test run and either quiescent for free convection or the measured air flow speed for forced convection. The numerical model was not adjusted to match any experimental fuel particle temperature data and the same version was used for all the experiments.

4.3 Results and Discussion

Fuel particle size strongly influenced the rate of particle heat exchange, primarily as result of the variation in convective flow length and boundary layer development of the radiantly heated sides. Irradiating 1, 3, 6, 9 and 12 mm fuel particles with free and forced convection resulted in only the 1 mm particles remaining below 300 C. The experiments and numerical model produced similar results (Fig. 4.10). The schlieren visualization of particle boundary conditions along with corresponding particle surface vertical temperature profiling indicated convective cooling as a principal mechanism of fuel particle heat exchange. The schlieren images and temperature profiles were strong evidence for the importance of convective cooling and fine fuel heat exchange. Using experiments and modeling I described the different influences of surface area-to-volume ratio (SAV) and particle boundary conditions. SAV determined particle response to surface temperatures but boundary conditions primarily govern the surface heat exchange and thus surface temperatures that drives fuel particle heating.

4.3.1 Fuel Particle Size and Convective Heat Exchange

In Chapter 3 I did an exploratory experiment that indicated significant heat exchange differences between a 1 mm and a 12 mm particle. As a follow-up to that exploratory experiment I did three replications of 1, 3, 6, 9 and 12 mm fuel particles under free convective conditions (quiescent air flow) and three replications of each particle size for forced convective conditions. The irradiance range was 29.8 kW/m^2 to 36.4 kW/m^2 and a forced flow of 1.00 m/s (± 0.02 m/s). All of the fuel particles but the 1 mm particles exceeded 300 C (front thermocouple) and were observed to significantly pyrolyze. To examine particle heat exchange, I used the numerical model with the measured initial and boundary conditions for each experimental test to predict particle temperatures for the last set of experiments. The results of the measured temperatures and the corresponding modeled temperatures are presented in Fig. 4.10.

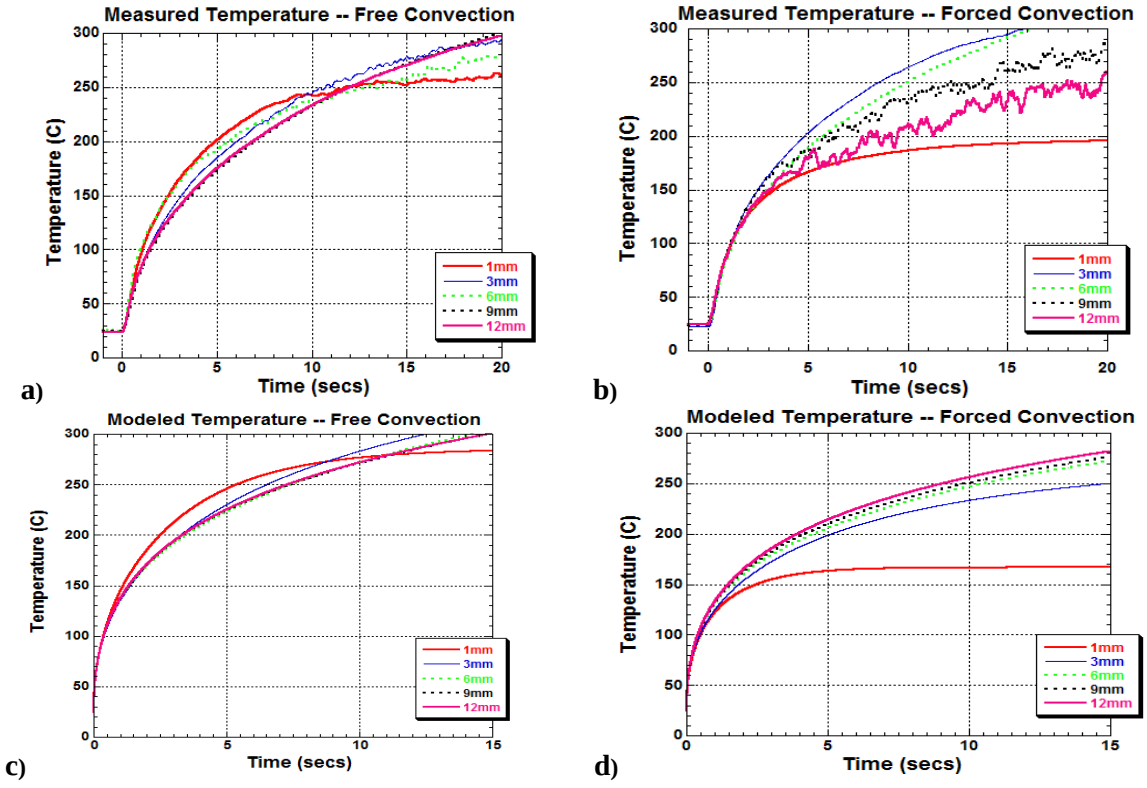

Fig. 4.10 Measured temperatures from experiments for a) free convection and for b) forced convection. Modeled temperatures given the measured experimental boundary conditions for c) free convection and d) forced convection. Note that model reliability is questionable beyond 275 C.

I found close correspondence between the modeled temperatures and the measured temperatures for free convection (Fig. 4.10) indicating that the model has largely captured the dominant heat exchange processes. That is, the ranking of the measured temperature profiles is closely approximated by the model results. In both the experimental data and model output, the initial 1 mm particle rate of temperature increase is greater than the coarser particles. With increasing surface temperature and thus increasing convective heat exchange, the 1 mm rate of temperature change reduces and at about 10 seconds all the fuel particles have similar front surface temperatures. Subsequently, the 1 mm temperatures vary with little increase while the coarser particle temperatures continue to rise.

Using the experimental data and modeled particle temperatures I found characteristics primarily contributing to the different 1 mm temperature profile compared to the coarser particles. First, the convective heat exchange (cooling) is higher for the 1 mm particle. The higher convective cooling of the 1 mm particle was demonstrated by the experimental results (Fig. 4.10) and consistent with the physical principals represented in the numerical model and the numerical modeling discussion above. And second, the higher surface area-to-volume ratio of the 1 mm particle results in a faster thermal response rate of the whole particle. From the experimental data I found significantly higher back-side temperatures for the 1 mm particle compared to the 3 and 6 mm particles and this difference begins within one second of the initial exposure (Fig. 4.11). Using the numerical model I provide the computed cross-sectional temperatures after 10 seconds (Fig. 4.12) when the three particles shared similar front side temperatures (Fig. 4.10a). It is clear from these diagrams that the 1 mm particle heats quicker, producing the initial rapid temperature rise. However, with greater convective cooling, the net heating approaches zero as the temperature profile of the 1 mm particle crosses the coarser particle profiles (Fig. 4.10a).

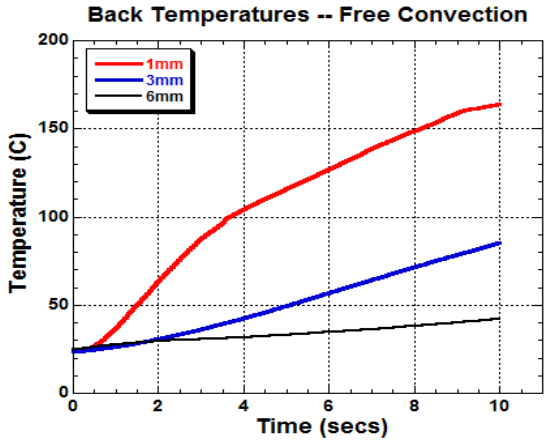

Fig. 4.11 These temperature profiles correspond to the back side thermocouples of the 1 mm, 3 mm and 6 mm particles in Fig. 10a.

The measured and modeled forced convection temperature profiles look similar;

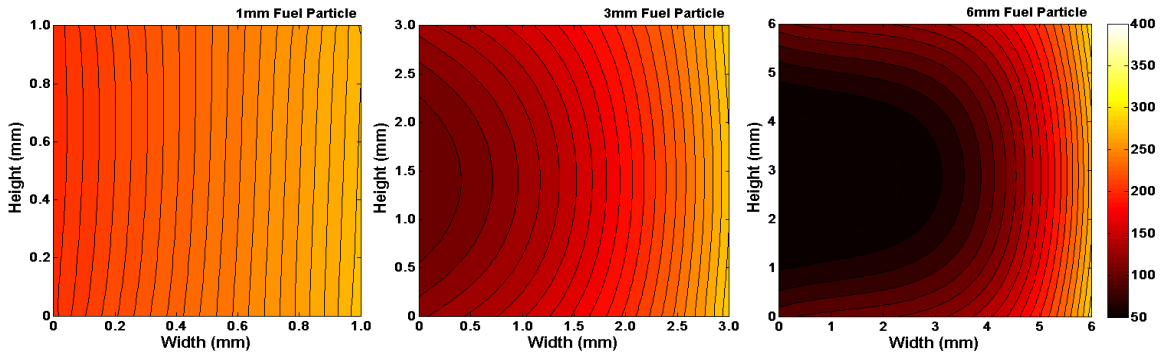

Fig. 4.12 These cross-sectional temperatures correspond to the 1mm, 3mm and 6mm particle temperature profiles shown in Fig. 10c at 10 seconds after the initial exposure.

however, the modeled temperatures are lower and the temperature profiles rank differently (Fig. 4.10b and c). A significant contribution to these differences is likely the forced convection heat transfer coefficients used in the model (see model assumption 15 above). These convection coefficients were developed for isothermal particle surfaces that were maintained by internal (±) heat generation with the convective heat transfer averaged for the entire particle (Incopera and DeWitt 2002, p. 387). A radiantly heating fuel particle does not have an isothermal surface (see next section) and the surface temperatures are not maintained by internal heat generation. The particle sides are heated differently resulting in different temperatures and thus, different convection heat transfer for each side. The larger the particle, the greater the internal temperature gradients (Fig. 4.12) and the greater difference in heat transfer between the sides. The calculated average convective heat transfer for the experimental particle does not describe the heat transfer for a specific side. For comparison, the modeled free convection coefficients (see model assumption 14 above) were calculated for each side. Although the available free convection coefficients were also for isothermal surfaces, the mid-surface temperature (the experimental data) closely approximates the average temperature for a radiantly heated surface (Incopera and DeWitt 2002, p. 546). If greater accuracy is required for fire spread modeling, convection coefficient correlations will need to be developed for the conditions of fuel particle heat exchange during wildland fire spread.

The measured temperature profiles exhibit wavy variations in temperature that did not occur in the modeled profiles (Fig. 4.10). For modeling particle temperatures, the radiative and convective boundary conditions were assumed constant. Variations about the mean (less

than ±0.2 kW/m^2) in measured irradiance were similar for all particle sizes. Variations in air temperatures during the tests were negligible compared to the variations in measured particle temperatures. In addition, the variations began after particle temperatures significantly increased and after the temperature rate of change decreased. This indicates the measured variations were from significant changes in convective heat transfer due to variations in air flow at the particle surface. Note that the finer particles varied for free convection but the coarser particles varied for forced convection. This suggests different factors for free and forced convection.

The experimental and corresponding modeling results presented in Fig. 4.10 are consistent with previous research by Tibbals et al. (1964). They found from their experiments and computations of radiant heating and ambient air cooling that both free and forced convective heat exchange was primarily determined by particle size and shape (conifer needles and deciduous leaves) and to a lesser extent orientation (cross flow and parallel flow). For their computations they used a maximum assumed growing season irradiance of 1.7 kW/m^2 while my experimental and modeled irradiances for flame front conditions were ~ 35.0 kW/m^2 (Fig. 4.10). Tibbals et al. (1964) used silver castings of spruce (*Picea*) and fir (*Abies*) needles to experimentally determine convection heat transfer coefficients. Because of the high conductivity of silver (silver, k = 425 W/mK; my fuel particle, k = 0.11 W/mK) their resulting coefficients were virtually particle averaged and nearly the same as the Hilpert cylindrical correlations (Incopera and DeWitt 2002, Equation 7.55b with Table 7.2) I used for my numerical model.

4.3.2 Convective Cooling and Boundary Conditions

I conducted demonstration experiments to gain further insight on how convection heat transfer varies by particle size. In Chapter 3 I suggested that the boundary layer increases with increased particle size. The increased flow length increases boundary layer development, and thereby convection heat transfer decreases (Incopera and DeWitt 2002, p. 409). Using schlieren optics I produced visualizations of boundary layers for radiantly heated 12 mm particles having free and forced convection (Fig. 4.13a and b). As described in the

Experimental Equipment section above, the dark areas correspond to an air density gradient from higher to lower densities. The dark pattern for free convection increases on the outer margin with upward flow length but the inner margin remains unchanged after a few millimeters. The absence of a dark patch at most of the particle surface indicates relatively uniform density and little ambient air flow for cooling. The exception is at the bottom of the heated surface especially for free convection but also for forced convection.

I instrumented the irradiated face with five, vertically arranged thermocouples (Fig. 4.7) to associate temperature profile rankings with the schlieren images. The 12 mm x 12 mm and 12 mm x 1 mm particles each had a different irradiance between 28.4 kW/m^2 and 30.4 kW/m^2 for both free convection (quiescent air) and forced convection (1.00 m/s, ± 0.01 m/s).

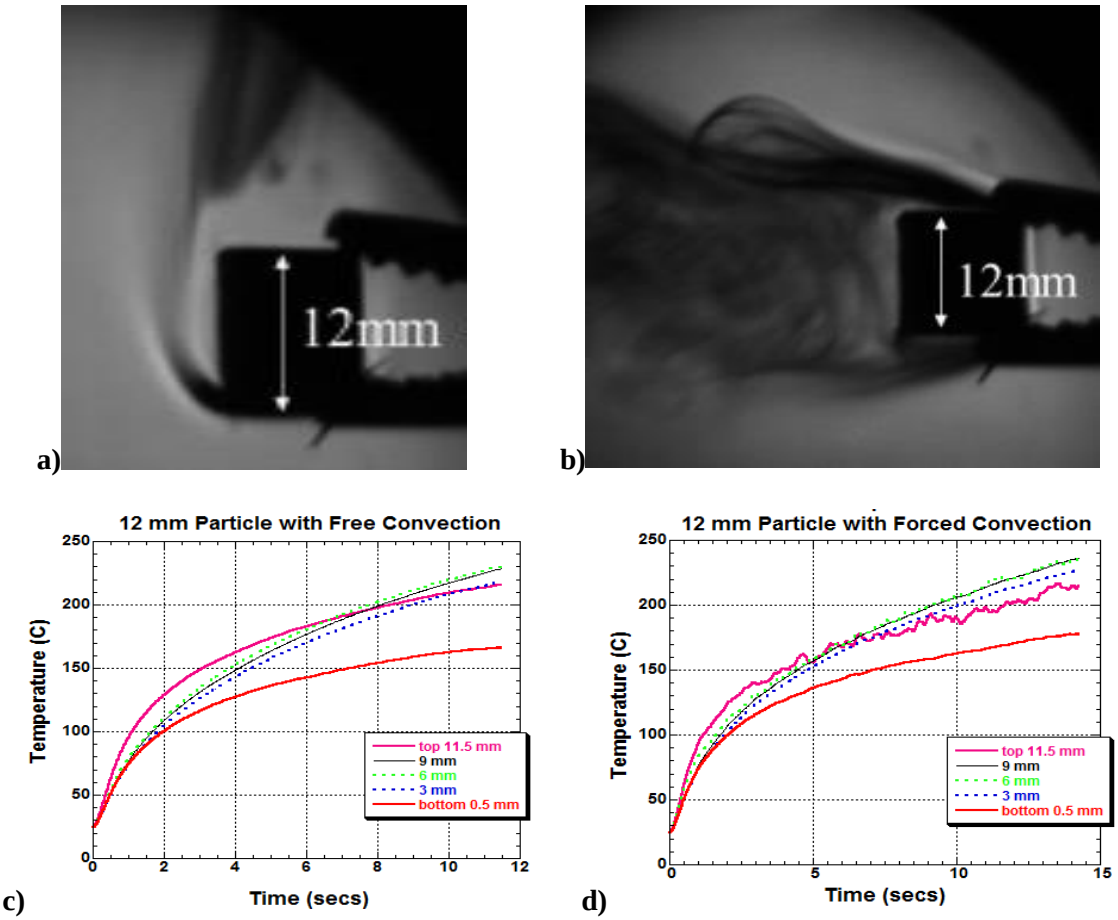

Fig. 4.13 a) This schlieren image is of free convection buoyant flow at the radiantly heated left side of a 12 mm fuel particle. b) This schlieren image is of forced convection, flowing from right to left around a 12 mm fuel particle being radiantly heated on the left side. c) and d) The temperature profiles are from 5 vertically arranged thermocouples on the heated side of the particle exposed to similar irradiance and air flow that occurred during the schlieren images.

All of the experimental runs resulted in similar temperature profiles (Fig. 4.13 c and d) both in temperatures and rankings of the profiles. The 0.5 mm thermocouples had the lowest temperatures with thermocouples at vertically higher positions having higher, comparable temperatures (Fig. 4.13 c and d). Both the free and forced convection temperature profiles are consistent with the schlieren images. The 0.5 mm position temperatures correspond to the dark area contact with the vertically higher thermocouple temperatures corresponding to more uniform conditions (Fig. 4.13). In addition, I noticed from different sets of experiments that 12 mm x 12 mm, 12 mm x 1 mm and 12 mm x 0.5 mm fuel particles exposed to 30 – 35 kW/m^2 irradiances resulted in a low char strip at the bottom of the particle (Fig. 4.14). The results from these three independent methods support convective cooling being the primary mechanism for cooling a radiantly heated particle and flow length/boundary layer development determining the rate of cooling.

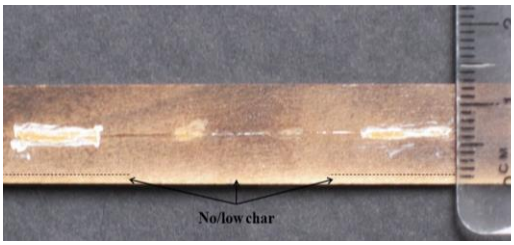

Fig. 4.14 This 12 x 1 mm particle with its low char strip at the bottom is similar to low char strips that appeared on all the particles with 12 mm heights. I have identified the low char strip with two thin dashed lines on either side of the particle mid-section. The low char strips varied in width from 0.5 mm to 1 mm.

My findings of boundary layer development using schlieren visualization associated with vertical surface temperatures as an indicator of free and forced convective heat transfer is consistent with boundary layer theory (Incopera and DeWitt 2002; Kays et al. 2005) and interferograms of free convection thermal boundaries presented by Alvares et al. (1970). However, the limited range of my irradiances (less than ~ 35.0 kW/m^2) may not address higher irradiances where convection and thus, particle geometry does not significantly influence surface cooling. For high intensity wildland fires such as crown fires (Stocks et al. 2004) the maximum average flame temperatures were about 1300 K (Butler et al. 2004; Taylor et al. 2004). From the Stefan-Boltzman law (Incopera and DeWitt 2002, Eq. 12.28), the maximum emissive power at 1300 K is 162 kW/m^2 so the maximum irradiance possible would be 162 kW/m^2. Alvares et al. (1970) report a critical irradiance of 167 kW/m^2 above which heating to ignition is not influenced by the vertical surface length. Martin (1964) reports a critical irradiance of 209 kW/m^2. This indicates that particle surface length influences convective cooling within the expected range of wildland fire irradiances and greater than my experimental radiant conditions.

4.3.3 Boundary Conditions and Surface Area-to-Volume Ratio (SAV)

In Chapter 3 I used reasoning based on physical principles to find that surface area-to-volume ratio (SAV) would not determine fuel particle surface heating. Rather, SAV would determine the fuel particle thermal response given the surface temperatures. I confirmed this result using experiments and modeling of radiantly heated fuel particles having different surface lengths and SAVs with free and forced convection.

I irradiated fuel particles having cross-sections of 1 x 1 mm, 12 x 12 mm, 12 x 1 mm and 12 x 0.5 mm having SAVs of 4000 m^{-1}, 333 m^{-1}, 2167 m^{-1} and 4167 m^{-1}, respectively. As with the previous particle heating experiments irradiance of 35.0 kW/m^2 (± 0.1 kW/m^2). The experimental results for all the tests were similar so I used the more precise radiant exposures of the last replication for modeling and forced convection wind speeds of 1.00 m/s (± 0.01 m/s). As before, I used the specific initial conditions of each experimental run for the modeling inputs.

The experimental results indicate SAV does not determine the convective cooling. Importantly, for all the experimental results, the 4000 m^{-1} (1 x 1 mm) fuel particle has the lowest final temperature and the 4167 m^{-1} (12 x 0.5 mm) particle has the highest (Fig. 4.15). In addition, for the three fuel particles with a height of 12 mm, the SAV ranking is the same as the temperature profile ranking; that is, the higher the SAV the higher the front side surface temperatures.

The model results have the same relative ranking of the particle temperature profiles as the experimental results (Fig. 4.15). The analysis I used in the *Fuel Particle Size Experiments* section regarding heat exchange at the particle surface and SAV (Fig. 4.12) equally applies to these experiments. Note that the same 1mm x 1 mm free convection temperature profile relative to the other particle profiles (Fig. 4.10) occurs with these free convection temperature profiles (Fig. 4.15a and c). The experimental and modeled temperature profiles (Fig. 4.15) along with the cross-sectional temperatures (Fig. 4.16) for forced convection indicate significantly faster thermal response rates for the 0.5 mm and 1.0 mm thick particles than the 12 mm x 12 mm particle. Given the same irradiance, the higher 12 mm x 1 mm particle temperatures compared with the 1 mm x 1 mm particle temperatures

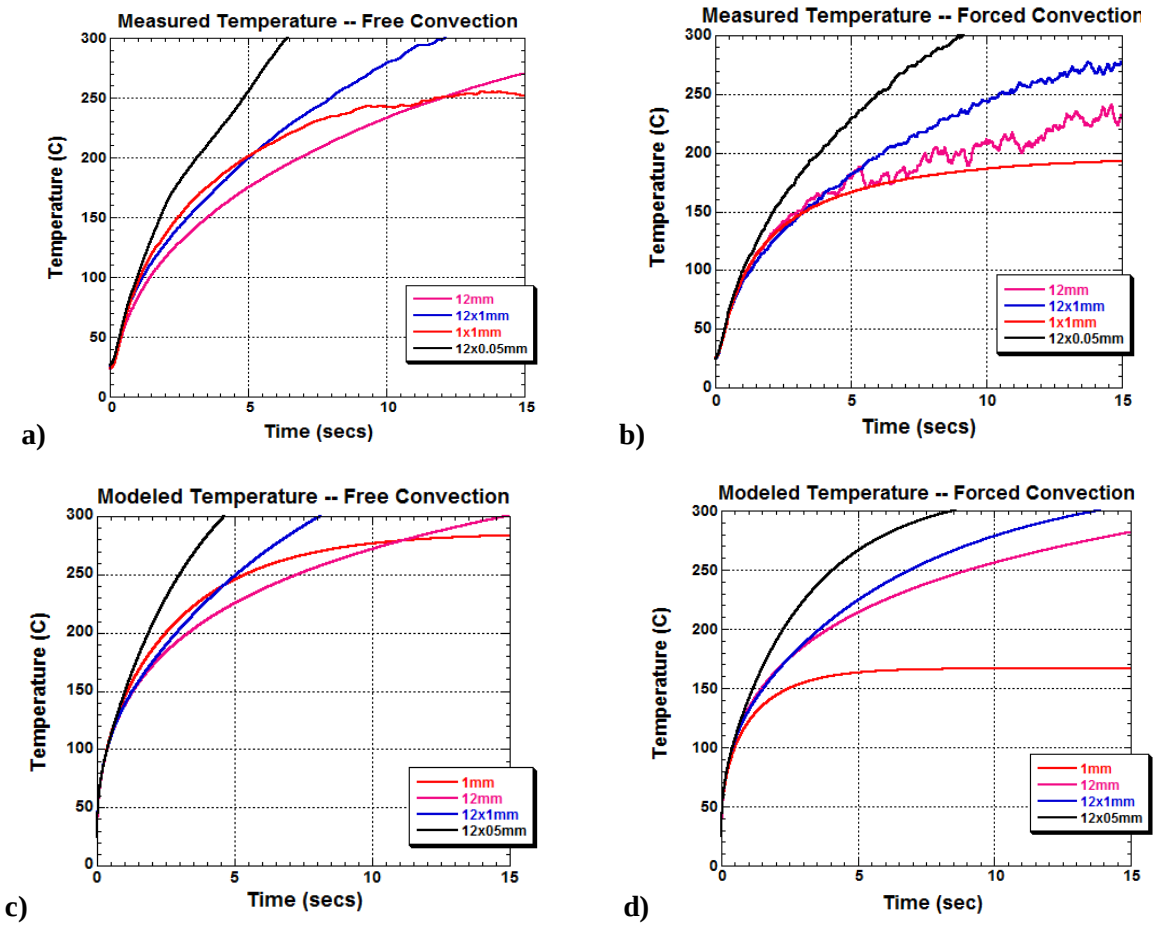

Fig. 4.15 Graphs a and b are experimental temperature profiles from the radiantly heated side of a fuel particle. With the exception of the 1 mm x 1mm particle, the other particles have heated sides that are 12 mm in height. Graphs c and d are the results of modeled heat exchange based on the specific initial and boundary conditions for each particle.

indicates significantly greater 1 mm x 1 mm particle convective heat exchange. Based on the experimental and modeling results I describe the effects of surface length and SAV on fuel particle surface temperatures and thermal response in the following:

1) The surface length for free and forced convection determines boundary development – the shorter the length the less the boundary development and the greater is the convective heat exchange. Regardless of SAV, the 12 mm high particles had similarly low convective heat exchange compared to the 1 mm x 1 mm particle (Fig. 4.16).

2) The SAV determines the thermal response of a particle to the changing surface temperatures. For similarly low convective heat exchange nearly the entire 12 mm x 0.5 mm particle is heated compared to the 12 mm x 12 mm particle (Fig. 4.15a and c).

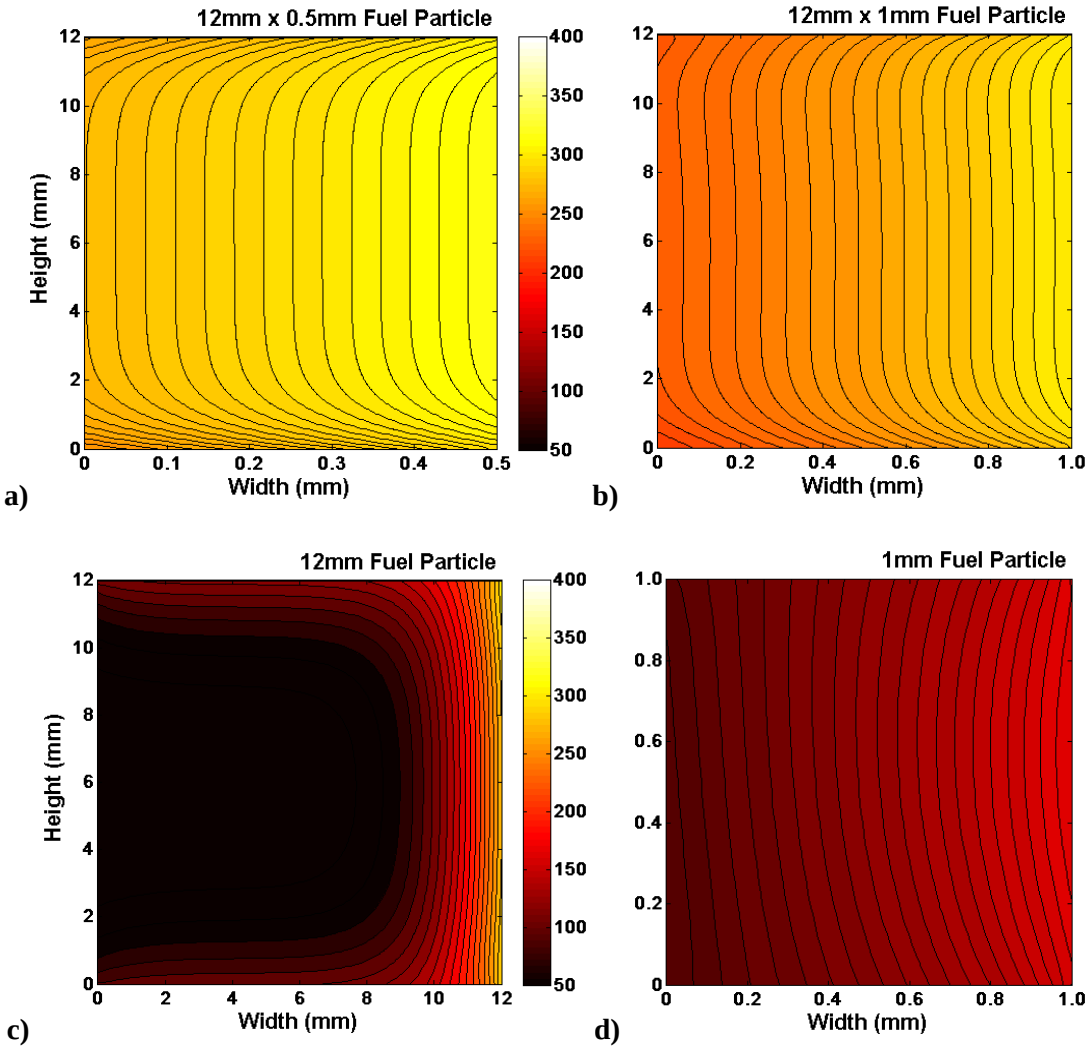

Fig. 4.16 These diagrams are the modeled forced convection cross-sectional temperatures of the fuel particles in Fig. 12. The 2-dimensional temperature field is for the last time step (maximum temperatures) of the model run. Temperatures are in degrees Celsius. Note that the graphs are square but the scales range from 0.5 mm to 12 mm.

Notably, Tibbals et al. (1964) found from their computational model that an irradiated deciduous leaf attained nearly twice the temperature difference as a conifer needle (leaf – air). This model finding is qualitatively consistent with my experimental and computational findings of flow length influences on convective heat exchange and the above findings regarding boundary conditions and surface area-to-volume ratio (SAV). However, Tibbals et al. (1964) assumed the difference between leaves and needles was due to SAV without experimentally examining the difference between surface heat exchange due to boundary conditions and thermal response rate due to SAV.

4.4 Conclusions

In concert with the experiments, I developed a numerical heat transfer model to understand the fuel particle heat exchange processes during the experimental conditions. Based on the experiments and modeling I showed that particle size influences convective heat exchange. For fine fuels such as my experimental 1 mm particles and smaller, convective cooling can result in insufficient radiation heating to ignite fine fuel sizes. Using schlieren images and multi-level temperature measurements I related boundary layer development and convective heat exchange to surface temperatures. Based on these experiments I showed how particle size related to convective length governs convective heat transfer rates and thus particle heating. With experiments and modeling I showed that SAV does not determine particle boundary conditions and thus, surface temperatures. The 12 mm x 0.5 mm and 1 mm x 1 mm fuel particles have similar SAVs but had significantly different heating characteristics due to the longer 12 mm length. Based on the experiments and modeling I showed how fuel particle heating leading to ignition involves two interrelated processes – the convective heat exchange between the particle surface and its boundary conditions, and subsequently the SAV determining the thermal response of the particle. With these experiments and modeling, I have taken initial steps towards theoretically understanding the heat exchange processes responsible for fuel particle heating during wildland fire spread.

4.5 Literature

Alvares NJ, Blackshear PL Jr, Kanury AM (1970) The influence of free convection on the ignition of vertical cellulosic panels by thermal radiation. *Combustion Science and Technology* **1**, 407-413.

Bell JH, Mehta RD (1988) Contraction design for small low-speed wind tunnels. NASA – Stanford University, Joint Institute for Aeronautics and Acoustics, Technical Report JIAA-TR-84. (Stanford, CA)

Butler BW, Cohen J, Latham DJ, Schuette RD, Sopko P, Shannon KS, Jimenez D, Bradshaw LS (2004) Measurements of radiant emissive power and temperatures in crown fires. *Canadian Journal of Forest Research* **34**(8), 1577-1587.

Drysdale D (1998) 'An Introduction to Fire Dynamics.' (John Wiley: New York)

Fairbridge C, Ross RA, Sood SP (1978) A kinetic and surface study of the thermal decomposition of cellulose powder in inert and oxidizing atmospheres. *Journal of Applied Polymer Science* **22**, 497-510.

Martin S (1965) Diffusion-controlled ignition of cellulosic materials by intense radiant energy. In 'Tenth Symposium (International) on Combustion.' 17-20 August 1964, Cambridge, England. pp. 877-896. (The Combustion Institute: Pittsburgh, PA)

Medtherm Corporation. (1997) 'Heat Flux Transducers.' Bulletin 118. (Huntsville, Alabama)

Mehta R D; Bradshaw P (1979) Design rules for small low-speed wind tunnels. *Aeronautical Journal*, **83**(827), 443-449.

Oreskes N, Shrader-Frechette K, Belitz K. (1994) Verification, validation and confirmation of numerical models in the Earth sciences. *Science* **263**, 641-646.

Patankar SV (1980) 'Numerical heat transfer and fluid flow.' (Hemisphere Publishing: Washington, DC)

Sasaki S, Masuda H, Higano M, Hishinuma N (1994) Simultaneous measurements of specific heat and total hemispherical emissivity of chromel and alumel by a transient calorimetric technique. *International Journal of Thermophysics* **15**(3), 547-565.

Settles GS (2001) 'Schlieren and shadowgraph techniques: Visualizing phenomena in transparent media.' (Springer-Verlag: New York)

Simmons RF (1995) Fire Chemistry, Ch. 7 'Combustion Fundamentals of Fire.' (Academic Press: New York)

Sparrow EM, Abraham JP, Tong JCK (2004) Archival correlations for average heat transfer coefficients for non-circular and circular cylinders and for spheres in cross-flow. *International Journal of Heat and Mass Transfer* **47**, 5285-5296.

Stocks BJ, Alexander ME, Lanoville RA (2004a) Overview of the International Crown Fire Modelling Experiment (ICFME). *Canadian Journal of Forest Research* **34**, 1543-1547.

Taylor SW, Wotton BM, Alexander ME, Dalrymple GN (2004) Variation in wind and crown fire behaviour in a northern jack pine – black spruce forest. *Canadian Journal of Forest Research* **34**, 1561-1576.

Tibbals EC, Carr EK, Gates DM, Kreith F (1964) Radiation and convection in conifers. *American Journal of Botany* **51**(5), 529-538.

Tillman DA, Amadeo JR, Kitto WD (1981) 'Wood Combustion.' (Academic Press: New York)

Chapter 5

Fuel Particle Heating Leading to Ignition in Spreading Laboratory Fires

5.1 Introduction

Ignition of wildland fuel particles depends upon heating by radiation and convection (Fons 1946) but the relative roles of heat transfer mechanisms have remained uncertain (Fang and Steward 1969; Baines1990; Finney et al. 2013). To investigate the physics of heat transfer and particle heating, I used laboratory experiments and mathematical modeling (reported in Chapter 4). These studies involved individual wooden fuel particles subjected to a well characterized, controlled, and constant radiant heat flux. From these studies, I found that particle size and shape strongly affected the heating response to radiation because the surface geometry controlled the potential for convective cooling by ambient air flow (Chapter 4). Using both laboratory experiments and modeling, I determined that free and forced convection by ambient air effectively cooled fine particles with short boundary-layer flow-length such that pyrolysis and thus ignition did not take place for fine particles under conditions in which coarse particles ignited. I concluded that radiation is not sufficient for fine fuel ignition and, therefore, that convective heating is critical. Convective heating is known to exhibit the same relationships to particle surface geometry as convective cooling (Incropera and DeWitt 2002), being far more efficient for fine particles than coarse ones. In this chapter, I investigate how convective and radiative heating occurs in spreading fires.

In contrast to the constant and persistent radiant fluxes used in my previous experiments (Chapter 3 and 4), spreading fires produce both radiation and convection that vary in time and limited to a finite period, as the flame front approaches each particle. Indications of how convective heating can take place come from recent experiments on flame characteristics using repeated wind-driven laboratory burns (Finney et al. 2014). Flames in these experiments were observed to extend forward from the flame front with predictable average frequencies and impinge intermittently on fuel particles within close proximity to the

leading edge of the flame front. Analysis of high speed video (Finney et al. 2014) suggested that flame contact was necessary for heating to ignition. Rothermel and Anderson (1966); Fang and Steward (1969); and Baines (1990) made similar observations. If radiation heating from the flame front is insufficient for fine fuel ignition then fire spread must occur by convective heating through some variation of the following sequence:

- The flame front radiation heats fuels ahead resulting in increased fuel temperature but not sufficiently to produce pyrolysis capable of piloted ignition;
- Fuels are convectively heated by intermittent contact with flames laterally extending from the non-steady flame front;
- At sufficient frequency and duration, sufficient pyrolysates are produced; and a
- Combustible pyrolysate-air mixture is pilot-ignited by flames;
- The fire advances to the ignited fuel particles to become part of the flame front.

5.2 Methods

I investigated fuel particle heating using spreading fires in the laboratory to measure radiation and convection and a numerical model to test the relative influences of measured radiation and convection in producing the fuel particle heating. Surface temperature of wood particles was measured along with the adjacent irradiance and gas temperatures during experimental burns in the large wind tunnel at the Missoula Fire Science Laboratory (MFSL, Rothermel and Anderson (1966) describe the facility). These measurements were used to model the particle heat exchange in response to its thermal boundary conditions.

5.2.1 Laboratory Fuel Beds

The fuel beds were engineered using 1.25 mm thick cardboard (Finney et al. 2013b). Each "comb" was laser cut from a 1.2 m long sheet to specified tine heights and widths (Fig. 5.1). Fuel particles were mounted on combs having tine widths of 2.31 mm, 6.20 and 12.4 mm and comb heights ranging from 102 mm to 203 mm. To change flame zone characteristics, fuel beds were constructed with combs at various spacing widths between rows and combinations

of combs with different tine heights and widths. For fuel beds with a combination of more than one comb size, fuel particles were mounted on the combs with the tallest tines. Fuel bed dimensions were 2.4 meters wide by 6 meters long and ignited as a line along the upwind edge. Fires spread the entire bed length with a largely linear front (Fig. 5.2). Air entrainment around the edges was minimized by using paper sideliners treated with diammonium phosphate flame retardant (see Finney et al. 2013b). Particle instrumentation was installed in the bed within 30cm of the down-wind edge.

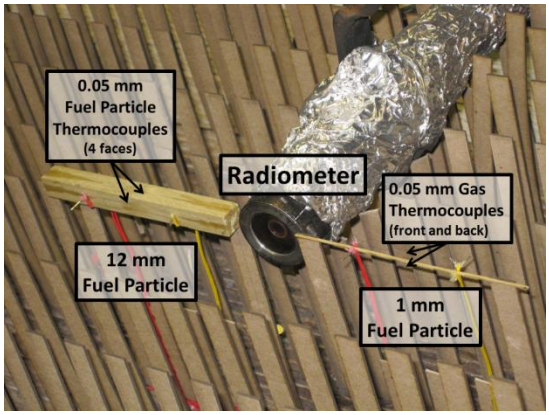

Fig. 5.1 The 1-mm and 12-mm fuel particles were instrumented with 50-µm thermocouples. The 1-mm particle had thermocouples embedded in the centers of front and back faces only; the 12mm particle had thermocouples centered in four faces (ends are neglected). The wood particles were attached to the top of a "fuel comb" in the cardboard fuel bed. The comb fuel bed shown had tines 152 mm tall by 12.4 mm wide and spaced 46 mm between rows. I used a water-cooled radiometer at fuel particle height to measure particle irradiance and 50-µm thermocouples to estimate gas temperatures.

5.2.2 Particle Instrumentation

Machined yellow poplar (*Liriodendron tulipiferia*) wood particles with 1 mm and 12 mm square cross-sections and 120 mm long were instrumented with fine thermocouples (K Type, 50 µm diameter). The 1 mm fuel particles had thermocouples embedded at the center of the front (facing the approaching flames) and back vertical surfaces; the 12 mm particles had thermocouples embedded at the center of each vertical and horizontal surface (front, top, back and bottom) (Fig. 5.1). The fuel particles were horizontally attached to the top of precisely constructed cardboard "comb" fuel beds (Finney et al. 2013b). The particles were located 130 mm to one side of

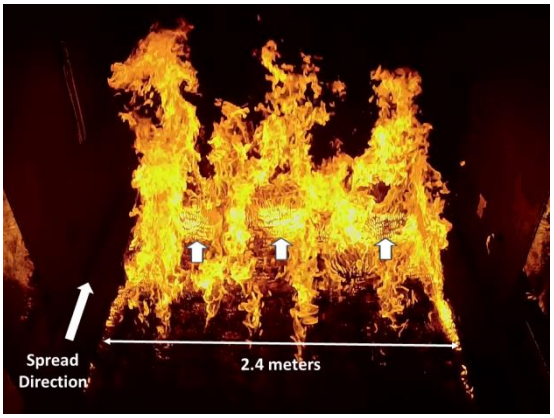

Fig. 5.2 The flame zone of a laboratory fire spread experiment (experiment 'e' in Table 5.1) from behind as it spreads away from the viewpoint. Three arrows point to locations where buoyancy generated downdrafts push flames downward and forward toward unburned fuels at the front (Finney et.al. 2014).

the center line of the 2.44 m wide fuel bed in the experimental wind tunnel burning facility at the MFSL.

The fuel particle irradiance was measured during the approaching flame front. For the irradiance measurement, I used a water-cooled Medtherm® radiometer placed even with the fuel particles (Fig. 5.1). The radiometer was calibrated using a black body cavity having temperatures in the range of a spreading flame front (1000 K – 1400 K). Gas temperatures immediately adjacent to the particles were measured using fine thermocouples (K Type, 50 μm) suspended approximately 5 mm from and centered at the particle's front and back vertical faces (Fig. 5.1).

All experimental fire measurements were taken at a sampling rate of 500 per second (500 Hz). At this rate, the sampling time interval (0.002 sec) is less than one-half the time constant (0.04 sec) of the fastest responding sensor (thermocouple) and meets Nyquist frequency aliasing criteria (Fritschen and Gay 1979). Measurements began before fuel bed ignition and continued through fuel particle ignition and burning. I used persistent particle and gas temperatures above 400 C as the criterion for particle ignition and confirmed this determination with video recordings whenever possible.

5.2.3 Numerical Model

I predicted 1 mm fuel particle temperatures using a two-dimensional numerical model of transient heat transfer (see Chapter 4) for the fire spread experiments. As in Chapter 4, I used the model as a heuristic tool and a theoretical basis for further examining the physical processes of the 1 mm particle heat exchange during the fire experiments. The model calculates fuel particle surface and interior temperatures for the mid-section profile given the measured initial conditions and radiative and convection boundary conditions during an approaching flame front. For the wind tunnel experiments, I altered the model assumptions (see Chapter 4, assumptions 9, 12, 14 and 16) because of the conditions specific to the fire spread experiments. These different assumptions are as follows:

- The fuel particle irradiance from the flame front was only absorbed by the vertical side facing the flame front.
- Quiescent conditions did not exist during the fire spread experiments. Two wind speeds were assumed based on the measured gas temperature at the fuel particle. For temperatures less than 500 C, the air speed was the average wind tunnel air speed (assumed constant) and, for temperatures 500 C and greater, the gas speed was 7 times the air speed (based on my observations from video taken during the experiments).
- The 1 mm fuel particle was always forced convection dominated.
- The gases at 500 C and greater had the same physical properties as air.

The computation of 1 mm particle temperatures began with the initial ambient air (gas) temperatures and irradiance of the wind tunnel surroundings before fire spread, and of initial measured front surface particle temperature assumed to be uniform through the interior. Temperatures were computed for the entire two-dimensional particle cross-section but only the front surface, center temperature corresponding to the measured front surface temperature was used for comparison.

5.3 Results

Seven fire spread experiments were conducted with instrumented fuel particles (Table 5.1). Based on the flame lengths I observed (Table 5.1), I suggest the fire characteristics are similar to those burning fuel beds composed of short grasses or surface forest litter under dry conditions and low wind speeds.

All of the seven experiments produced similar time profiles of the measured boundary conditions and particle temperatures. I chose three of the experiments, d, e and f, as example results. Similarly, the physical modeling using the measured boundary conditions and calculating particle temperatures resulted in similar results. In the following discussion I have presented experiment d as an example comparison between measured and modeled results as well as an analysis of the particle heat transfer mechanisms.

Table 5.1. Fire spread conditions in laboratory experiments. Bed depth was the maximum fuel comb height. Wind speed was a constant wind tunnel setting. Rate of spread was measured in the middle of the fuel bed using a series of 64 thermocouples oriented in the spread direction. Flame length and spread rate measurements were made beyond the influence of the ignition. Flaming depth was the estimated distance from the forward edge of the propagating flame front to the rear where coherent flaming ceases due to fuel consumption. The fuel particle irradiance range is from the last four seconds before the 1 mm particle ignition.

Fire Exp. ___	Bed Depth (m)	Wind Speed (m/s)	Rate of Spread (m/s)	Flame Length (m)	Flaming Depth (m)	Irradiance [4 s to ign.] (kW/m^2)
a	0.15	0.34	0.028	1.0	0.54	20 - 29
b	0.15	0.34	0.024	1.2	0.41	20 - 30
c	0.15	0.22	0.016	1.4	0.57	22 - 40
d	0.15	0.56	0.032	1.2	0.68	17 - 34
e	0.20	0.34	0.031	1.3	0.56	25 - 44
f	0.15	0.67	0.034	1.5	0.60	13 - 25
g	0.12	0.34	0.031	0.6	0.28	10 - 22

5.3.1 Comparison of 1 mm and 12 mm Particle Temperature

I found in every experiment, regardless of the wind speed, spread rate, or flame dimensions, that 1 mm particles responded more quickly to changing thermal conditions compared to the 12 mm particles (Fig. 5.3). Within the last four seconds of the approaching flame front, the temperatures of the 1- mm particle rapidly increased resulting in sustained ignition while the 12 mm particle had not yet ignited (Fig. 5.3). In all seven experiments, the 1 mm particles

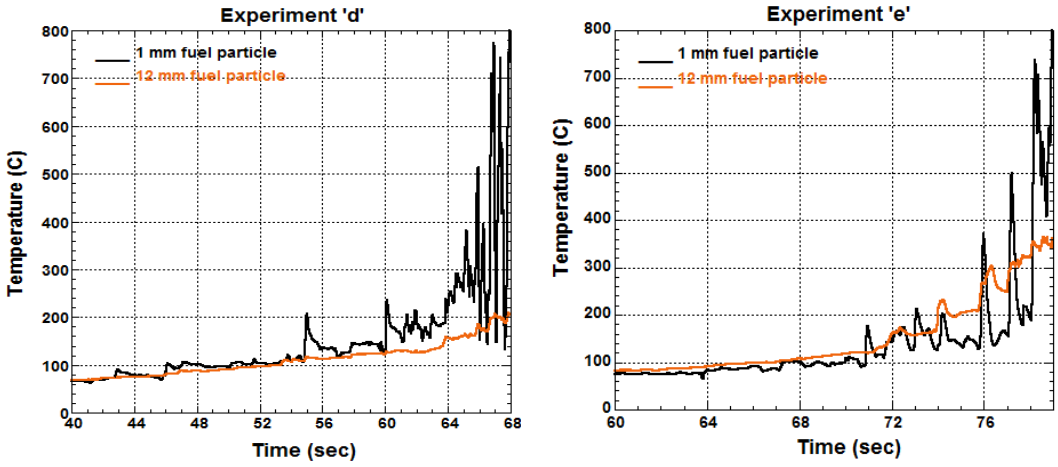

Fig. 5.3. The 1mm particle (black) had large temperature variations compared to the 12mm particle (orange) for all experiments as exemplified by these results of experiments d and e (see Table 5.1). In the last second, the 1mm particle has ignited in both experiments while the 12mm particle has not. In experiment d, the flame front had not reached the 12mm particle when the 1 mm particle ignited. In Experiment e the flame front contacted the 12mm particle at 77 seconds and the 1mm at 78 seconds but the 1mm particle ignited before the 12-mm particle.

ignited (exceeded 400 C) before the 12 mm particles.

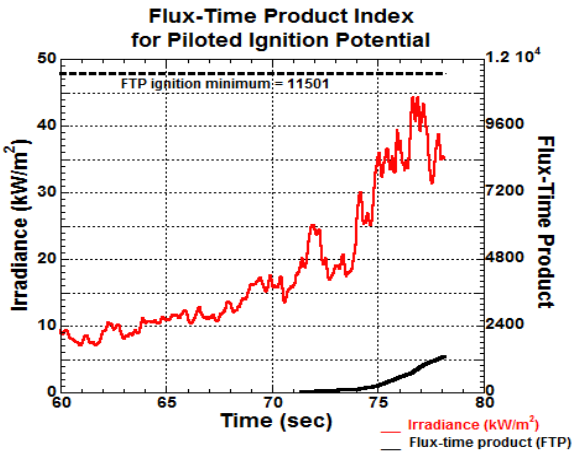

Fig. 5.4 The FTP (solid black) is calculated based on the measured irradiance (red, from Experiment e). If the minimum FTP for ignition (broken black) is met and exceeded by the actual FTP, sustained ignition is likely.

5.3.2 Radiation Heating Alone is Insufficient for Fuel Particle Ignition

None of the experiments produced measured fuel particle irradiances capable of piloted ignition before the flame front arrived at the particle. The piloted-ignition correlation equation (Cohen 2004) discussed in Chapter 3 indicates that a flux-time product of 11501 is required for radiation to ignite flat wall surfaces. Yet, even with the maximum measured irradiance of 44 kW/m^2 among all experiments (Table 5.1, Experiment 'e') the 1mm particle ignited when the FTP value of only 1313 was achieved (Fig. 5.4). This means that at a constant irradiance of 44 kW/m^2, the 12-mm particle time-to-ignition based on the FTP calculation would be about 22 sec. which is longer than the actual duration of significant irradiance during the experiment (Fig. 5.4). Because 44kW/m^2 was the maximum irradiance measured in any of these experiments, radiation heat transfer was clearly insufficient for particle ignition in any of the experiments.

5.3.3 Measured Thermal Boundary Conditions

The thermal boundary conditions shown in Fig. 5.5 are the measured irradiance for both the 1-mm and 12-mm particles and the front gas thermocouples of each particle (Fig. 5.1). The boundary conditions of Experiments e, d and f shown in Fig. 5.5 largely cover the experimental range of maximum irradiances and ambient wind speeds even though the experiments resulted in similar spread rates and flame lengths (Table 5.1). When experiments e, d and f are arranged in descending order of maximum measured irradiance (Fig. 5.5), their corresponding ambient wind speeds are in increasing order. Despite having similar fire

Measured 1-mm and 12-mm Irradiance and Gas Temperatures

a) [0.34 m/s wind speed]

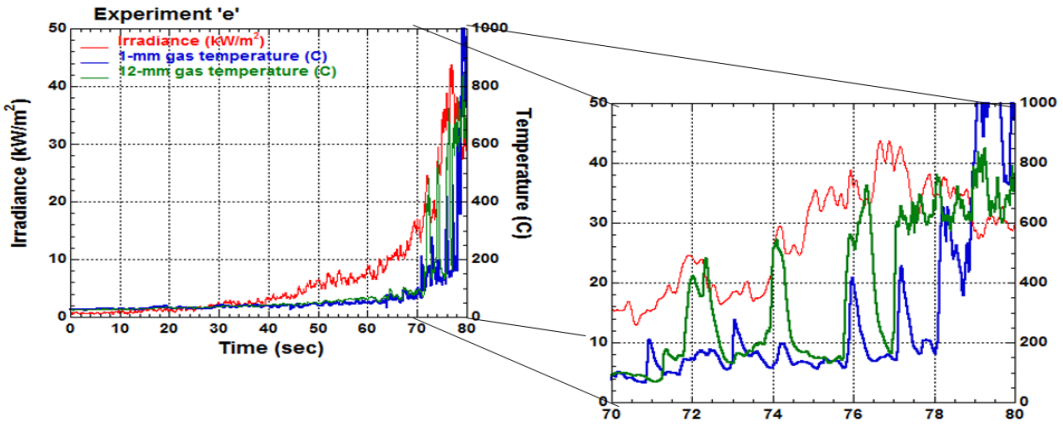

b) [0.56 m/s wind speed]

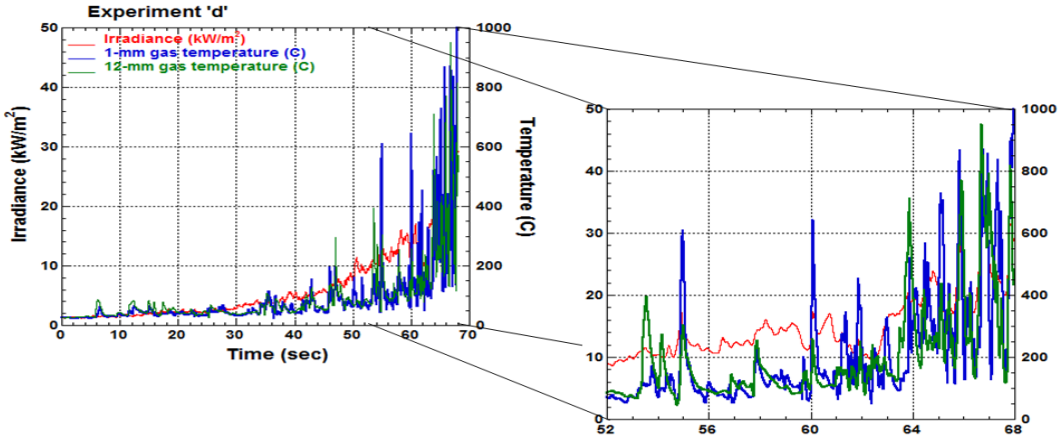

c) [0.67 m/s wind speed]

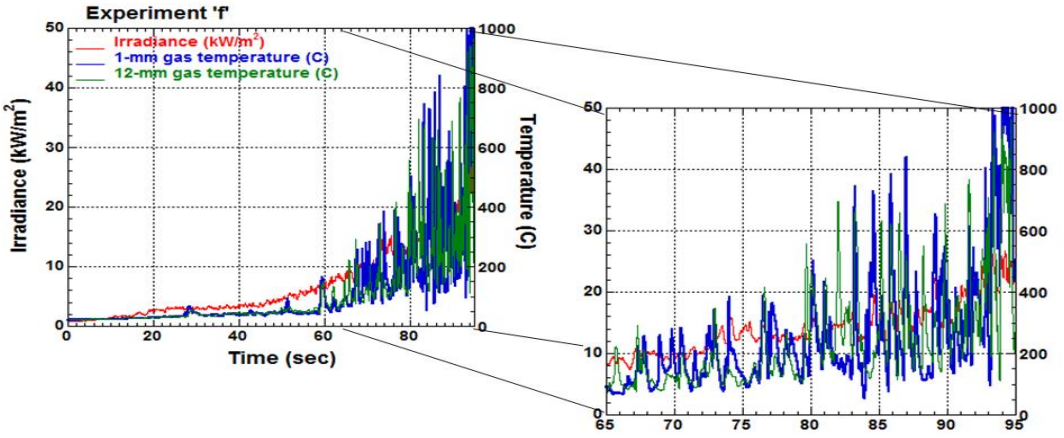

Fig. 5.5 Graphs a, b, and c correspond to Experiments e, d and f (Table 5.1), respectively. The experiments are ordered downward by decreasing maximum irradiance that corresponds to increasing ambient (wind tunnel) wind speed. All the graphs have the same y-axes but the x-axes vary. Left graphs range from negligible flame front exposure to flame front arrival. Expanded (right) graphs begin when convective pulses begin to exceed 200 C. Note: the period of gas temperature pulses above 200 C from the expanded graphs is about 8 seconds, 15 seconds and 30 seconds for graphs a, b and c, respectively.

behavior (spread rate and flame length, Table 5.1), the radiation and convection boundary conditions are significantly different. Further, gas temperature profiles differed among experiments. With increasing wind speed, the particle experiences higher gas temperatures for longer periods as evidenced in the full profile graphs (left side of Fig. 5.5). The expanded graphs (right side of Fig. 5.5) indicate increased frequency of gas temperature pulses greater than 200 C and these pulses extend over longer periods. Pulses greater than 200 C began about 8 seconds, 15 seconds and 30 seconds before flame front arrival for Experiments e, d and f, respectively. From the average spread rates of each experiment (Table 5.1), the times corresponded to distances when the flame front was 0.23 meters, 0.45 meters and 0.97 meters from the instrumented fuel particles. Pulses having temperatures greater than 600 C produce enough visible light to be seen. For example, an observer could have seen flame pulses contacting particles out to 0.13 m ahead of the leading edge of the flame zone during experiment d (Fig. 5.5b at time 64 seconds) and 0.41 ahead during Experiment f (Fig. 5.5c at time 83 seconds).

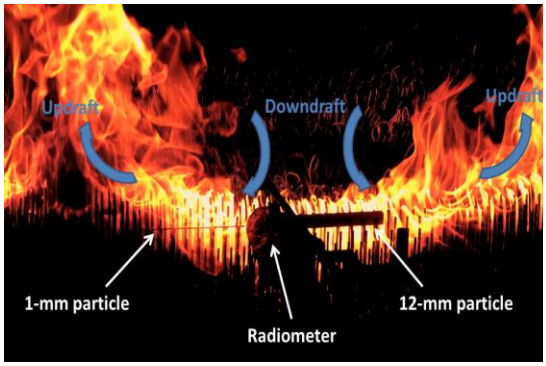

Fig. 5.6 The flame front is approaching the fuel particles during Experiment 'g' (Table 5.1). Note the downdraft (down arrows) forcing flame down and forward from burning comb fuel. This produces intermittent convective heating of the 1-mm and 12-mm fuel particles.

The phenomenon of high temperature gas pulses extending ahead of the flame zone occurred in all experimental conditions reported here. Finney et al. (2014) observed flame peaks and troughs that resulted from alternating upward and downward flows (paired counter-rotating vortices) across the flame front. The downward flows deflected flames down and forward to make flame intermittent contact with fuels adjacent to the flame front (Fig. 5.6) and I suggest the same occurred here.

While the general tendency of increasing frequency of hot gas pulses over longer periods occurs for the 1 mm and 12 mm particles, the peak temperatures of the pulses at the particles is different and specific to the experiment. For example, inspection of the expanded graph (right) in Fig. 5.5a shows pulse temperatures of the 12-mm particle were significantly greater than for the 1 mm particle during the approaching fire spread. Also, the flame front

arrived at the 12 mm particle at 77 seconds (graph time), about 2 seconds before arriving at the 1 mm particle and 1 second before 1 mm particle ignition (identified in Fig. 5.3). The convective boundary conditions are temporally and spatially transient (Fig. 5.5) and this indicates such transience of the flame front.

5.3.4 Measured 1 mm Fuel Particle Temperatures

Given the importance of fine fuels as the primary fuel contributor to flame front intensity and spread (Rothermel 1972), I now focus on the 1 mm particle response to the thermal boundary conditions during approach flame fronts. The 1 mm particle temperature (Fig. 5.7a, b, c, full graphs) starts at ambient particle temperatures before significant thermal exposure from the flame front. At the end of the experiment, the particle temperatures were above 400 C consistent with sustained ignition of the 1 mm particle (Fig. 5.3). The gas temperature profiles (Fig. 5.7) show intermittently high temperature pulses with a more steady increase in irradiance with the 1 mm particle temperatures included.

The time-history of 1 mm particle temperatures shown in Figure 5.7 can be interpreted in terms of the boundary conditions. When the gas temperature (blue line) is lower than the particle (black) convective cooling occurs. Higher gas temperature compared to particle temperature indicates convective heating. As the flame front approaches, particles are warmer than gas temperatures when they absorb flame radiation. This causes 1 mm particle temperatures to remain higher than ambient gas temperatures until the flame front is close enough for hotter gas pulses to contact the particle. The 1-mm particle temperatures responded quickly to changes in gas temperature, both heating and cooling. Although radiation heating can raise particle temperatures to 100 C, graphs Fig. 5,7 a, b and c indicate 1 mm particles heat to ignition only when convectively heated by hot gasses. Each of the experiments (Fig. 5.7a, b and c) have a different pattern of high temperature gas pulses leading to ignition but particle ignition occurs only after gas temperatures are persistently over 400 C in the last two seconds. For example, between 78 seconds and 80 seconds in Fig. 5.7a particle temperatures increase with the corresponding gas temperatures. Importantly, at about 79 seconds gas temperatures and particle temperatures increase leading to particle ignition

Measured 1-mm Particle Temperature

a) [0.34 m/s wind speed]

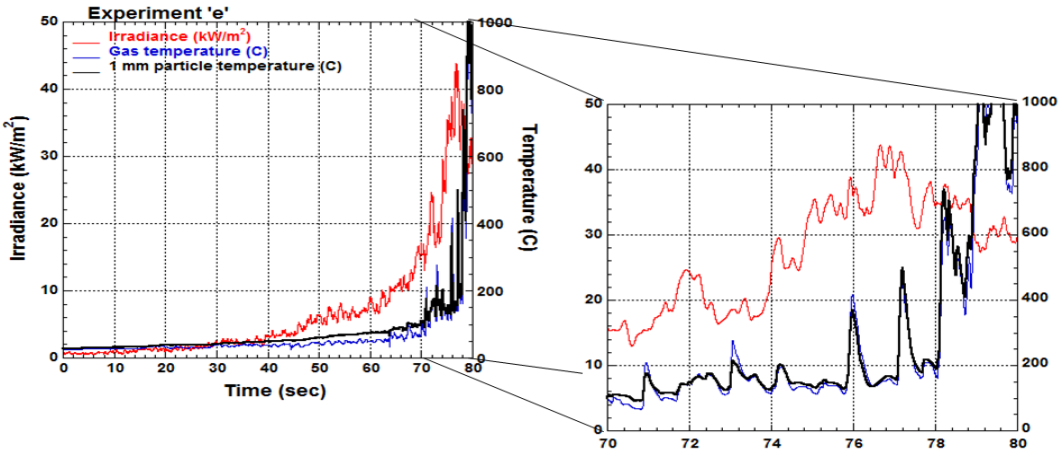

b) [0.56 m/s wind speed]

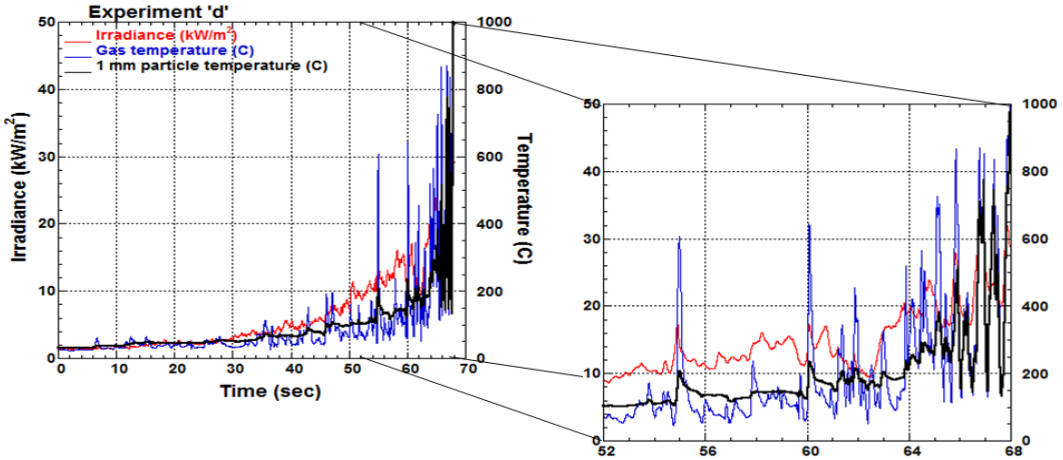

c) [0.67 m/s wind speed]

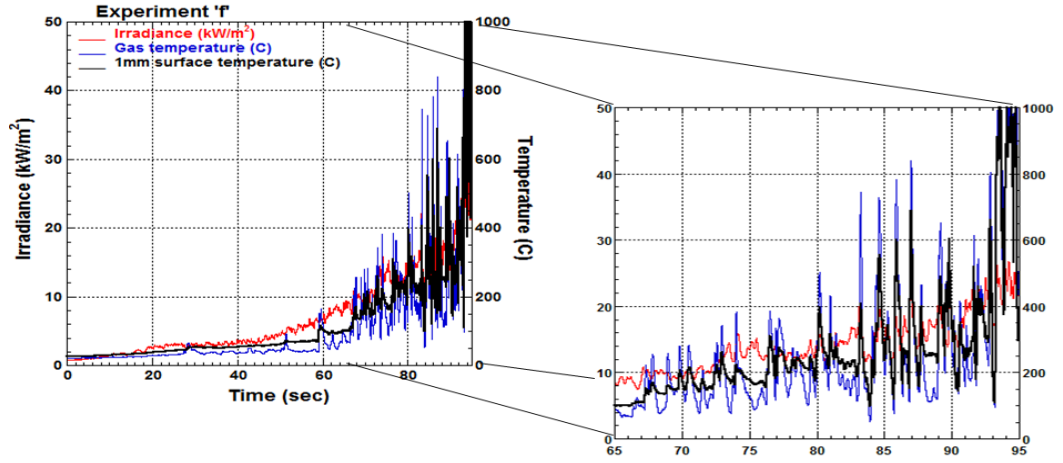

Fig. 5.7 Measured 1-mm particle temperature (black) is graphed in association with measured irradiance (red) and gas temperature (blue). Particle temperatures are from the 1-mm front surface thermocouple and gas temperatures are from the 1-mm adjacent front thermocouple (Fig. 5.1). The y-axes are the same for all graphs but the x-axes are not. Graphs a, b and c correspond to Experiments e, d and f, respectively.

while irradiance decreases. Fig. 5.7b demonstrates significant particle temperature increases during hot gas pulses at 55, 60 and 64 seconds. In Fig. 5.7c particle ignition occurs after gas temperatures remain over 400 C in the last two seconds leading to ignition.

The spatial and temporal variability of the flame zone characteristics during fuel particle heating experiments, the interactions of heat transfer mechanisms, and the difficulty of sufficiently high resolution instrumentation makes the physics elusive and the results difficult to interpret. Physically modeling the heat transfer mechanisms of fuel particle heating were thus, used to provide further insights to particle heating related to thermal boundary conditions.

5.3.5 Modeled 1 mm Fuel Particle Temperatures

I found that the model accounted for the observed 1 mm particle heating response using the time-series of irradiance and air temperature measured in the experiments as boundary conditions in the numerical heat transfer model (Chapter 4). The modeled 1 mm particle temperature (dotted purple line, Figure 8) rose quickly when contacted by high temperature air pulses and cooled more slowly between pulses, similar to the measured particle surface temperature (black line). Inspection of Fig. 5.8 indicates the model responded to the high temperature gas pulses at 55 seconds, 60 seconds, and during the last second of the graph similar to the measured temperatures. I calculated the correlation coefficient ('r,' DeVeaux et al. 2005, p.121) of the modeled temperatures to the measured temperatures to be r = 0.993. This indicates a strong linear association of the modeled and experimental data. Although particle

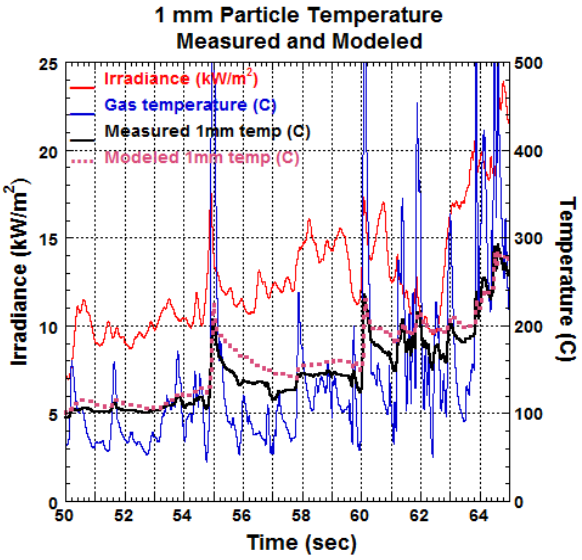

Fig. 5.8 The measured irradiance and gas temperatures shown in Figure 7b are used as inputs for computing the 1 mm particle face temperature (dotted purple). The measured 1 mm face temperature (black) is presented for comparison with the modeled temperature (50 seconds to 65 seconds of Fig. 5.7b).

temperature modeling began before flame front influences occurred, the data displayed in Fig. 5.8 begin when the particle reaches 100 C (50 seconds for both measured and modeled). The graph ends at 65 seconds when the measured particle temperature begins to reach and exceed 275 C, the upper limit of model reliability.

Modeled temperature response times appear to be longer than the measured response as indicated by the modeled temperatures remaining higher than measured temperatures after contact by hot gases. This could be due to using an average convection heat transfer coefficient that does not account for a highly non-uniform temperature distribution across the particle. However, based on the strong linear association of the model with measured data, I used the model to examine heat transfer mechanisms.

5.3.6 Modeled Without Flame Radiation

It is difficult to differentiate the radiation and convection heat transfer mechanisms during fire spread even with fine scale sampling. Modeling "experiments" thus, provide the opportunity to overcome practical limits of experimentation to explore questions such as "What would be the resulting particle temperatures if the flame radiation was blocked without affecting flame convection and vice versa?" Using the model, I conducted modeling experiments to examine particle heating from only convection. The measured irradiance was replaced by a constant irradiance from 300 K (27 C) blackbody surroundings and the particle could radiate to the suroundings. The measured gas temperatures were used as previously modeled. Inspection of Fig. 5.9 indicates that without flame radiation the modeled particle displayed similar temperature response characteristics to the measured particle principally due to

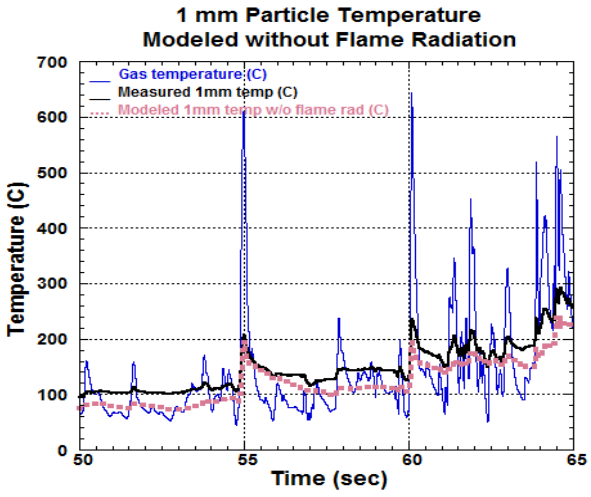

Fig. 5.9 A constant irradiance of 300 K surroundings was substituted for the measured flame irradiance. The measured gas temperatures (blue) were used to compute convection heat transfer as before. The last 15 seconds of the computed particle temperature (purple) was compared to the measured particle temperature (black).

convective heat exchange. Without flame radiation the modeled particle temperatures were never more than 50 C below the measured particle temperatures (Fig. 5.8).

5.3.7 Modeled Without Flame Convection

With a similar modeling experiment I examined the particle heating from radiation. The measured gas temperatures were replaced by a constant ambient temperature of 300 K (27 C) at the constant wind tunnel flow speed of 0.56 meters/second. With ambient gas temperatures, convection only cools the particle as it absorbs flame radiation. The measured irradiance from Experiment 'd' was used as previously modeled. Inspection of Fig. 5.10 indicates a major change in the modeled temperatures compared to the measured particle temperatures. The rapid increases in measured particle temperatures corresponding to 55 seconds and 60 seconds (Fig. 5.10 graph time) were absent without flame convection. Notably, at 63 seconds the modeled temperature dropped corresponding to the measured decrease in irradiance while the measured particle temperature increased. Just prior to actual particle ignition the final modeled temperature was about 100 C, well below temperatures associated with piloted ignition. The measured temperature was approaching 300 C. This result is consistent with the previously discussed FTP analysis indicating that the irradiance was radically less than sufficient for piloted ignition.

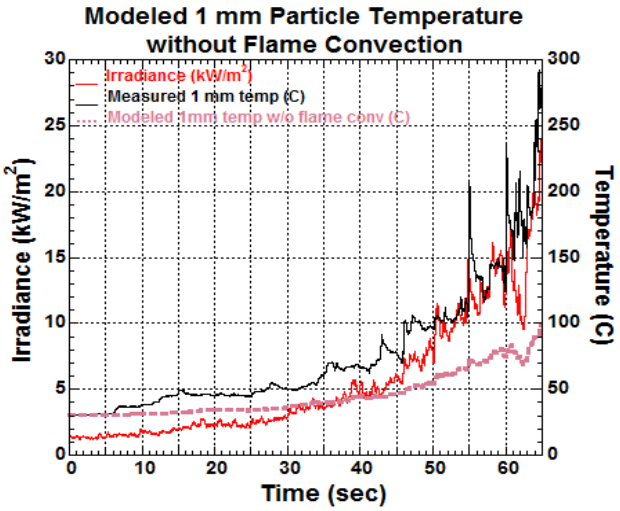

Fig. 5.10 A constant 300 K gas flow was substituted for the flame gases. The measured flame irradiance was used as before. The 65 second sequence shows how the measured particle temperature (black) diverges from the computed temperature (purple) without hot flame gases.

5.4 Discussion

The flame spread experiments with engineered cardboard fuel beds were used to obtain data on radiation and convection that heated the 1-mm and 12-mm fuel particles. The two instrumented particles did not influence the spread and intensity of the experimental fires and thus, the particle time-temperature profiles leading to ignition cannot be interpreted in terms of spread rate, flame zone depth and flame length of the propagating flame zone. For example, the fuel beds and wind speeds of experiments e, d and f (Fig. 5.7a, b, and c) were all different resulting in significantly different measured flame radiation and convection heating of the 1-mm fuel particles.

The measured 1 mm and 12 mm particle surface temperatures indicated the importance of particle size on heat transfer response time (Fig. 5.3). The 1 mm particle demonstrated shorter heat exchange response times with rapid temperature changes over a wider range of temperatures than the 12 mm particles. Importantly, with increasing convective heating from hot gas pulses the 1 mm particle attained higher temperatures and ignited before the 12 mm particle during every experiment. This reinforces the Chapter 2 discussion of the importance of fine fuels as the principal fuel influencing wildland fire propagation.

The experimental results were contrary to the common modeling assumption of flame radiation as the mechanism primarily responsible for fire spread (Albini 1985; Sen and Puri 2008; Butler et al. 2004, see Chapter 2 for in-depth explanation). The FTP analysis of the measured irradiances from all the experiments indicated radiation heating for piloted ignition was insufficient (Fig. 5.4). Therefore, convective heating being the only alternative mechanism for fuel heating, must heat the fuels to ignition. In support of the FTP findings, Fig. 5.7a, b and c demonstrate that convection is the principal mechanism responsible for the 1 mm temperature changes and thus heat exchange. Each of the graphs (Fig. 5.7a, b and c) show significant particle heating only after hot gas pulses contacted particles (blue lines above black lines). Several instances of flame contact with corresponding temperature increases occurred during decreasing irradiance. For example, Fig. 5.7a at 79-80 seconds and Fig. 5.7b at 67-68 seconds indicate convective heating as the primary heat transfer mechanism. The modeling experiment with radiation heating and only convection cooling resulted in a 1-mm

particle surface temperature of 100 C while the measured particle temperature approached 300 C leading to ignition (Fig. 5.10). This modeling result is similar to that of Baines' (1990) radiation heating and convective cooling model compared to the modeled fuel temperatures without convective heating shown in Chapter 2, Fig. 2.1. The experimental and modeling results indicate the importance of convection heating in determining fire spread and support the convection heating ignition sequence presented in this chapter's Introduction.

Most of the fuel particle heating required for ignition occurred in the final few seconds before ignition. This is the heating time discussed in Chapter 2 that was specifically noted by Fang and Steward (1969) and demonstrated in graphs of experimental data from Rothermel (1972; Fig. 2.3) where the mechanisms of particle heating leading to ignition were unresolved. An inspection of Fig. 5.5a, b and c reveals an increase in particle contacts from hot gas pulses corresponding to increased wind speed. Because the 1-mm particles always ignited before the 12-mm particles, I focused my examination on the 1-mm temperature profiles with boundary conditions (Fig. 5.7a, b and c). Although hot pulse contacts occurred with increased durations before particle ignition, the 1 mm front surface temperatures repeatedly cooled to temperatures less than 200 C. The final temperature increase from 200 C to ignition occurred within 2 seconds for all experiments. Given the experimental average spread rates (Table 5.1), the flame zone ranges from within 0.032 m to 0.068 meters from the particle when sufficient heating results in ignition. Because pyrolysis is negligible at particle surface temperatures less than about 275 C and above 325 C is typical for piloted ignition (Fairbridge et al. 1978; Tillman et al. 1981; Simmons 1995; Drysdale 1998), the significance of prior heating from hot gas pulses is unclear. Based on experimental measurements and analyses using the theoretical physical model, convective particle heating from flame contact was the primary mechanism for fuel particle ignition during the laboratory fire spread experiments. Figs. 5.5 and 5.7 indicate changes in the frequency, duration and temperature of intermittent hot gas pulses with the different experimental fire spread conditions. Knowing the hot pulse characteristics as the flame front approaches and the particle response characteristics, one could calculate what might be termed the "effective heating length," that is, the maximum fuel bed gap distance across which an ignition can occur.

5.5 Conclusions

My findings do not support the general assumption that wildland fire spread is primarily governed by flame radiation. Based on experiments and modeling I have described how radiation is not sufficient for fine fuel particle ignition and how convection heating can be the principal mechanism determining fire spread. With convection being the only alternative fuel heating mechanism to radiation, the experimental and modeling results support convection heating from intermittent hot gas pulses as the primary mechanism for particle ignition. However, convection heat transfer rates are different for fine and coarse fuels depending convective surface lengths. From experimental results, I show that fine fuels (1-mm particles), the principal fuel component governing fire spread, respond faster with greater per unit area heat exchange than coarse fuels (12-mm particles). Although these experimental results may not apply to all wildland fire spread situations, and thus further study is needed as described in Chapter 6), the laboratory fire spread experiments matched the flame zone characteristics of most wildland fire spread in surface litter (as I discussed in Chapter 2). I therefore suggest non-steady convection as the principal mechanism for wildland surface fires both actual and experimental.

5.7 References

Albini FA (1985) A model for fire spread in wildland fuels by radiation. *Combustion Science and Technology* **42**(5-6), 229-258.

Baines PG (1990) Physical mechanisms for the propagation of surface fires. *Mathematical Computer Modelling* **13**(12), 83-94.

Butler BW, Finney MA, Andrews PL, Albini FA (2004) A radiation-driven model for crown fire spread. *Canadian Journal of Forest Research* **34**(8), 1588-1599.

Cohen, J. D. (2004) Relating flame radiation to home ignition using modeling and experimental crown fires. *Canadian Journal of Forest Research* **34**(8): 1616-1626.

DeVeaux RD, Velleman PF, Bock DE (2005) 'Stats: Data and Models.' (Pearson-Addison Wesley: Boston)

Drysdale, D. (1998) 'An Introduction to Fire Dynamics.' (Wiley: New York)

Fairbridge C, Ross RA, Sood SP (1978) A kinetic and surface study of the thermal decomposition of cellulose powder in inert and oxidizing atmospheres. *Journal of Applied Polymer Science* **22**: 497-510.

Fang JB, Steward FR (1969) Flame spread through randomly packed fuel particles. *Combustion and Flame* **13**, 392-398.

Finney MA, Cohen JD, McAllister SS, Jolly WM (2013a) On the need for a theory of wildland fire spread. *International Journal of Wildland Fire* **22**, 25-36.

Finney MA, Forthofer JD, Grenfell IC, Adam BA, Akafuah NK, Saito K (2013b) A study of flame spread in engineered cardboard fuel beds, Part I: Correlations and Observations. 6-9 August, 2013, 'Seventh International Symposium on Scale Modeling.' Hirosaki, Japan.

Finney MA, Cohen JD, Forthofer JA, McAllister SS, Adam BA, Akafuah NK, English J, Saito K, Gorham DJ, Gollner MJ (2014) Experimental evidence of buoyancy controlled flame spread in wildland fires. 17-20 November 2014, 'Seventh International Conference on Forest Fire Research.' (Coimbra, Portugal)

Fons WL (1946) Analysis of fire spread in light forest fuels. Journal of Agricultural Research **72**, 93–121.

Fritschen LJ, Gay LW (1979) 'Environmental Instrumentation.' (Springer-Verlag: New York)

Incropera FP, DeWitt DP (2002) 'Introduction to Heat Transfer.' (Wiley: New York)

Rothermel RC, Anderson HE (1966) Fire spread characteristics determined in the laboratory. USDA Forest Service, Intermountain Forest and Range Experiment Station, Research Paper INT-RP-30. (Ogden, UT)

Rothermel RC (1972) A mathematical model for predicting fire spread in wildland fuels. USDA Forest Service, Intermountain Forest and Range Experiment Station, Research Paper INT-RP-115. (Ogden, UT)

Sen S, Puri IK (2008) Thermal radiation modeling in flames and fires. Ch. 8 ‘Transport Phenomena in Fires.’ (WIT Press-Cambridge Printing: Southampton, UK)

Simmons RF (1995) Fire chemistry, Ch. 7 In ‘Combustion Fundamentals of Fire.’ (Academic Press: New York)

Tillman DA, Amadeo JR, Kitto WD (1981) ‘Wood Combustion.’ (Academic Press: New York)

Chapter 6

The Research: Significance, Limitations and Further Considerations

6.1 The Research

I conducted my fuel particle heat exchange research to examine the fundamental processes of fuel particle heating leading to ignition and thus, fire spread. Surprisingly, in the decades since Fons (1946) identified fire spread as a series of ignitions, a theory for how wildland fire spreads has not been developed (Finney et al. 2013). I described in Chapter 2 that research has largely focused on predicting rate of spread rather than understanding the heat exchange processes leading to particle ignition that results in fire spread. Thus, there is an absence of experimental evidence as a basis for describing the mechanisms of wildland fire spread for physical modeling. The perception that radiation heating is the governing mechanism of wildland fire spread has been widely held and commonly assumed in physical fire spread models. However, the assumption of radiation as the primary mechanism determining fire spread has never been experimentally confirmed in terms of fuel particle heating and ignition. What little experimental evidence that does exist indicates otherwise (Anderson 1969, Fang and Steward 1969, Baines 1990, Weber 1991).

I approached wildland fire spread by examining fuel particle ignition based on the premise that fire spread results from ignition. I justified this premise in Chapter 2. I described in Chapter 3, 4, and 5 the experiments and modeling of fuel particle heat exchange leading to ignition. Using experiments I measured radiation and convection boundary conditions and the resulting fuel particle surface temperatures. However, the experimental measurements did not describe fuel particle heat exchange. In the experiments, the fuel particle thermally responds to the boundary conditions resulting in the particle temperatures. To reveal these processes I created a theoretically based model to generate particle temperatures from the measured particle boundary conditions. The modeled particle temperatures in Chapters 4 and 5 exhibited the same responses and similar temperature ranges as the measured temperatures.

Based on these results I concluded that the model reasonably represented particle heat exchange processes for the experimental conditions.

From the experimental and modeling results I showed how convective boundary conditions governed fuel particle heat exchange leading to ignition (Chapter 4). I conducted controlled experiments to examine fuel particle cooling during radiative heating. I exposed square cross-section 1, 3, 6, 9 and 12 mm fuel particles to constant exposures of irradiance (29.8 – 36.4 kW/m^2) and free and forced convection (0.0 - 1.0 m/s). Of these 5 particle sizes tested only the 1 mm fuel particle did not exceed measured temperatures of 275 C. Due to greater convective cooling of the smaller 1 mm particle, radiation was not sufficient for ignition. Using schlieren imaging and vertically arranged thermocouples on the particle surface, I demonstrated that convective heat exchange increased with decreasing particle size due to reduced flow length and thus, less boundary development. From experiments and modeling I showed how particle boundary conditions are largely independent of particle surface area-to-volume ratio (SAV), that is, surface boundary conditions govern the particle surface temperatures and SAV determines the thermal response of the particle.

The greater convection heat exchange that cooled the 1 mm particle during radiant heating compared to coarser particles also increased its convective heating from contact with hot flame gases. Because burning fine fuels govern fire spread (Chapter 2) I focused attention on the 1 mm particle. As described in Chapter 5, I conducted experiments using spreading laboratory fires to primarily examine 1 mm fuel particle heat exchange and its response rate to the flame zone radiation and convection. For comparison I also included a 12 mm particle. Of the seven fire spread experiments, none of the measured irradiances were sufficient for piloted ignition and the 1 mm particles always ignited before the 12 mm particles. This is the opposite result of the radiative heating-convective cooling experiments (Chapter 4). During the spreading laboratory fires I measured the radiative and convective boundary conditions and surface temperatures of the 1 mm and 12 mm fuel particles. Notably the 1 mm particles rapidly responded to intermittent pulses of hot gases and the 12 mm particles did not. From my measurements of boundary conditions and fuel particles I resolved the heat exchange mechanisms to less than 250 milliseconds, the radiometer time constant. Based on these measurements and physical modeling, I found the principal particle heating mechanism of the

1 mm fuel particle to be convection from intermittent pulses of hot gases within the last 6 cm (or less than 2 seconds) of fire spread before particle ignition.

6.2 Research Limitations and Further Research

Although my research has taken an important initial step for considering fuel particle convective heat exchange it does not definitively describe fuel particle heat exchange for the broad range of fuel conditions and flame front exposures during the spread of wildland flame fronts. These research limitations are with both my experiments and modeling. Because my approach relied on the coupling of experimental and modeling results, broadening the research to include more factors over a wider range of conditions will require further experiments and model development.

The experimental limitations include fuel particle conditions, irradiance levels and wind speeds and direction. My research used fuel particles fabricated from yellow poplar (*Liriodendron tulipifera*) lumber, having square cross-sections of 1 mm and larger. For the controlled experiments the particle moisture contents were less than 3 percent (dry weight basis) and for the fire spread experiments less than 6 percent. Fuel particles were mounted singly and horizontally. The experiments did not examine dead moisture content influences and did not include potential differences between the fabricated particles and dead vegetative fuels such as grasses, twigs and foliage that would include a variety of materials, sizes and shapes (for example, circular cross-section). The effects of vertical orientation and multi-particle clusters on radiative and convective fuel particle heat exchange were not examined and live foliage was not considered. The experimental particle irradiance was limited to a maximum continuous irradiance during the controlled experiments of about 35 kW/m^2 and a maximum transient fire spread irradiance of 44 kW/m^2. Higher particle irradiances and potential irradiances of 80 to 100 kW/m^2 have been measured during crown fires (Cohen 2004; Butler et al. 2004; Taylor et al. 2004). The experiments did not examine fuel particle heat exchange of air flows directed at front and back particle sides higher than 1.0 m/s.

The research results from the controlled and fire spread experiments suggested that the physical model accurately captured the fuel particle heat exchange processes for the

experimental conditions but these conditions were limited as just discussed. While the experimental limitations largely corresponded to the apparatus and ability to measure particle temperatures, the numerical model limitations were more related to computational complexity and theoretical limits as discussed in the model assumptions section of Chapter 4. The numerical model did not account for phase changes both water and pyrolysis and did not account for mass transfer and material property changes due to water movement and thermal decomposition. Cylindrical particle shapes were not considered because the 2-dimensional numerical solver for the heat conduction equation was based on a square grid unit of computational nodes (Chapter 4). The model was limited in appropriately accounting for free and forced convective boundary conditions because available convection coefficient correlations did not match the transient, non-isothermal, externally heated conditions of the experimental fuel particles, and for forced convection, low Reynolds number flows for non-cylindrical particles ($Re_L \approx 10^1 - 10^2$). The numerical model only considered a single, horizontally oriented fuel particle.

An added limitation of this research is replication and this relates to its applicability for operational use or a broader inference to a larger wildland fire behavior and fire effects context. The experiments conducted in this research were from a physics and engineering context, within a highly monitored laboratory setting, whereby each run was characterized by near unique conditions. The laboratory fire spread experiments were repeatable within a narrow range of attributes such as spread rate, burning residence time and flame length but conditions were not repeatable at my scale of particle heat exchange. Due to the non-linearity between boundary conditions and resulting particle temperatures, verification of the observations and determination of heat exchange was achieved through comparison with the theoretical physical model, on a case-by-case basis. An aspect of repeatability was exercised with each set of boundary measurements as the basis for comparing modeled particle temperatures with measured particle temperatures. I conducted tests on each of five different particle sizes for free and forced convection and observed similarly good comparisons with the model making me confident on the soundness of the results. When experiments are performed during wildland fire spread, the same high spatial and temporal measurement resolutions will be essential along with the replication of as many parameters as possible held

constant to ensure that the observed effects are not an artifact of variation brought in by extraneous variables.

The limitations of my research provide a guide for further research that will expand the experimental range of conditions and increase the factors considered by the numerical model to more comprehensively account for wildland fire spread conditions. Further research is needed to examine whether the current numerical model continues to accurately capture the heat exchange processes at higher irradiances and air flow speeds including air flowing toward the irradiated side of the particle. Further experimental research might initially involve experiments to examine the effects of various factors such as moisture content, live foliage, particle shape (rectangular or circular across) and horizontal to vertical orientation. These experiments would examine the significance of a factor's influence on particle heat exchange for determining inclusion in the numerical model. Without theoretical comparisons, these experiments would require sufficient replication for determining the degree of significance. Given that a factor has significant influence, further model development might use empirical correlations within the theoretical framework. For example, additional laboratory experiments would be used to determine empirical convection coefficient correlations based on appropriate fire spread conditions. Without experimentation the numerical model can be modified to calculate circular cross-sections and two-phase mass and energy transfer for water evaporation and initial pyrolysis. However, without an experimental basis, developers should resist complicating the numerical model. Ultimately, further research might include boundary condition and fuel particle measurements during field fire spread experiments to sample actual wildland fire conditions and evaluate numerical model capabilities to accurately capture the principal processes of fuel particle heat exchange and ignition.

6.3 Significance to Physical Fire Spread Modeling

My research findings contribute to a developing theory of wildland fire spread (Finney et al. 2013) related to fuel particle heat exchange leading to ignition. Thus, my findings potentially become incorporated into a fire spread theory that provides the basis for future physical fire spread models. From my findings I conclude that a physical fire spread model will have to

appropriately account for fuel particle size and shape related to radiation and convection heat exchange. Because of the non-linear relationship between particle size and convective heat exchange, characterizing bulk fuel bed properties for a mix of fuel particle sizes and shapes must be done according to the component heat exchange rates and not particle dimensions. For example, for a mix of fine and coarser fuel particles, the heat exchange of the average fuel particle size will not be the same as the heat exchange for the fine fuel particles that govern the fire spread. I found that fuel particle heat transfer processes related to surface length (boundary conditions) primarily determine surface temperature and given surface temperatures, surface area-to-volume ratio primarily determines particle thermal response rate. Based on my findings from Chapters 4 and 5, both of these fuel descriptors require consideration to physically model fire spread. My finding that fine fuel particles primarily heat to ignition from contact with intermittent pulses of hot flame gases indicates a physical fire spread model must describe flame front dynamics such as the pulse frequencies, pulse durations and convective temperatures as a function of fuel particle distance from the flame front. With these research findings I provide a foundation for understanding fuel particle heat exchange leading to ignition and the basis for physical fire spread models to more appropriately describe fuel heating and ignition.

6.4 A Probabilistic Consideration for Physical Model Applications

From Chapters 4 and 5 it is apparent that particle size and configuration determine particle heating and thus, fuel heat exchange and ignition processes occur at particle scales. However, applying a physical model to actual wildland fire spread will require modeling scales significantly larger than fuel particles whether for research or operational purposes. This dictates the need to appropriately account for heat exchange processes at the particle scale while modeling the fire spread at significantly larger scales. I suggest that the small scale properties might be inferred using probability distributions from larger, modeling scales. For example, the small scale composition and structure of a wildland fuel bed might be probabilistically designated based on prior research that has described small scale patterns as probability distributions (Parsons et al. 2011). Perhaps the particle scale heat exchange and ignition processes can be more appropriately represented at practical modeling scales by

physically modeling particle scale ignition processes to pre-determine the probability distribution of the expected larger scale fuel response to the radiative and convective exposure probabilities of the flame front. I am suggesting that fire spread modeling would become a stochastic processor for probabilistic diagnostic descriptions of spread thresholds and probabilistic predictions of spread rates.

6.5 References

Anderson HE (1969) Heat transfer and fire spread. USDA Forest Service, Intermountain Forest and Range Experiment Station, Research Paper INT-RP-69. (Ogden, UT)

Baines PG (1990) Physical mechanisms for the propagation of surface fires. *Mathematical Computer Modeling* **13**(12), 83-94.

Butler BW, Cohen J, Latham DJ, Schuette RD, Sopko P, Shannon KS, Jimenez D, Bradshaw LS (2004) Measurements of radiant emissive power and temperatures in crown fires. *Canadian Journal of Forest Research* **34**(8), 1577-1587.

Cohen JD (2004) Relating flame radiation to home ignition using modeling and experimental crown fires. *Canadian Journal of Forest Research* **34**(8), 1616-1626.

Fang JB, Steward FR (1969) Flame spread through randomly packed fuel particles. *Combustion and Flame* **13**, 392-398.

Fons WL (1946) Analysis of fire spread in forest fuels. *Journal of Agricultural Research* **72**: 93-121.

Finney MA, Cohen JD, McAllister SS, Jolly WM (2013) On the need for a theory of wildland fire spread. *International Journal of Wildland Fire* **22**(1): 25-36.

Parsons RA, Mell WE, McCauley P (2011) Linking 3D spatial models of fuels and fire: effects of spatial heterogeneity on fire behavior. *Ecological Modeling* **222**(3): 679-691.

Taylor SW, Wotton BM, Alexander ME, Dalrymple GN (2004) Variation in wind and crown fire behaviour in a northern jack pine – black spruce forest. *Canadian Journal of Forest Research* **34**, 1561-1576

Weber RO (1991) Modelling fire spread through fuel beds. *Progress in Energy Combustion Science* **17**: 67-82.